NUREG/CR-2018
SAND80-1870
RT

A Comparison of Analytical Techniques for Analyzing a Nuclear-Spent-Fuel Shipping Cask Subjected to an End-On Impact

Charles R. Adams, John H. Biffle
Matt H. Gubbels, Michael Huerta

RECEIVED
AUG 28 1981
U.S. NUCLEAR REGULATORY COMMISSION

Printed June 198

Sandia National Laboratories

SF 2900-

Prepared for

U.S. NUCLEAR REGULATORY COMMISSION

8109180566 810831
PDR NUREG
CR-2018 R PDR

NOTICE

This report was prepared as an account of work sponsored by an agency of the United States Government. Neither the United States Government nor any agency thereof, or any of their employees, makes any warranty, expressed or implied, or assumes any legal liability or responsibility for any third party's use, or the results of such use, of any information, apparatus product or process disclosed in this report, or represents that its use by such third party would not infringe privately owned rights.

Available from

GPO Sales Program
Division of Technical Information and Document Control
U.S. Nuclear Regulatory Commission
Washington, D.C. 20555

and

National Technical Information Service
Springfield, Virginia 22161

NUREG/CR-2018
SAND80-1870
RT

A Comparison of Analytical Techniques for Analyzing a Nuclear-Spent-Fuel Shipping Cask Subjected to an End-On Impact

Charles W. Adams
John M. Biffle
Matt H. Gubbels
Michael Huerta

Date Published: June 1981

Sandia National Laboratories
Albuquerque, New Mexico 87185
operated by
Sandia Corporation
for the
U. S. Department of Energy

Prepared for
Division of Safeguards, Fuel Cycle and Environmental Research
Office of Nuclear Regulatory Research
U. S. Nuclear Regulatory Commission
Washington, DC 20555
Under Memorandum of Understanding DOE 40-550 75
NRC FIN No. A-104

Abstract

A requirement of the design of a nuclear shipping cask (10 CFR 71 Appendix B) is that it survive a free drop of 30 feet onto a flat, essentially unyielding target. This report compares various analytical techniques which can be used to determine the dynamic response of a cask. These techniques are compared by defining two hypothetical cask designs, one lead-steel-balsa and the other uranium-steel. The end-on axial impact orientation condition was selected and one-, two-, and three-dimensional analyses were performed. The analysis techniques include strength-of-materials methods, lumped-parameter dynamic modeling, and both static and dynamic two- and three-dimensional finite element techniques. The results are compared in terms of kinematic and stress levels at different points on the casks. The study will be valuable as a guide in selecting analysis techniques for evaluating the dynamic response of shipping casks.

Contents

1.0 Introduction 11
1.1 Scope of Study 11
1.2 Types of Analysis 11
1.2.1 One-Dimensional Analysis Procedures 12
1.2.1.1 Constant Acceleration Method Analysis 12
1.2.1.2 Dynamic Analysis 17
1.2.2 Multidimensional Analyses Procedures 18
1.3 References 20
2.0 Description and Design of Casks 21
2.1 Cask Model Design Overview 21
2.2 Lead-Steel-Balsa Cask Model 22
2.3 Uranium-Steel Cask Model 22
2.4 LWR-Spent-Fuel Shipping Cask Structural Survey 23
2.4.1 Survey Summary 23
2.4.2 NFS-4 23
2.4.3 NLI 1/2 27
2.4.4 TN-8 and TN-9 27
2.4.5 NFS-5 27
2.4.6 IF 300 27
2.4.7 NLI 10/24 27
2.4.8 TN-12 27
2.5 References 28
3.0 Material Properties 29
3.1 304 Stainless Steel 29
3.2 Lead 29
3.3 Uranium 30
3.4 Balsa Wood 30
3.5 Water 33
3.6 References 33
4.0 Analysis of End-On Impact 35
4.1 Lead-Steel-Balsa Cask 35
4.1.1 Cask Analysis 35
4.1.1.1 Two-Dimensional Dynamic Analysis 36
4.1.1.2 Two-Dimensional Static Analysis 40
4.1.1.3 One-Dimensional Dynamic Analysis 40
4.1.1.4 One-Dimensional Static Analysis 44
4.1.2 Comments on Accomplishing Analyses 46
4.1.3 Comparison of Results for the Lead-Steel Cask 47
4.2 Uranium-Steel Cask 49
4.2.1 Fin Impact Analysis 49
4.2.1.1 Three-Dimensional Dynamic Analysis 49
4.2.1.2 Two-Dimensional Dynamic Analysis 52
4.2.2 Cask Analysis 54
4.2.2.1 Two-Dimensional Dynamic Analysis 54
4.2.2.2 Two-Dimensional Static Analysis 59
4.2.2.3 One-Dimensional Dynamic Analysis 59
4.2.2.4 One-Dimensional Static Analysis 64
4.2.3 Comparison of Results for the Uranium-Steel Cask 66
4.3 References 69
5.0 Summary and Conclusions 71

Illustrations

Figure

1.2.1 Balsa Wood Impact Limiter Schematic 13
1.2.2 Side-Impact End View 14
1.2.3 Corner-Impact Schematic 15
1.2.4 Corner-Impact Parameter Plot No. 1 15
1.2.5 Corner-Impact Parameter Plot No. 2 15
1.2.6 Strength-of-Materials Modeling of Cask End Plates 16
1.2.7 Illustration of a One-Dimensional Lumped Parameter Model for a Shipping Cask 17
1.2.8 Illustration of a Load-Deflection Curve for an Impact Limiter 18
1.2.9 Quadrilateral Element Approximation 18
2.1 Lead-Steel-Balsa Cask 22
2.2 Uranium-Steel Cask 23
3.1.1 Stress-Strain Curve for 304 Stainless Steel at 70°F 29
3.2.1 Stress-Strain Curve for Chemically Pure Lead at 70°F 30
3.4.1 Balsa-Wood-Weight Model for Material Model Calculations 30
3.4.2 Axial Acceleration of Plate at Point A When Elastic-Plastic Material Model Is Used 31
3.4.3 Axial Velocity of Plate at Point A When Elastic-Plastic Material Model Is Used 31
3.4.4 Axial Displacement of Plate at Point A When Elastic-Plastic Material Model Is Used 32
3.4.5 Axial Acceleration of Plate at Point A When Crushable Foam Model Is Used 32
3.4.6 Axial Velocity of Plate at Point A When Crushable Foam Model Is Used 32
3.4.7 Axial Displacement of Plate at Point A When Crushable Foam Model Is Used 32
3.4.8 Total Force vs Time at the Balsa-Wood-Foundation Interface 33
4.1.1 Axisymmetric Outline Lead-Steel-Balsa Cask 36
4.1.2 Finite Element Mesh of Lead-Steel Cask for End-On Impact Analysis 36
4.1.3 Radial Stress vs Time at Location A for the Lead-Steel-Balsa Cask End-On Two-Dimensional Dynamic Impact Calculation 37
4.1.4 Radial Stress vs Time at Location B for the Lead-Steel-Balsa Cask End-On Two-Dimensional Dynamic Impact Calculation 37
4.1.5 Axial Stress vs Time at Location C for the Lead-Steel-Balsa Cask End-On Two-Dimensional Dynamic Impact Calculation 38
4.1.6 Circumferential Stress vs Time at Location C for the Lead-Steel-Balsa Cask End-On Two-Dimensional Dynamic Impact Calculation 38
4.1.7 Effective Stress vs Time at Location C for the Lead-Steel-Balsa Cask End-On Two-Dimensional Dynamic Impact Calculation 38

Illustrations (cont)

Figure

4.1.8 Axial Acceleration vs Time at Location E for the Lead-Steel-Balsa Cask End-On Two-Dimensional Dynamic Impact Calculation 38

4.1.9 Axial Velocity vs Time at Location E for the Lead-Steel-Balsa Cask End-On Two-Dimensional Dynamic Impact Calculation 39

4.1.10 Axial Displacement vs Time at Location E for the Lead-Steel-Balsa Cask End-On Two-Dimensional Impact Calculation 39

4.1.11 Axial Acceleration vs Time at Location A for the Lead-Steel-Balsa Cask End-On Two-Dimensional Dynamic Impact Calculation 39

4.1.12 Axial Velocity vs Time at Location A for the Lead-Steel-Balsa Cask End-On Two-Dimensional Impact Calculation 39

4.1.13 Axial Displacement vs Time at Location A for the Lead-Steel-Balsa Cask End-On Two-Dimensional Impact Calculation 40

4.1.14 Schematic of the Lumped Parameter Model 40

4.1.15 Force Input to the Bottom End (Location E) of Cask vs Time for the Lead-Steel-Balsa Cask End-On One-Dimensional Impact Calculation 41

4.1.16 Displacement of Location E vs Time for the Lead-Steel-Balsa Cask End-On One-Dimensional Impact Calculation 41

4.1.17 Velocity of Location E vs Time for the Lead-Steel-Balsa Cask End-On One-Dimensional Impact Calculation 42

4.1.18 Acceleration of Location E vs Time for the Lead-Steel-Balsa Cask End-On One-Dimensional Impact Calculation 42

4.1.19 Displacement of Location F vs Time for the Lead-Steel-Balsa Cask End-On One-Dimensional Impact Calculation 42

4.1.20 Velocity of Location F vs Time for the Lead-Steel-Balsa Cask End-On One-Dimensional Impact Calculation 43

4.1.21 Acceleration of Location F vs Time for the Lead-Steel-Balsa Cask End-On One-Dimensional Impact Calculation 43

4.1.22 Axial Stress at Location C vs Time for the Lead-Steel-Balsa Cask End-On One-Dimensional Impact Calculation 43

4.1.23 Axial Stress at Location D (Lead) vs Time for the Lead-Steel-Balsa Cask One-Dimensional End-On Impact Calculation 43

4.1.24 Tangential and Radial Stress at Location A vs Time for the Lead-Steel-Balsa Cask End-On One-Dimensional Impact Calculation 44

4.1.25 Radial Stress at Location B vs Time for the Lead-Steel-Balsa Cask One-Dimensional End-On Impact Calculation 44

4.1.26 Tangential Stress at Location B vs Time for the Lead-Steel-Balsa Cask End-On One-Dimensional Impact Calculation 45

4.2.1 Outline of Axisymmetric Parts of the Uraium-Steel Cask 50

4.2.2 Finite Element Mesh for Three-Dimensional Fin Impact Analysis 50

4.2.3 Total Force vs Time on End of Fin from Three-Dimensional Transient Analysis 51

4.2.4 Z Acceleration vs Time for Simulated Cask 51

4.2.5 Z Velocity vs Time for Simulated Cask 51

4.2.6 Z Displacement vs Time for Simulated Cask 51

4.2.7 Deformed Mesh of Fin at 7.00×10^{-3} s After Impact 52

Illustrations (cont)

Figure

4.2.8 Deformed Mesh of Fin at 7.75 x 10^{-3} s After Impact 52
4.2.9 Cask Fin Finite Element Model 53
4.2.10 Deformed Fin Model at 4.25 ms 53
4.2.11 Cask Acceleration During Impact 54
4.2.12 Cask Velocity During Impact 54
4.2.13 Side View of End Fin 54
4.2.14 Axisymmetric Finite Element Model of Uranium-Steel Cask Without Fins 55
4.2.15 Circumferential Stress vs Time at Location A for the Uranium-Steel Cask End-On Two-Dimensional Impact Calculation 55
4.2.16 Circumferential Stress vs Time at Location B for the Uranium-Steel Cask End-On Two-Dimensional Impact Calculation 56
4.2.17 Axial Stress vs Time at Location C for the Uranium-Steel Cask End-On Two-Dimensional Impact Calculation 56
4.2.18 Circumferential Stress vs Time at Location C for the Uranium-Steel Cask End-On Two-Dimensional Impact Calculation 56
4.2.19 Effective Stress vs Time at Location C for the Uranium-Steel Cask End-On Two-Dimensional Impact Calculation 56
4.2.20 Axial Stress vs Time at Location D for the Uranium-Steel End-On Two-Dimensional Impact Calculation 57
4.2.21 Circumferential Stress vs Time at Location E for the Uranium-Steel Cask End-On Two-Dimensional Impact Calculation 57
4.2.22 Circumferential Stress vs Time at Location F for the Uranium-Steel Cask End-On Two-Dimensional Impact Calculation 57
4.2.23 Axial Acceleration vs Time at Location F for the Uranium-Steel Cask End-On Impact Calculation 57
4.2.24 Axial Velocity vs Time at Location F for the Uranium-Steel Cask End-On Two-Dimensional Impact Calculation 58
4.2.25 Axial Displacement vs Time at Location F for the Uranium-Steel Cask End-On Two-Dimensional Impact Calculation 58
4.2.26 Axial Acceleration vs Time at Location H for the Uranium-Steel Cask End-On Two-Dimensional Impact Calculation 58
4.2.27 Axial Velocity vs Time at Location H for the Uranium-Steel Cask End-On Two-Dimensional Impact Calculation 58
4.2.28 Axial Displacement vs Time at Location H for the Uranium-Steel Cask End-On Two-Dimensional Impact Calculation 59
4.2.29 Schematic of the Lumped Parameter Model 59
4.2.30 Force Input to the Front End of the Cask vs Time for the Uranium-Steel Cask End-On One-Dimensional Impact Calculation 60
4.2.31 Displacement of the Bottom End of the Cask (Location G) vs Time for the Uranium-Steel Cask End-On One-Dimensional Impact Calculation 60
4.2.32 Velocity of the Bottom End of the Cask (Location G) vs Time for the Uranium-Steel Cask End-On One-Dimensional Impact Calculation 60
4.2.33 Acceleration of the Bottom End of the Cask (Location G) vs Time for the Uranium-Steel Cask End-On One-Dimensional Impact Calculation 60

Illustrations (cont)

Figure

4.2.34 Displacement of the Top End of the Cask (Location H) vs Time for the Uranium-Steel Cask End-On One-Dimensional Impact Calculation 61

4.2.35 Velocity of the Top End of the Cask (Location H) vs Time for the Uranium-Steel Cask End-On One-Dimensional Impact Calculation 61

4.2.36 Acceleration of the Top End of the Cask (Location H) vs Time for the Uranium-Steel Cask End-On One-Dimensional Impact Calculation 61

4.2.37 Axial Stress at Location C vs Time for the Uranium-Steel Cask End-On One-Dimensional Impact Calculation 62

4.2.38 Axial Stress at Location D vs Time for the Uranium-Steel Cask End-On One-Dimensional Impact Calculation 62

4.2.39 Radial Stress at Location E vs Time for the Uranium-Steel Cask End-On One-Dimensional Impact Calculation 62

4.2.40 Tangential Stress at Location E vs Time for the Uranium-Steel Cask End-On One-Dimensional Impact Calculation 62

4.2.41 Tangential and Radial Stress at Location F vs Time for the Uranium-Steel Cask End-On One-Dimensional Impact Calculation 63

4.2.42 Tangential and Radial Stress at Location A vs Time for the Uranium-Steel Cask End-On One-Dimensional Impact Calculation 63

4.2.43 Radial Stress at Location B vs Time for the Uranium-Steel Cask End-On One-Dimensional Impact Calculation 63

4.2.44 Tangential Stress at Location B vs Time for the Uranium-Steel Cask End-On One-Dimensional Impact Calculation 63

Tables

2.1 Lead-Steel-Balsa Cask Model Data 22

2.2 Uranium-Steel Cask Model Data 23

2.3 Size Data for Truck Spent-Fuel Shipping Casks 24

2.4 Size Data for Rail Spent-Fuel Shipping Casks 25

2.5 Construction Material Data for Truck Spent-Fuel Shipping Cask 26

2.6 Construction Material Data for Rail Spent-Fuel Shipping Cask 26

4.1 Kinematic Comparison of Dynamic Analyses, End-On Impact of Lead-Steel-Balsa Cask 47

4.2 Stress Components Comparison, End-On Impact of Lead-Steel-Balsa Cask 48

4.3 Kinematic Comparison of Dynamic Analyses, End-On Impact of Uranium-Steel Cask 66

4.4 Stress Component Comparison, End-On Impact of Uranium-Steel Cask 67

A Comparison of Analytical Techniques for Analyzing a Nuclear-Spent-Fuel Shipping Cask Subjected to an End-On Impact

1.0 Introduction

1.1 Scope of Study

The objective of this study is to describe analytical techniques which can be used to assess the response of a nuclear shipping cask to a free fall of 30 ft onto an unyielding surface. Analyses have been performed by several methods of differing sophistication, as discussed below. For one-dimensional calculations, an equivalent static approach using a strength-of-materials method and a dynamic analysis using a lumped-parameter model[1] are described. The two- and three-dimensional calculations rely on static and dynamic finite element analysis techniques. In order to compare the various analytical techniques, the designs of existing casks were studied and are described in the report. Based on a survey of actual cask configurations, two hypothetical casks were designed, with all the pertinent structural features of the actual casks retained. One of the two hypothetical casks is a lead-steel-balsa design. The lead is used as the primary radiation shielding material, the balsa wood as an impact limiting material, and the steel as the main structural material. In the second cask, uranium is used as the radiation shielding material, steel fins as an impact limiting device, and steel as the main structural material.

Properties of the various materials used in the calculations are discussed and presented in forms useful for analysis purposes.

In order to compare the analytical techniques, one design condition of a 30-ft drop and end-on axial impact of the casks is used. In these analyses, it is assumed that the casks impact the unyielding surface in a perfectly normal orientation. One-, two-, and where needed, three-dimensional analyses were performed. The results are then compared in terms of kinematic quantities and stress levels at different points on the casks. This report can serve as a guide in selecting analysis techniques capable of producing adequate but economical evaluations of shipping casks.

1.2 Types of Analysis

The method of finite elements has greatly enhanced the ability of the structural analyst to calculate stress, strain, and displacement histories at given points in a structure. The analyst need not restrict himself with as many assumptions as with strength-of-materials methods in order to obtain the value of a parameter at a point. However, though the method is very powerful, it does not relieve the analyst of the responsibility of understanding structural mechanics. To obtain valid answers, the analyst must have enough mechanics insight to realize where accurate results are needed before proceeding to calculate numbers.

Traditionally, strength-of-materials methods have been used for design of structures which are then experimentally tested. In the technology of the present day, basic engineering methods, i.e., use of strength-of-materials formulas and experimental tests, have their place in the safety assessment of a nuclear fuel cask. However, over the past 10 years, the finite element method has been used increasingly for design and safety analyses of structures. This technique will be discussed to some extent.

In two dimensions, and with elastic material properties, the finite element method is inexpensive and can be very accurate if the analyst performs his

task well. In safety analyses, where large displacements occur and nonlinear material properties must be taken into account, a two-dimensional solution to a problem which accurately calculates the needed answers can be very expensive. This is especially true for a static solution. Although the technique is powerful, considerable engineering judgment is needed to accurately model the structure and the material properties, to define the loads, and to interpret the results.

Finite element computer programs have been written which are capable of solving three-dimensional, large displacement, materially nonlinear, static or dynamic problems. However, except possibly for linear static problems, three-dimensional analyses are extremely expensive. A three-dimensional solution is rarely used for design purposes and should be used in safety analyses only when a two-dimensional idealization of a three-dimensional problem will not suffice. The solution to transient dynamic problems, while still expensive, can be obtained economically for simple structures such as a cask fin. However, for three-dimensional, nonlinear static problems solutions are extremely expensive, and quite often the capability of the computer programs will not allow an accurate solution even if the cost could be justified.

In this report, two-dimensional static and dynamic finite element techniques are demonstrated for use in an end-on impact calculation of shipping casks. A three-dimensional dynamic calculation of an impact limiter steel fin is also included. A one-dimensional lumped parameter technique is also examined for its usefulness in analyzing an end-on impact. These computer techniques, as well as some of the more traditional methods, will be described in detail.

1.2.1 One-Dimensional Analysis Procedures

1.2.1.1 Constant Acceleration Method Analysis

The elementary techniques used to perform the stress analysis for both the lead-steel-balsa cask and the uranium-steel cask are discussed in this section. The approach used is to analyze the cask impact problem by applying the most simple, direct means available to estimate the stresses in the cask. The intent of this simple analysis is to simulate the most elementary analyses that have appeared in the spent-fuel-shipping-cask safety analysis reports (see Section 2.5) so that comparisons can be made with the other techniques used in this report.

The basic approach used is to analyze the cask impact as an equivalent static problem. This is accomplished by applying D'Alembert's Principle, which states that the laws of static equilibrium apply to the dynamical cask problem if the inertial forces due to cask deceleration during impact are applied as forces acting on the cask. The strength-of-materials method is then employed as the basis for the analysis technique to calculate the stresses in the cask. To apply the method, the portion of the cask to be analyzed is isolated from the remainder of the cask by passing imaginary planes or surfaces through the cask. The isolated section or free body is then analyzed by considering all the external forces that originally act upon it plus the forces that act at the cutting planes. The free body is generally chosen so that the stresses may be calculated with known formulas for stress and strain.[12] In this case, the forces that act at a cutting plane are replaced with an assumed boundary condition. For example, the end of a typical cask might be analyzed as a circular plate with fixed boundaries and a uniform inertial force acting on it.

The fundamental objective of the elementary cask analysis is to produce a conservative stress analysis while retaining a representative model of the structural behavior of the cask. Unfortunately, the degree of conservatism in a particular analysis can only be evaluated with a more detailed structural analysis and/or an experimental study of the problem. The conservatism of an analysis is a function of the modeling assumptions used in setting up the analytical model of the free body. Assumptions regarding the external loads generally tend toward increasing the load or increasing its effect on the structure. The structural modeling assumptions in general are made to create a model that is more flexible than the real structure. Another form of assumption is made when a load or portion of the structure is ignored in the analysis. In this case, the assumption may be either conservative or nonconservative, but is justified only if the effect upon the analysis results is very small.

In the remainder of this section, the simple analyses performed for the vertical impact of the two casks are discussed. Also, some discussion of the side and corner impacts is included. It should be emphasized that the use of a particular analysis procedure is not necessarily an endorsement of its use for performing a stress analysis of a cask. In fact, more precise analysis techniques, for example, the finite element method, are available to the structural analyst and are recommended.

The simple analysis approach is applied to the spent-fuel shipping cask by dividing the analysis into two parts. First, the deceleration force on the cask

body is determined by evaluating the impact limiter performance. The balsa wood impact limiter is analyzed with the strength-of-materials approach. However, the plastic deformation of the fin impact limiter is too complex to be analyzed with these simple techniques. Thus, the deceleration load for the fin impact must be obtained by other means, such as experiment or finite element analysis. In this report, the deceleration force for the uranium-steel cask vertical impact is estimated by using a two-dimensional finite element analysis (see Section 4.2.1.2). The second phase of the cask impact analysis concerns the calculation of stresses in the cask body which result from the impact deceleration load determined in the first phase of the analysis. For the present analysis of the vertical impact, the calculations are directed toward estimating the stresses in the end plates and the side walls of the cask.

The deceleration analysis of the balsa wood impact limiter is now discussed. The balsa wood impact limiter on the lead-steel-balsa cask is a cylindrical cap structure encased in a thin shell of steel (see Section 2.1). During the vertical impact, the end section of the impact limiter absorbs the energy of impact (Figure 1.2.1). The balsa wood is assumed to crush uniaxially at a constant crush stress. Then, the constant deceleration force, F, is given by

$$F = \sigma_c A$$

where σ_c is the crush stress and A is the cross-sectional or footprint area of the impact limiter. The deceleration, d, is expressed in g's by applying Newton's second law of motion,

$$F = ma = \frac{W}{g}a = Wd = \sigma_c A$$

or

$$d = \frac{\sigma_c A}{W} ,$$

where:

m = the mass of the cask
a = the acceleration, L/S^2
g = the gravitational constant
W = the cask weight = mg
d = the cask deceleration = (a/g), g's .

The crush, h, of the balsa impact limiter is calculated with an energy formulation. The energy, E, absorbed by the balsa wood crush is given by

$$E = Fh = \sigma_c Ah = \sigma_c V ,$$

where V is the crush volume. The impact energy is equal to the potential energy of the cask at a height, H, of 30 ft and is expressed as

$$E = WH .$$

Since the impact energy is equal to the energy absorbed, the latter two energy expressions yield the formula for the crush height,

$$h = \frac{WH}{\sigma_c A} .$$

Also note that the cask deceleration for vertical impact may conveniently be calculated from

$$d = \frac{\sigma_c A}{W} = \frac{H}{h} .$$

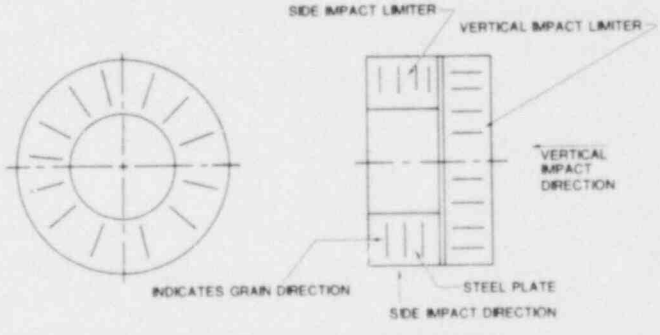

Figure 1.2.1 Balsa Wood Impact Limiter Schematic

The deceleration force in the vertical impact of the balsa wood impact limiter is a constant because both the crush stress, σ_c, and the crush area, A, are assumed to be constant. The analysis is conservative in that the deceleration force may be made larger than the actual average deceleration force by choosing σ_c judiciously. The assumption of a constant deceleration force is not correct, since it is well known that the deceleration associated with an impact exhibits an initial peak and a definite time dependence. However, the significance of this with respect to a cask impact is questionable and can only be resolved with further research. In any case, the static methods of analysis used in this portion of the report and a time-dependent load are not compatible.

The present analysis of the balsa wood impact limiter ignores the energy absorbing capacity of the shell encasement. This is primarily because a credible analysis of the plastic deformation of the shell is not within the scope of a strength-of-materials analysis. However, it is presumed that the shell would absorb a

negligible amount of energy. Even if the energy absorbed by the shell is small, it should be noted that the neglecting of the shell is a nonconservative assumption with respect to calculation of the deceleration force. The energy absorbed by the shell causes the cask to stop in a shorter distance than predicted by the above analysis and, consequently, produces a larger deceleration force than is calculated above.

Both increased temperature and water content of the balsa wood can degrade its energy absorbing characterisitics, and both have been neglected in the above analysis. Since spent-fuel shipping casks are normally operated at a few hundred degrees Fahrenheit, temperature effects should be addressed in the analysis of an actual cask. The effect of water on the balsa wood is generally neglected since the problem can be alleviated by ensuring that the shell encasement is watertight.

The side-impact analysis of the balsa wood impact limiter is very similar to the vertical-impact analysis with respect to both method and limitations. The impact limiters on each end of the cask are identical and are assumed to dissipate equal amounts of impact energy. In side-drop, the balsa wood impact ring (Figure 1.2.2) is assumed to be the sole energy absorbing structure. For the end-on orientation, the impact limiter and the circular steel plate are neglected since they would be expected to shear off during impact.

For the side drop, the impact limiter is assumed to crush as indicated in Figure 1.2.2, which shows an end view of the balsa wood ring. The assumed crush sequence will now be described. The deceleration force increases as the outer rim of the ring (as indicated by Area I) crushes. When the deceleration force at the rim equals the upward force on the cask, the cask will start to crush through the balsa ring (as represented by Area II) with no increase in the deceleration force. Thus, the maximum effective crush area, A_e, for side impact is

$$A_e = 4r_i\ell \ ,$$

where r_i is the cask radius at the impact limiter and ℓ is the length of one side-drop-impact-limiter ring. If the radial grain direction of the balsa wood is neglected, then the deceleration force is conservatively calculated as

$$F = \sigma_c A_e = 4\sigma_c r_i \ell \ ,$$

and the decleration in g's is

$$d = \frac{F}{W} = \frac{4\sigma_c r_i \ell}{W} \ .$$

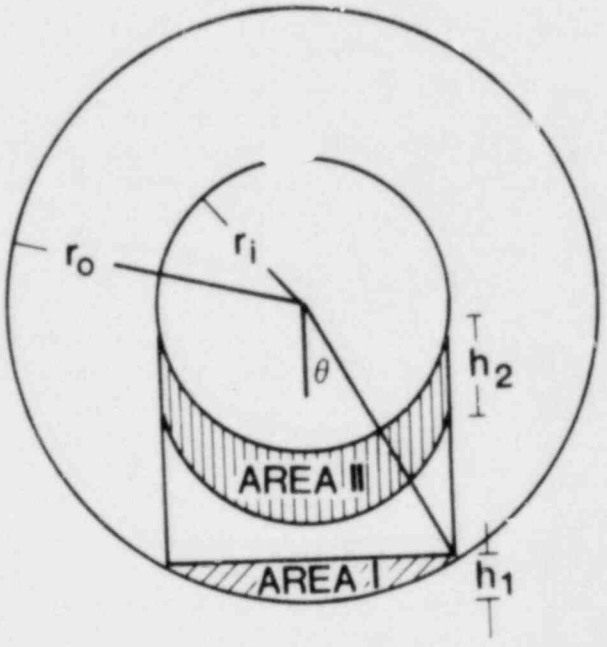

Figure 1.2.2. Side-Impact End View

Again, the corner-impact analysis of the balsa wood impact limiter is similar to the previous two analyses of the vertical- and side-impact orientations, and similar limitations apply. The corner-impact orientation (Figure 1.2.3) is defined by assuming the cask center of gravity is directly over the corner of the impact limiter during the impact sequence. The inclination angle, α, is defined by

$$\tan\alpha = \frac{2r_o}{L} \ ,$$

where L is the overall length of the cask with impact limiters attached and r_o is the radius of the impact limiter.

As with the previous analyses, the energy absorbed by the balsa wood impact limiter is assumed to be equal to the crush volume times the crush stress. For the corner impact, the crush volume is a complex function of the impact limiter parameters. Referring to Figure 1.2.3, the impact limiter footprint area is a portion of an ellipse for crush up to line a-a, and is an ellipse for crush up to line b-b. The energy absorbed by the impact limiter when deforming up to line a-a is expressed by the relationship,

$$\bar{E} = \frac{WH}{\sigma_c \pi r_o^3 \tan\alpha}$$

$$= \frac{1}{\pi}\left(\frac{2}{3}\sin^3\psi + \cos^2\psi\sin\psi - \psi\cos\psi\right) \ ,$$

where WH is the impact energy of the cask and $\bar{E}$ is an energy parameter. The cask deceleration, d, in g's is defined by the expression

$$\frac{dW \cos \alpha}{\sigma_c \pi r_o^2} = \frac{1}{\pi}(\psi - \tfrac{1}{2} \sin 2\psi) ,$$

where ψ is a convenient parameter defined by the equation

$$\cos \psi = 1 - \frac{h}{r_o \tan \alpha} , \quad 0 \leq 4 \leq 180$$

in which h is the crush depth measured parallel to the cask axis along the side being crushed and has the values defined by the height parameter, $\bar{h}$,

$$0 \leq \bar{h} = \frac{h}{2r_o \tan \alpha} \leq 1.0 .$$

Nondimensional plots produced from the above relationships are shown in Figures 1.2.4 and 1.2.5. These plots may be used to estimate the deceleration for crush up to line a-a in Figure 1.2.3 or when $\bar{h} = 1.0$. The above relationships can be used to solve for the cask deceleration, but numerical techniques or a trial-and-error solution must be used. If the energy parameter, $\bar{E} \geq 1.0$, then the cask deceleration is given by

$$d = \frac{\sigma_c \pi r_o^2}{W \cos \alpha} ,$$

and the balsa crush height will proceed beyond line a-a to some level represented by line b-b (Figure 1.2.3). For this case, the crush height, h', above line a-a is given by

$$h' = r_o \tan \alpha + \frac{WH}{\sigma_o \pi r_o^2} .$$

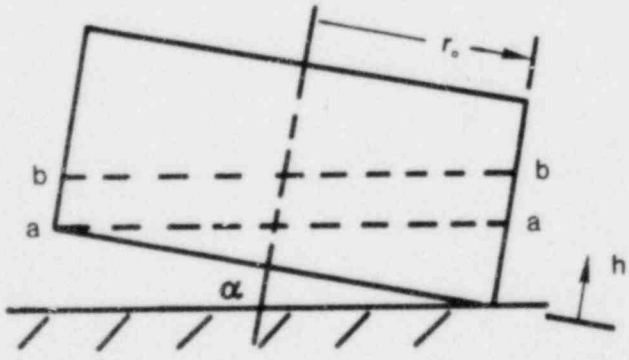

Figure 1.2.3. Corner-Impact Schematic

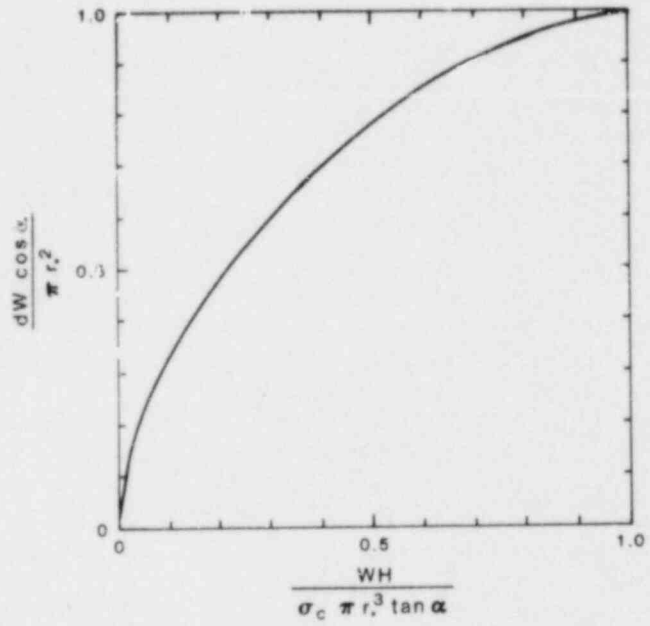

Figure 1.2.4. Corner-Impact Parameter Plot No. 1

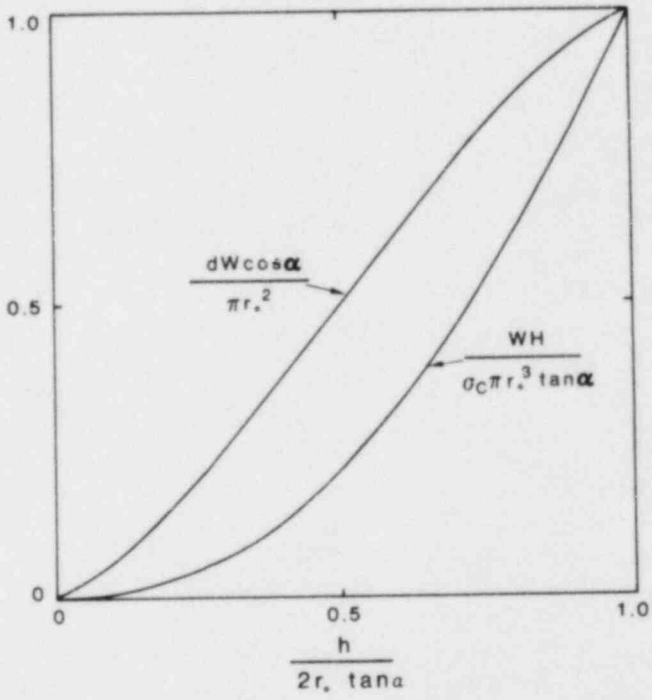

Figure 1.2.5. Corner-Impact Parameter Plot No. 2

Note that the present balsa wood impact limiter analysis is nonconservative from an impact limiter design viewpoint. The assumptions made to produce conservative deceleration force results will produce nonconservative crush depth results because of their inverse relationship. The crush depth is obviously an important design parameter for an impact limiter

since it is needed to adequately size the impact limiter to prevent bottoming out during impact. A conservative analysis with respect to the crush depth calculations can be attained by considering the effects of balsa wood grain direction, which are particularly significant in the side-and corner-drop orientation. Neglecting the energy absorbed by the shell encasement is also a conservative assumption in the design of an impact limiter.

The second phase of the elementary stress analysis for both the lead-steel-balsa cask and the uranium-steel cask will now be discussed. The methods used to calculate the vertical impact stresses in the side walls and the end plates of the cask are described in general terms; the analysis details are reserved for Section 4. A few remarks pertaining to the side and corner impacts appear at the end of this discussion.

Since the method of analysis used in this section is restricted to statics, D'Alembert's Principle is applied to define the impact load on the cask body. The cask body, as a structure, supports the inertial impact force due to its own weight. Thus, two impact loads must be considered in the analysis of any free-body section of the cask: one is the body force associated with the weight of the free body; the other is any external load on the free body which may result from a portion of the cask supported structurally by the free-body structure. For example, the side walls taken as a free body would have an external load resulting from the top end plate weight and the top impact limiter weight. Both of these impact loads are considered in the analyses discussed below.

The inertial body force for a free body is simply calculated as the body weight multiplied by the deceleration (in g's) as determined in the impact limiter analysis. Since the impact load is a constant, the weight times the average deceleration of the cask, the stress values obtained with this static analysis can at best be only a measure of the average stress in the cask body.

The stresses in the cask side walls are calculated by assuming that a uniaxial state of stress exists. Then, in simplest terms, the compressive axial stress is calculated on the axial inertial force in the wall divided by the cross-sectional area of the cask walls. The calculation is complicated slightly by the layered construction of the cask walls, which consist of a layer of radiation shielding material sandwiched between layers of stainless steel. In the case of the lead-steel-balsa cask, the compressive wall stress is calculated by neglecting the lead as a structure. That is, the cross-sectional area is calculated only from the steel wall layers. A separate calculation for the lead stress is performed by considering only the axial load due to the lead weight and the cross-sectional area of the lead. For the uranium-steel cask, the steel layers and the uranium layer are treated as parallel elastic systems. By assuming the uranium and steel layers must have the same axial deflection, the portion of the total axial load carried by each layer is calculated.

The cask wall analysis is limited in several ways. Again, the severity of the limitations can only be judged by a more detailed study. Bonding between the cask wall layers is neglected since the wall layers are essentially treated as independent structurally or as parallel structures. By assuming a uniaxial state of stress, the hoop stresses associated with an internal cavity pressure, water hammer effects, and lead slump are neglected. Also, the wall bending stresses associated with the moment load due to end plate deflection are neglected.

The end plates for both types of casks are analyzed alike. Stress formulas from Reference 1.2 for linear elastic thin circular plates are used for the end plate analysis. The cask end plate is modeled as shown in Figure 1.2.6. The end plate model has a diameter equal to the inside diameter of the cask. As indicated in Figure 1.2.6, the end plate is modeled as three separate circular plates that are required to have equal center axial displacements. The steel layers are assumed to have a fixed boundary condition because the steel layers are integrally attached to the walls. The hinged, or simple, support boundary for the shield layer is chosen to represent no bonding to the cask wall.

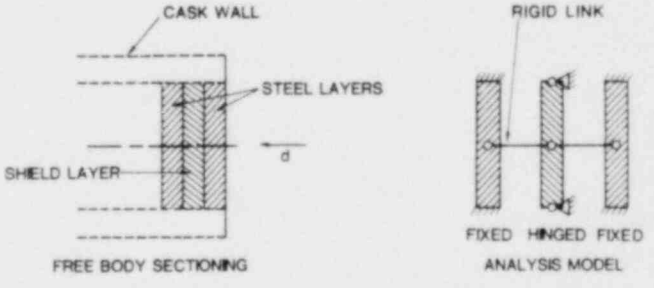

Figure 1.2.6. Strength-of-Materials Modeling of Cask End Plates

The composite structure consisting of the three layers is assumed to support the total inertial load. The compatibility condition, that the center deflections of all the plate layers are equal, is used to determine the portion of the total end plate load that is carried by each plate layer. Once the load on each plate layer is found, the stresses may be determined according to thin plate theory for each layer. For all of these plate calculations, the inertial load is applied as a uniform load over the circular plates. In addition

to the inertial load resulting from the end plate weight, the inertial load due to the impact limiters and cask contents are considered where appropriate. These additional loads are also applied as uniform distributed loads.

The stresses determined for the center of the stainless steel plate layers should be conservative since the analysis model is more flexible than the actual end plate. Steel plate layer stresses are also calculated for a location near the boundary. Since there may be a complex state of stress in the vicinity of the end plate and cask wall interface, it is not possible to judge from the present analysis whether the edge stresses calculated are conservative or nonconservative.

The end plate analysis is limited since bonding between the end plate layers is neglected. Also, interaction between the end plate and the cask wall is not considered with the strength-of-materials solution.

For the side-impact orientation, the cask body can be analyzed with beam bending theory. In this case, the cask body is modeled as a simply supported beam subjected to a uniform load that is equivalent to the inertial force of the cask weight. Since the cask cross section consists of layers of two materials, the analysis can be made conservative and performed more simply by neglecting the structural behavior of the shield material. Also, the thin shell surrounding the water gamma radiation shield may be neglected for like reasons.

The strength-of-materials analysis of the corner-drop orientation can be handled by resolving the corner deceleration into two component decelerations--one parallel to the cask axis and the other transverse to the cask. The effect of the axial component of deceleration is then analyzed like the end-on impact. The effect of the transverse component may be neglected, since the impact angle is small and the transverse component is generally small in comparison to the side-impact deceleration.

1.2.1.2 Dynamic Analysis

In this analysis the cask and impact limiter are discretized into a number of masses and springs or couplings (a lumped parameter model). The mass and coupling definitions are calculated by hand and then input into a computer program which solves the system of equations for a given impact condition and provides the response of the system. In this study, the SHOCK[11] computer program was used. The information obtained includes time resolved displacements, velocities, and accelerations for the various masses as well as the forces in the couplings. This information must then be interpreted in terms of stresses in the cask structure. The example discussed below explains the technique in some detail.

Figure 1.2.7 illustrates a cask structure and a possible lumped parameter model. Not shown but included in the model are balsa wood impact limiters which are attached to the ends of the cask. In the schematic illustration of the discretized structure, masses 2-11 correspond to the cask structure and impact limiters. The impact limiter masses, which are relatively small, are lumped into the end mass elements, numbers 2 and 11. The fuel elements are simulated with mass element number 12 and the water shield with number 13.

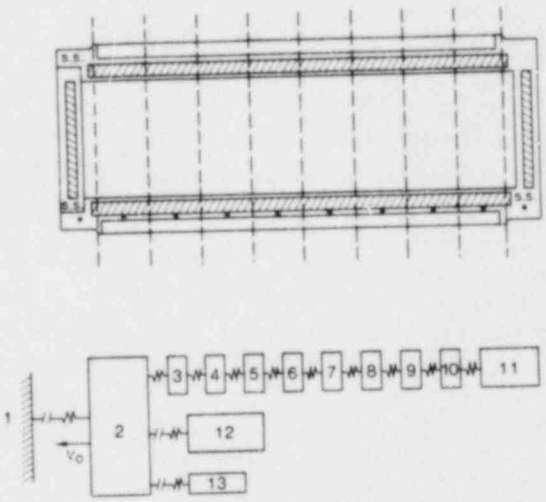

Figure 1.2.7. Illustration of a One-Dimensional Lumped Parameter Model for a Shipping Cask

On the impact end, the force-deflection characteristic of the impact limiter is dominant. The stiffness of the cask mass element is much higher and can be neglected. Therefore, only the characteristic of the impact limiter is used to define coupling 1-2. This coupling definition will be discussed in more detail later.

The rest of the couplings are linear springs. Couplings 2-12 and 2-13 represent the interactions between the fuel elements and water shield and the cask structure. They are allowed to load only in compression. The spring values for the structure are computed by simply using

$$K = \frac{AE}{\ell},$$

where

A = cross-sectional area
E = material modulus
ℓ = distance between mass centers.

Spring constants between mass element centers must be computed considering the different materials and whether they are loaded in series or in parallel. That is, effective constants must be calculated. The values for the spring constants which connect the fuel and water shield to the cask structure are estimated using material properties for the fuel and the bulk modulus of water. The same basic relationship described above is used.

The coupling defining the force-deflection characteristic for the impact limiter is described by using a piecewise linear curve with provisions for different loading and unloading paths, allowing for energy absorption. Figure 1.2.8 illustrates the type of curve that would be used for a balsa wood impact limiter. This deflection characteristic exhibits a constant crush force up to a "bottoming" condition. For plate type impact limiters the crush portion of the curve could be given a negative slope to better represent the behavior of this type of structure. The curve could also be defined with a larger number of straight line segments. Unloading past the initial yield point follows a different path (Figure 1.2.8) allowing energy absorption and simulating a crush behavior.

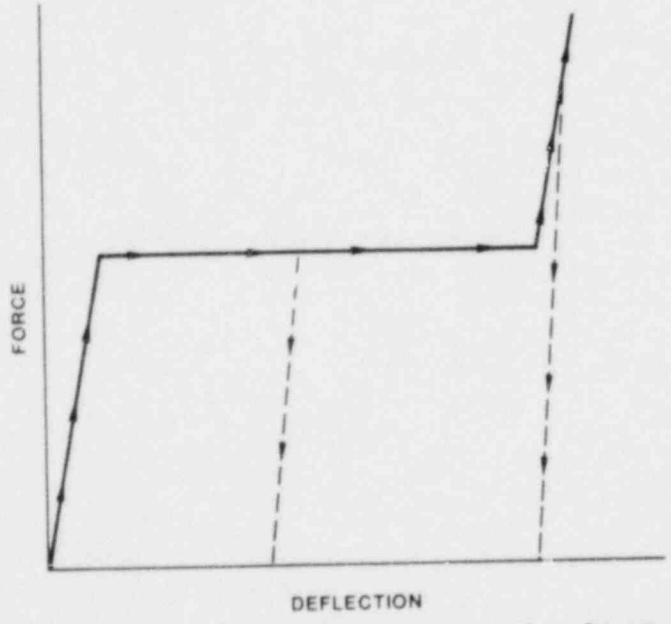

Figure 1.2.8. Illustration of a Load-Deflection Curve for an Impact Limiter

The values of the mass elements are calculated in a straightforward manner, simply by using the material densities and volumes of the descretized structure. To simulate an impact condition, all the mass elements are given an equivalent initial velocity into a fixed mass (Figure 1.2.7).

Axial stresses in the cask walls can be calculated from the computed forces in the couplings or more directly from the computed relative displacements between mass elements, which can be converted to strain and stress. Stresses in the cask ends can be computed by using an elastic plate equation.[12] Simply supported end conditions can be conservatively assumed. The loading to the plate can be obtained from the loading in the adjacent coupling or the acceleration time plot for the mass element corresponding to the plate surface. If the computed acceleration (g level) is used, then this must be multiplied by the plate weight to obtain the proper loading. Section 4 includes cask analyses made utilizing this technique.

1.2.2 Multidimensional Analyses Procedures

The two- and three-dimensional analyses presented here are dynamic and static techniques based upon the finite element method.[13] The finite element method is similar to the classical Rayleigh-Ritz procedure. The unknowns, usually displacements of a body, are described by a set of functions which contain some undetermined coefficients. Substitution of the functions into the first variation of a functional, which is set equal to zero, results in a set of equations that have the coefficients as the unknowns. First, using a two-dimensional problem as an example, the body is divided into quadrilateral or triangular regions called elements. Within each element a class of interpolating functions is selected to describe the displacements. The functions contain, as variables, the values of the displacements at discrete points (the corners of the quadrilaterals) called nodes. An example of a finite element mesh is shown in Figure 1.2.9.

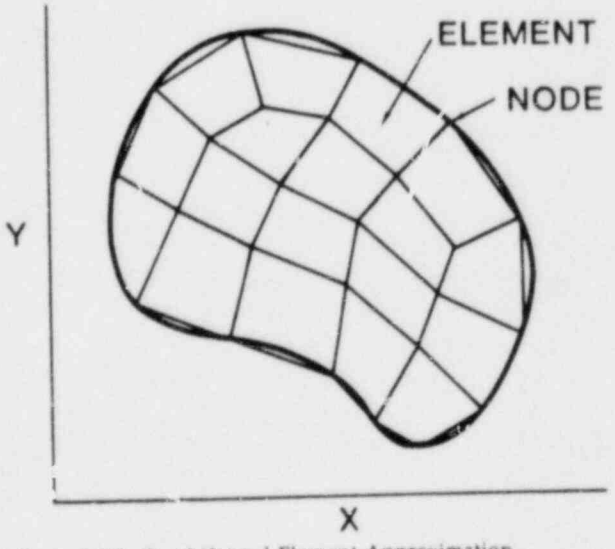

Figure 1.2.9. Quadrilateral Element Approximation

For two- or three-dimensional static solutions the computer code ADINA[14] is used for the analyses in this report. ADINA is a general purpose code capable of solving large problems in two or three dimensions. The structural systems that can be analyzed using ADINA can be composed of combinations of a number of different finite elements. The program presently contains the following element types:

(a) Three-dimensional truss element
(b) Two-dimensional plane stress and plane strain element
(c) Three-dimensional plane stress element
(d) Two-dimensional axisymmetric shell or solid element
(e) Three-dimensional solid and thick shell elements
(f) Three-dimensional beam element
(g) Thin shell element
(h) Two- and three-dimensional fluid elements

The nonlinearities may be due to large displacements, large strains, and nonlinear material behavior. The material descriptions presently available are:

For the truss elements:

(a) Linear elastic
(b) Nonlinear elastic
(c) Thermo-elastic
(d) Elastic-plastic
(e) Thermo-elastic-plastic and creep

For the two-dimensional elements:

(a) Isotropic linear elastic
(b) Orthotropic linear elastic
(c) Isotropic thermo-elastic
(d) Curve description model
(e) Concrete model
(f) Elastic-plastic materials; von Mises and Drucker-Prager yield conditions
(g) Thermo-elastic-plastic-creep, von Mises yield condition
(h) Mooney-Rivlin material

For the three-dimensional elements:

(a) Isotropic linear elastic
(b) Orthotropic linear elastic
(c) Isotropic thermo-elastic
(d) Curve description model
(e) Concrete model
(f) Elastic-plastic materials, von Mises and Drucker-Prager yield conditions
(g) Thermo-elastic-plastic-creep, von Mises yield condition

For the beam element:

(a) Linear elastic
(b) Elastic-plastic, von Mises yield condition

For the shell element:

(a) Linear elastic
(b) Elastic-plastic, von Mises yield condition

For two-dimensional dynamic analyses the HONDO computer code[15,16] was chosen over the ADINA code because it is more efficient for the class of problems to which it applies. HONDO is a finite element method computer program designed to calculate the large deformation elastic- and inelastic transient dynamic response of two-dimensional solids. To accommodate a wide variety of applications, finite strain calculations are incorporated. Spatially the program employs a 4-node isoparametric quadrilateral element. To advance the solution in time, the program performs the integration using a central-difference-method time integrator. Since the time integration scheme is only conditionally stable with respect to step size, the program continuously monitors the step size and adjusts it to maintain stability. The program contains five material subroutines covering elastic, viscoelastic, elastic-plastic, crushable foam, and soil behavior. Initial conditions on velocity but not displacement are allowed. Pressure loadings are allowed. Thermal loads are not implemented. The program functions entirely in the core memory of the computer, and, because no stiffness matrices need be calculated and stored, rather large problems are easily accommodated.

For three-dimensional impact problems the special purpose computer code WULFF[17] is used. A mixed displacement finite element formulation is implemented, in the WULFF set of computer codes, which calculate the large displacement dynamic response of three-dimensional solids. Two constitutive models are available: an elastic-plastic relationship, and a crushable foam and soil model. Loading conditions can be pressure vs time functions or initial velocity conditions.

The complete set of computer programs is designed to generate a three-dimensional finite element mesh, input boundary conditions and material descriptions, solve the problem, and then graphically display the results.

As discussed for the general problem of finite element analysis for large displacement dynamic response in Reference 1.8, it is possible to formulate the problem so all the variables—the stress, velocity, and displacement components—are nodal-point valued

functions. The formulation, a particular alternative described in Reference 1.8, and called the mixed displacement formulation, has the following characteristics.

All quantities are calculated at the nodes of a finite element mesh: mass, volume, acceleration, velocity, displacement, position, stress, and velocity gradient. Stress boundary conditions are treated implicitly using boundary integrals in a variational statement of the equilibrium equations. Fixed boundaries are accommodated by setting the acceleration vector equal to zero. Spatial discretization is accomplished by the use of 8-node three-dimensional trilinear isoparametric elements. Integration of the equations is advanced in time using central difference expressions for acceleration and velocity. Artifical viscosity is used to smooth shock fronts.

The computer programs used in this report are representative of the large number of codes which are available. The designer and/or analyst of shipping casks should have little trouble in acquiring computer codes to use.

1.3 References

1.1 V. K. Gabrielson and R. T. Reese, *SHOCK Case User's Manual - A Computer Code to Solve the Dynamic Response of Lumped Parameter Systems*, Report No. SCL-DR-L9-98 (Livermore, CA: Sandia Laboratories, 1969).

1.2 R. J. Roark, *Formulas for Stress and Strain* (McGraw-Hill Publishing Co., 1965).

1.3 O. C. Zienkiewicz, *The Finite Element Method in Engineering Science* (London: McGraw-Hill Publishing Company Limited, 1971).

1.4 K. J. Bathe, *ADINA, A Finite Element Program for Automatic Dynamic Incremental Nonlinear Analysis*, Report 82448-1 (Cambridge, MA: Massachusetts Institute of Technology, 1978).

1.5 S. W. Key, "A Finite Element Procedure for the Large Deformation Dynamic Response of Axisymmetric Solids," *Computer Methods in Applied Mechanics and Engineering*, 4, 1974, pp 195-218.

1.6 S. W. Key, Z. E. Beisinger, and R. D. Kreig, *HONDO II - A Finite Element Computer Program for the Large Deformation Dynamic Response of Solids*, Report SAND78-0422 (Albuquerque,NM: Sandia Laboratories, 1978).

1.7 J. H. Biffle and M. H. Gubbels, *WULFF -- A Set of Computer Programs for the Large Displacement Dynamic Response of Three-Dimensional Solids*, Report SAND76-0096 (Albuquerque, NM: Sandia Laboratories, 1976).

1.8 J. H. Biffle and S. W. Key, "Finite element Formulations for Large Displacement Transient Dynamic Problems in Solids Using Explicit Time Integration," *Computer Methods in Applied Mechanics and Engineering*, 12, 1977, pp 323-336.

2.0 Description and Design of Casks

2.1 Cask Model Design Overview

The design of the cask analysis models used in this study is based upon the results of a survey of the structural characteristics of the present generation of LWR-spent-fuel shipping casks. These are the casks licensed in this country since 1970 or those expected to be licensed in the future. The details of the two cask analysis models used for this study, the lead-steel-balsa cask and the uranium-steel cask, are given in Sections 2.2 and 2.3. The results of the cask survey are presented in Section 2.4.

The LWR-spent-fuel shipping casks are manufactured in two size classes according to their primary mode of transportation, which is either truck or rail. The legal-weight truck casks are characterized by a payload of less than two PWR or three BWR fuel assemblies weighing about 50 000 lb. The rail casks have a maximum payload of either 12 PWR or 32 BWR fuel assemblies, weighing between 135 000 and 225 000 lbs.

The present generation of spent-fuel shipping casks is a large cylindrical vessel with an impact limiter system provided at each end to reduce the effects of collision accidents. The impact limiters are designed to attenuate the impact force for all orientations of the cask against a flat, unyielding surface.[2.1] The most used system is a balsa-wood-filled cap structure or (a "soft" system).

The main cask body is designed specifically with containment and shielding of the fuel in mind. The cask is closed with a massive bolt-down lid. In some cases, double containment is accomplished with double side walls and two bolt-on lids. For most cask systems, the inner cavity is designed to accept either BWR or PWR fuel assemblies by interchanging fuel support baskets. A few casks have been designed to accept only one type of fuel assembly. Typicaily, the cask walls are made with two layers of radiation shielding material (one for gamma radiation and the other for neutron radiation), each sandwiched between stainless steel shells. The inner shell is the fuel cavity wall. The first shield layer that surrounds the fuel cavity is the gamma shield and is usually made from chemical-grade lead or depleted uranium. The second layer is the neutron radiation shield and is usually a borated water-ethylene glycol jacket surrounding the cask. A few casks use an alternate neutron shield of specially prepared polyester resin compound. The bolt-on lid and the bottom end of the cask are generally of a solid stainless steel construction or a gamma shield sandwich construction, since the radiation dose rate emitted from the ends of the fuel assembly is less than that emitted from the sides.

The large quantitites of decay heat (10 to 35 kW for a truck cask, for example) generated by the fuel assemblies is important in the design of the spent-fuel shipping cask. The present generation of casks depends primarily on passive heat transfer through the cask walls to dissipate the decay heat and to protect the cask during a fire accident. Cooling fins have been provided on some casks to increase their surface area. Auxiliary cooling systems are provided for some casks to facilitate handling during loading and unloading operations.

The cask analysis models used in this study are typical of the size used for railroad transport. The larger models were chosen primarily because the impact forces associated with the larger casks are expected to be more severe than the impact forces associated with the smaller, truck-size casks. However, results for the smaller casks may be inferred from the results of this study.

The cask models analyzed were sized to be representative of two classes of railroad casks. The lead-steel-balsa cask is constructed primarily from steel with lead being used for gamma radiation shielding. It has a balsa-wood-cap impact limiter system. The uranium-steel cask uses depleted uranium as the gamma shield material and steel as the containment structure. Steel fin structures are used for the impact limiter system. The neutron shield for each cask is borated water.

The cask models are not true spent-fuel shipping casks in that several cask design considerations were not addressed in their development. Heat transfer, radiation shielding, cask closure, and fuel support structures are some of the major design factors neglected in the analysis model development. The sizing of the steel containment and structural layers was

checked only to ensure that the model was structurally similar to a real spent-fuel cask. That is, no attempt was made to obtain an optimal design of the cask structure. Similarly, the cask impact limiter systems were sized to stop the cask without bottoming out and do not necessarily represent an optimal design for the particular cask structure.

2.2 Lead-Steel-Balsa Cask Model

The lead-steel-balsa cask analysis model is a 194 000 lb railroad cask. The cask body containment structure is primarily 304 stainless steel. Lead and water are used for radiation shielding. The impact limiter system consists of a balsa wood cap structure attached to each end of the cask. The essential data pertaining to the lead-steel-balsa cask are summarized in Table 2.1. The cask model is illustrated in Figure 2.2.1.

Table 2.1 Lead-Steel-Balsa Cask Model Data

Overall Structure	
Geometry	Circular Cylinder
Cask Body	77.75 in. OD x 200 in.
Overall	120 in. OD x 268 in.
Cavity	48 in. ID x 180 in.
Weight Empty	164 000 lbs
Weight Loaded	194 000 lbs
Wall Layers (inside out)	1 in. 304 ss
	6 in. Lead
	2 in. 304 ss
	5 in. Water
	¾ in. 304 ss
End Layers	3 in. 304 ss
	4 in. Lead
	3 in. 304 ss
Impact Limiters	
End-On	Balsa Disc (9 lb/ft)
	120 in. OD x 33 in.
Side-On	Balsa Ring (9 lb/ft)
	120 in. OD x 74 in. ID
	x 15 in. each end

The 120-in.-dia impact limiter cap structures attenuate the impact forces for all impact orientations. The vertical- and corner-drop impact limiter is a 33-in.-thick disc of balsa wood backed with a 1-in.-thick steel plate. The grain direction of the balsa wood disc is oriented parallel to the cask axis. The side-drop impact limiter is a ring of balsa wood composed of arc segments such that the balsa wood grain direction is essentially radial.

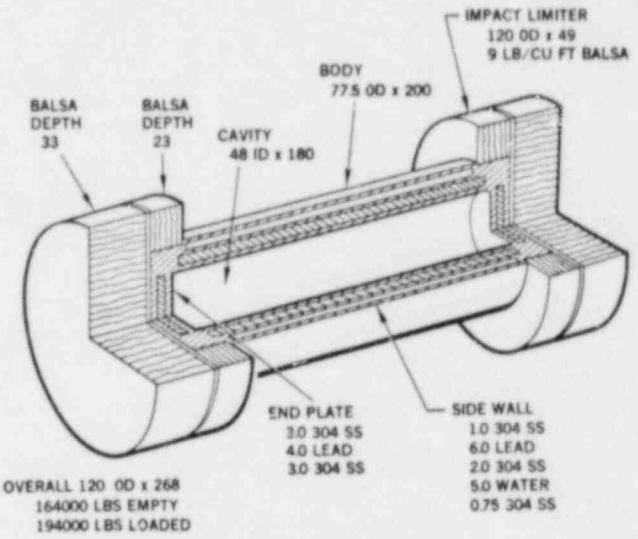

Figure 2.2.1. Lead-Steel-Balsa Cask

The balsa-wood-impact-limiter cap structure is encased with a thin metal shell. The encasement is assumed to be structurally adequate to contain the lateral expansion of the balsa wood but it is nonstructural with respect to impact energy absorption. The circular plate contained in the impact limiter cap is taken to be effective during end impact but is considered nonstructural during a side impact.

The cask body is a composite structure of 304 stainless steel and lead. From inside to outside, the cask walls consist of a steel layer, a lead layer, and two more layers of steel. The inner steel layer is the cavity liner and is the primary containment structure. The two remaining layers of steel serve as containment for the lead gamma shield and the water neutron shield. Toward each end of the cask, the wall is solid steel to provide added strength for tying the wall layers together and for the interface between the wall and the end plates. The end plates are a sandwich of lead contained between two layers of stainless steel.

2.3 Uranium-Steel Cask Model

The uranium-steel cask is a railroad cask having a loaded weight of nearly 120 000 lb. The cask body structure is made from 304 stainless steel with depleted uranium gamma shielding and water neutron shielding. Stainless steel fins make up the impact limiter systems. Cask data are summarized in Table 2.2, and the cask model is illustrated in Figure 2.3.1.

Table 2.2 Uranium-Steel Cask Model Data

Overall Structure

Geometry	
Cask Body	58 in. OD x 200 in.
Overall	66 in. OD x 216 in.
Cavity	36 in. ID x 188 in.
Weight Empty	98 500 lbs
Weight Loaded	119 500 lbs
Wall Layers (inside out)	1.0 in. 304 ss
	4.0 in. Depleted Uranium
	1.0 in. 304 ss
	5.0 in. Water
End Layers	1.5 in. 304 ss
	3.0 in. Depleted Uranium
	1.5 in. 304 ss

Impact Limiters

End-On	32 fins 1.25 in. Thick x 8 in. deep x 14 in. long
Side-On	End fins 1.25 in. thick x 8 in. deep x 16 in. long plus four rings 9 in. deep

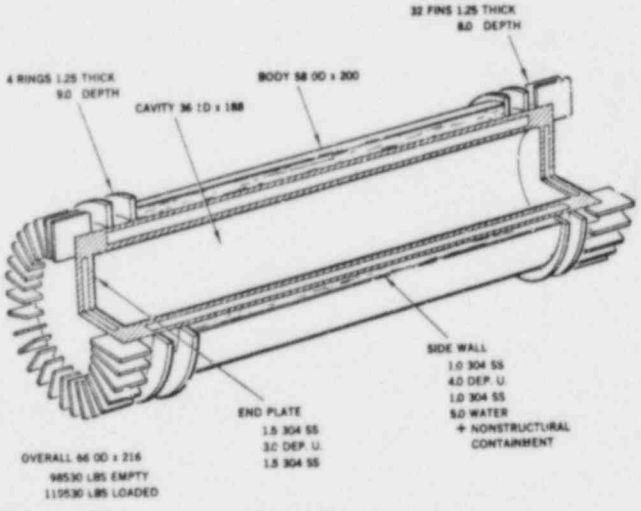

Figure 2.3.1. Uranium-Steel Cask

Impact energy absorption is provided by 1.25-in-thick stainless steel fins. Thirty-two fins (Figure 2.2) are uniformly spaced around the cask circumference at each end and are oriented radially. All of these fins dissipate energy during the end impact, and a few are involved in both the corner drop and the side drop. Additional side-impact protection is provided by two ring limiters placed near the ends of the cask.

The cask wall and end plates are composite structures made of depleted uranium sandwiched between stainless steel. The wall is solid steel near each end to provide added strength for the interface between the walls for neutron shielding. The containment for the water is assumed to be a metal shell which is nonstructural during impact.

2.4 LWR-Spent-Fuel Shipping Cask Structural Survey

2.4.1 Survey Summary

This section presents data from a survey of the structural characteristics of LWR-spent-fuel shipping casks licensed in this country since 1970 or expected to be licensed in the future. The data encompass five truck-size casks (the NFS-4, the NFS-5, the NLI 1/2, the TN-8 and the TN-9), and three railroad-size casks (the IF 300, the NLI 10/24, and the TN-12). Size and capacity data for the truck casks and the rail casks are summarized in Tables 2.3 and 2.4. Construction material layer information for the respective classes of casks is presented in Tables 2.5 and 2.6. The remainder of this section is devoted to brief descriptions of each spent-fuel shipping cask.

2.4.2 NFS-4

The Nuclear Fuel Services, Inc., spent-fuel shipping cask Model Number NFS-4[2.2-2.6] was the first cask licensed and fabricated to handle the larger physical sizes and higher burnups associated with the second generation nuclear reactors. It was licensed in 1972 for a design capacity of 1 PWR or 2 BWR fuel assemblies. The NFS-4 cask, designed primarily as a legal weight truck cask, but which may be shipped by rail, is a relatively small and simple cask used to satisfy Nuclear Fuel Services' early shipping schedule. The purpose was to provide lead time for the design and license of the NFS-5 cask. Six NFS-4 casks have been placed in operation and well over 200 shipments have been made with them.

Shielding for the NFS-4 is provided with chemical grade lead and borated water. A solid stainless steel base and bolt-on lid are used in the design, and the cask is sealed with double O-rings.

Balsa wood clad in stainless steel is used at each end of the cask for impact protection. The side and bottom limiters are permanently attached with the bottom limiter serving as a base when the cask is positioned vertically during loading and unloading operations. A removable top end limiter similar in design to the bottom limiter is used to protect the cask head.

Table 2.3 Size Data for Truck Spent-Fuel Shipping Casks

Cask	NFS-4 Nuclear Fuel Services, Inc.	NLI 1/2 N.L. Industries	TN-8 Transnuclear, Inc.	TN-9 Transnuclear, Inc.	NFS-5 Nuclear Fuel Services, Inc
License Date	1970	1973	1975	1975	Not licensed
No. available/ under construction	6/0	3/3	2 (Europe)/2 (USA)	2 (Europe)/2 (USA)	None
Docket No.	71-6696	71-9010	70-1375	70-1375	71-9031
CASK STRUCTURE					
Geometry	Circular Cylinder	Circular Cylinder	Circular Cylinder	Circular Cylinder	Circular Cylinder
Dimensions without impact limiter (in.)	50 OD x 202	40 OD x 193	66.9 OD x 192	66.9 OD x 201	38.3 OD x 180.5
Dimensions with impact limiter (in.)	50 OD x 214	75 OD x 238	80.1 OD x 217	80.1 OD x 227	60.0 OD x 221.5
Weight - Empty (lb)	47,400	--	76,640	76,200	44,080
Weight - Loaded (lb)	50,000	48,000	81,500	80,850	50,000
CAVITY					
Geometry	Circular	Circular	Special,3 Cells	Special,7 Cells	Rectangular
Dimensions (in)	13.5 ID x 178	13.375 ID x 178	Ea 9.1 s.q.x168.5	Ea 5.91 s.q.x178	9.6x18.2x165
Type of Shipment	Wet, Water	Dry, Helium	Dry, Air	Dry, Air	Wet, Water
IMPACT LIMITERS					
End-On Dimensions (in.)	Top-Balsa wood disc (9 lbs/ft) Bottom-Ring structure w/balsa wood fill 43 OD x 12 (top) and 8 (bottom)	Balsa wood disc (10.8 lbs/ft) 33 OD x 16.625 each end	Balsa wood disc 6.24 lbs/ft) 67 OD x 11.5 (top) 67 OD x 13.8 (bottom)	Same as TN-8	Balsa wood disc (15 lbs/ft) 80.75 OD x 20
Side Dimensions (in.)	Ring structure w/top balsa filled 50 OD x 30 ID x 17.25 each end	Balsa wood ring (10.8 lbs/ft) 75 OD x 34.75 ID x 10.44 (bottom) 75 OD x 32.5 ID x 11.75 (top)	Balsa wood ring (6.24 lbs/ft) 79.5 OD x 68.7 ID x 21 each end	Same as TN-9	Balsa wood rings at center & ends (11 lbs/ft) 60 OD x 30.75 ID x 10 (bottom) x 7 (center & top)
CAPACITY					
Fuel Assemblies	1 PWR/2 BWR	1 PWR/2 BWR	3 PWR	7 PWR	2 PWR/3 BWR
Fuel Decay-Min(days)	120	120	150	150	120
Fuel Burnup-Max (MWD/MTU)	40,000	40,000	38,500	36,500	35,000
Decay Heat-Max(kW)	12.4	10.63	35.5	24.5	20

Table 2.4 Size Data for Rail Spent-Fuel Shipping Casks

Cask	IF 300 General Electric Co.	NLI 20/24 N.L. Industries	TN-12 Transnuclear, Inc.
License Data	1973	1976	Future
No. Available/ under construction	4/0	0/4	0/1 (Europe)
Docket No.	--	71-9023	N.A.
CASK STRUCTURE			
Geometry	Circular Cylinder	Circular Cylinder	Circular Cylinder
Dimensions without impact limiters (in.)	N.A.	96 OD x 204	98 OD x 210
Dimensions with impact limiters (in.)	61.75 OD x 200	102 OD x 273	98 OD x 265
Weight - Empty (lb)	--	160,900	183,000
Weight - Loaded (lb)	13,500-145,000	194,000	213,800
CAVITY			
Geometry	Circular	Circular	--
Dimensions (in.)	37.5 ID x 180.25	45 ID x 179.5	183 (length)
Type of Shipment	Wet, Water	Dry, Helium	Dry, Air
IMPACT LIMITERS			
End-On Dimensions (in.)	Stainless Steel Fins 16 ea - 1.125 x 24.5 x 8 (bottom) x 9.5 (top) 16 ea - 1.5 x 15 x 6	Balsa wood annulus (10.8 lb/ft) 102 OD x 84 ID x 42	--
Side-On Dimensions (in.)	Stainless steel fins 16 ea - 1.125 x 17 (bottom) x 18.5 (top) x 6 16 ea - 1.5 x 15 x 6	Same as end-on	--
CAPACITY			
Fuel Assemblies	7 PWR/18 BWR	10 PWR/24BWR	12 PWR/32 BWR
Fuel Decay-Min (days)	120	120	150
Fuel Burnup-Max (MWD/MTD)	35,000	35,500	38,500
Decay Heat-Max (kW)	76.7	70.0	135

Table 2.5 Construction Material Data for Truck Spent-Fuel Shipping Casks

Cask	NFS-4		TN-8	TN-9	NFS-5
SIDE MATERIAL LAYERS	0.31 ss 6.63 lead 1.25 ss 4.50 water 0.17 ss	1.27 ss 7.0 depleted uranium 5.40 lead 2.22 ss 12.7 water 0.64 ss	0.24 ss 0.20 B C + Cu, min 5.79 lead, min 0.39 wet cement, min 0.79 SA 516 steel 5.91 resin, min	0.24 ss 0.20 B C + Cu, min 5.63 lead, min 0.39 wet cement, min 0.79 SA 516 steel 5.91 resin, min	0.25 ss 3.9-4.2 depleted uranium 1.0 ss 1.2-8.6 water 0.12 corrugated ss
BOTTOM MATERIAL LAYERS	8.0 ss 0.125 asbestos 8.0 balsa wood 0.5 ss	1.25 ss 3.50 ss 7.90 depleted uranium 3.18 ss	0.50 304 ss 7.09 lead 0.98 resin 0.79 304 ss 13.79 balsa wood 0.79 304 ss	Same as TN-8	1.0 ss 2.5 depleted uranium 1.5 ss
TOP MATERIAL LAYERS	7.50 ss 0.125 asbestos 12.0 balsa wood 0.104	1.9 ss 7.6 depleted uranium 3.18 ss 2.85 ss	1.57 304 ss 0.30 304 ss 5.87 lead 0.87 resin 0.90 304 ss 0.16 ss 9.65 balsa wood 0.79 304 ss	Same as TN-8	0.5 ss 2.5 depleted uranium 2.0 ss

Notes: 1. Layers listed from inside to outside of cask.
2. For NFS-4, ss indicates 321, 347, 94 348 ss.
3. Top and bottom data for TN-8 and TN-9 are estimated from half-scale model drawings for model used in drop tests.

Table 2.6 Construction Material Data for Rail Spent-Fuel Shipping Casks

Cask	IF 300	NLI 10/24	TN-12
SIDE MATERIAL LAYERS	0.5 317 ss 4.0 depleted uranium 1.56 317 ss 6.0 borated water 0.12 corrugated 304 ss	0.75 304 ss 6.0 lead 2.0 304 ss 7.0 borated water 0.75 304 ss	No data available
BOTTOM MATERIAL LAYERS	1.25 304 ss 3.75 depleted uranium 1.50 304 ss	2.0 ASME SA 336-F8 2.5 depleted uranium 4.0 ASME SA-336-F8 3.75 Ricorad PPC-V 0.13 ss	
TOP MATERIAL LAYERS	1.0 304 ss 3.0 depleted uranium 2.0 304 ss	0.75 304 ss 3.0 depleted uranium 3.0 304 ss 3.0 Ricorad PPC-V 2.5 304 ss 5.0 aluminum	

Note: 1. Layers listed from inside to outside of cask.

2.4.3 NLI 1/2

The NLI 1/2 spent fuel shipping cask[2.5-2.7] was designed by National Lead Industries and licensed in 1973. It is a legal-weight truck cask which has a payload capacity of 1 PWR or 2 BWR fuel assemblies. The cask is designed for double containment using an inner container and gasketed closure which is independent of the main cask body and its closure. The gamma radiation shield in the sides of the NLI 1/2 comprises a layer of lead and one of depleted uranium; uranium alone is used at the ends of the cask. A neutron shield water jacket is used along the axis of the cask, and hat-shaped balsa wood impact limiters encased in an aluminum weldment are attached to each end of the cask.

2.4.4 TN-8 and TN-9

The TN-8 and TN-9 spent fuel shipping casks[2.5 2.6 2.8 2.9 2.10] were designed initially for use in Europe by Transnuclear, Inc. of France and were licensed for use in the USA in 1975. The TN-8 and TN-9 are essentially the same cask. The difference is in their fuel capacity. The TN-8 has three compartments in the inner cavity for PWR fuel assemblies; the TN-9 has a capacity for 7 BWR fuel assemblies. The design of these casks permits their use for rail, water or truck transport; however, for truck transport they require an overweight permit since their loaded weight of almost 80 000 lb exceeds the legal weight truck limit. The main gamma shield for these casks is made of lead with an outer case of carbon steel. The neutron shield system on the TN-8 and TN-9 casks is unique among presently available LWR-spent-fuel transport casks. The neutron shield consists of a layer of polyester resin affixed to the outer surface of the cask. To enhance the heat transfer characteristics of the resin layer, fins that are welded to the outer cask surface pass through the neutron shield layer. Balsa wood impact limiters are used on each end of the casks for protection from both side and end impacts.

2.4.5 NFS-5

The NFS-5 spent fuel shipping cask[2.4 2.11] has been designed by Nuclear Fuel Services, Inc., as a legal weight truck cask to replace the NFS-4 shipping cask. The increased cask payload of 2 PWR and 4 BWR fuel assemblies makes the NFS-5 cask economically and operationally more attractive for truck shipment. The increased payload is possible because the fuel cavity has a rectangular cross section, which is unique among the present generation of LWR shipping casks. Depleted uranium is used for gamma radiation shielding, and the water jacket system is used for neutron radiation shielding. Balsa wood impact limiters at each end of the cask are used for collision protection. In addition to the balsa end caps, a balsa ring is positioned at the midsection of the cask for side-impact protection.

2.4.6 IF 300

The General Electric Company's IF 300 spent-fuel shipping cask,[2.6 2.10 2.12 2.13] which was licensed in 1973, is designed for normal shipment by railroad flatcar. The cask may be shipped short distances by a special overweight truck to service reactors that do not have rail facilities. The cask may be used to ship either 7 PWR or 18 BWR fuel assemblies. Shielding is provided by depleted uranium and an exterior water jacket. The IF 300 cask is unique in that it exclusively uses metal fins for impact protection. During shipment two diesel-driven blowers force air over the cask surface to provide auxiliary cooling.

2.4.7 NLI 10/24

The NLI 10/24 cask[2.14] was designed by National Lead Industries for the rail shipment of 10 PWR or 24 BWR fuel assemblies. This cask was licensed by the NRC in 1976. Gamma shielding along the length of the cask is provided by a lead layer. Gamma shielding at the ends of the cask is provided by depleted uranium. Similarly, two materials are used for neutron shielding: the water jacket system is used along the length of the cask, and Ricorad PPV-C, a silver based alloy, is used at the ends of the cask. Cylinder-shaped impact limiters made of balsa wood sandwiched between cylindrical aluminum shells, extend from each end of the cask.

2.4.8 TN-12

The TN-12,[2.9 2.15] which was designed by Transnuclear, Inc., is a rail shipping cask which is licensed in Europe. Licensing in the USA is anticipated at a future date. The TN-12 has a capacity of 12 PWR or 32 BWR fuel assemblies. Its basic structure is a steel forging, which also provides the gamma shielding. The main advantage of the steel forging design is that it is a well-known technology and has well known characteristics, thus reducing license evaluation time and eliminating manufacturing complications associated with casks that use unconventional materials in their designs. Little more information is available on

the TN-12 design; however, the remainder of the design is probably similar to that for the TN-8 and TN-9.

2.5 References

2.1 U. S. Nuclear Regulatory Commission Rules and Regulations, 10 CFR-Part 71, April 30, 1975.

2.2 *Safety Analysis Report for Nuclear Fuel Services, Inc. Spent Fuel Shipping Cask Model No. NFS-4*, September 1972 (71-6698).

2.3 V. J. Barnhart, J. D. Rollins, "The NFS-4 Spent Fuel Shipping Cask," *Transactions American Nuclear Society, No. 16, June 1973, 174.*

2.4 *K. H. Dufrane, "Design, Manufacturing, and Operational Experience with the NFS-4 Spent Fuel Shipping Cask," Proceedings of the 4th International Symposium on Packaging and Transportation of Radioactive Materials*, Vol 1, Miami Beach, FA, September 22-27, 1974.

2.5 R. W. Peterson, "Industrial Views on Federal, State, and Local Regulations and Regulatory Processes," AIF Conference on Transportation for the Nuclear Industry, Minneapolis, MN, May 25-28, 1976.

2.6 D. G. Maxwell, "Overview: Spent Fuel Transportation," AIF Conference on Transportation for the Nuclear Industry, Minneapolis, MN, May 25-28, 1976.

2.7 *NLI 1/2 Spent Fuel Shipping Cask Safety Analysis Report*, Amend No. 1, December 1972 (71-9010).

2.8 *Safety Analysis Report for Transnuclear, Inc., Spent Fuel Shipping Casks Model No. TN8 and TN9*, September 8, 1976, Rev 7 (70-1375).

2.9 Ltr from R. B. Pope, Organization 5431, Sandia National Laboratories, to Distribution, subject: "Information on Transnuclear, Inc., Spent Fuel Shipping Casks," January 20, 1976.

2.10 R. M. Jefferson and L. L. Bonzon, "Available Packaging and Transportation Systems," *Proceedings of The International Symposium on the Management of Waste From The LWR Fuel Cycle*, July 11-16, 1976, Denver, CO, sponsored by the Division of Nuclear Fuel and Production, ERDA.

2.11 *Safety Analysis Report for Nuclear Fuel Services, Inc. Spent Fuel Shipping Cask Model No. NFS-5*, Rev 3, May 3, 1976 (71-7031).

2.12 *Design and Analysis Report IF300 Shipping Cask*, NEDO-10084-1 (San Jose, CA: General Electric Co., February 1972).

2.13 E. Walker, "IF300 Spent Reactor Fuel Shipping Cask," *Transactions American Nuclear Society*, No. 18, June 1974, pp 168-170.

2.14 *Safety Analysis Report NLI 10/24 Spent Fuel Shipping Cask*, Rev 5, Wilmington, DE: Nuclear Transportation Department, Nuclear Division, N. L. Industries, Inc., February 1976 (71-9023).

2.15 B. R. Teer, "Spent Fuel Transportation," *Public Utilities Fortnightly*, August 14, 1975.

3.0 Material Properties

In performing a stress analysis of a shipping cask, the best available material properties and constitutive models should be used in the computer programs. In this study, however, only representative properties are needed for each material because the study is concerned only with evaluating the available analytical techniques and their application to shipping cask analyses. Hence, an extensive literature search for material properties was not undertaken. It is not implied that the properties listed are to be used in an actual cask analysis. To eliminate material modeling as a variable in the assessment of the results, the same material data fits are used in all of the computer programs.

All material properties are for 70°F and, as explained elsewhere, no thermal effects are included. The stainless steel and the uranium were considered to remain elastic except for the analysis of the stainless steel impact-limiting fins and for the plate directly between the balsa wood and the cask on the lead-steel-balsa wood cask. The lead shielding material and the balsa wood are considered to be nonlinear materials.

Since several of the computer programs which will be used permit only a bilinear representation of the nonlinear stress-strain curve, a bilinear model is used for all of the computer programs.

3.1 304 Stainless Steel

All the steel in each design will be represented by the following properties resulting from a bilinear fit (Figure 3.1.1) of a stress-strain curve in Reference 3.1 at 70° F for a strainrate of 10 s^{-1}.

Young's modulus, E = 28.0 x 10^6 psi
Poisson's ratio, υ = 0.33
Plastic modulus, E_T = 275 000 psi
Yield stress, σ_y = 45 000 psi
Density, ρ = 7.332 x 10^{-4} lb-s^2/$in.^4$.

In elastic-plastic components, i.e., the impact limiter analyses, isotropic hardening will be assumed because a decision was necessary without benefit of a complete materials evaluation. Also, it is probably not very important whether kinematic or isotropic hardening is used since only loading of the impact limiters is to be performed.

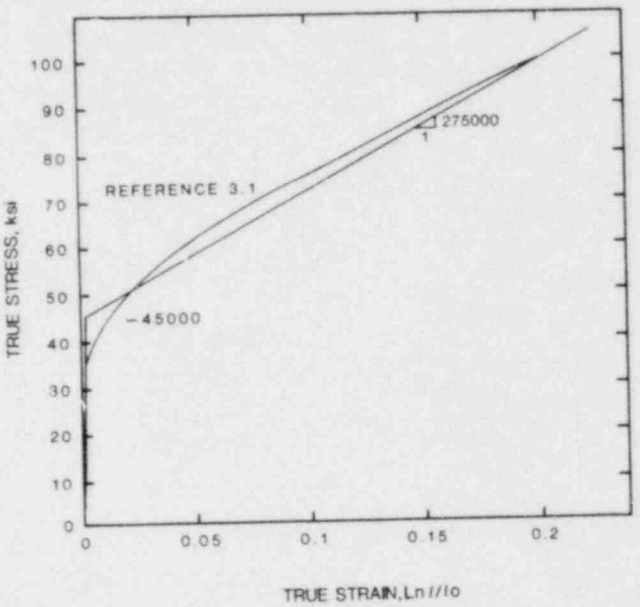

Figure 3.1.1 Stress-Strain Curve for 304 Stainless Steel at 70° F.

3.2 Lead

Lead will be modeled as an elastic-plastic material with the following properties.

Young's modulus, E = 27 750 psi
Poisson's ratio, υ = 0.42
Plastic modulus, E_T = 2 400 psi
Yield stress, σ_y = 4 300 psi
Density, ρ = 1.0389 x 10^{-3} lb-s^2/$in.^4$

A stress-strain curve taken from Reference 3.2 was fit with a bilinear stress-strain curve as shown in Figure 3.2.1. Isotropic hardening is to be used with no strain rate effects. Isotropic hardening conditions were chosen because of an incomplete materials evaluation. The type of hardening conditions chosen should not affect the results because unloading and subsequent yielding is not expected. If data were available, a better material model would be to prescribe bulk modulus and shear modulus data because the Poisson's ratio of lead is quite high. The data taken from Reference 3.3 were obtained under dynamic loading conditions. Since lead is strain rate sensitive, in an actual analysis strain rate effects should be included. The data in Reference 3.3 show

that, for strain rates of 100 to 700 s^{-1}, the stress-strain curve does not vary appreciably. In retrospect, the 30-ft-drop condition is not severe enough to warrant the high yield stress used in this study. Since lead is highly nonlinear, a bilinear representation is used for the stress-strain curve, with the yield point and the hardening modulus chosen so that the data are fit closely for the expected range of the strain. Obviously, if the computer program is not limited to a bilinear fit, this assumption does not have to be made.

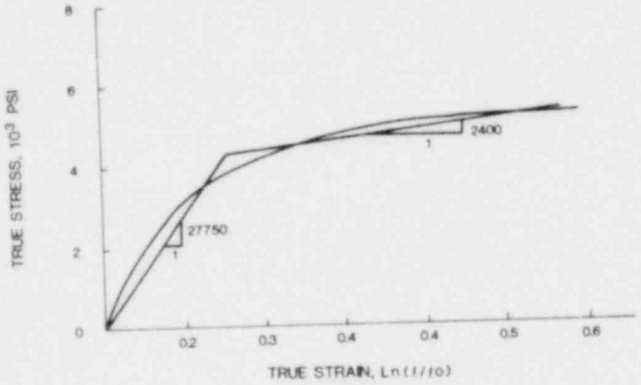

Figure 3.2.1 Stress-Strain Curve for Chemically Pure Lead at 70°F

3.3 Uranium

Depleted uranium will be modeled as an elastic material for this study, using data taken from Reference 3.7. At 70°F the yield strength is approximately 35 000 psi and stresses above 35 000 psi are not likely to occur under the 30-ft drop impact conditions.

Young's modulus, $E = 25.8 \times 10^6$ psi
Poisson's ratio, $\nu = 0.21$
Density, $\rho = 1.76 \times 10^{-3}$ lb-s^2/in.^{4}.

3.4 Balsa Wood

Balsa wood is highly orthotropic and the properties are very low in the radial, r, and tangential, θ, directions as compared to the longitudinal, L, direction. In anticipation of the material models which are generally available in computer programs, a study was conducted to determine how balsa wood properties should be input to the program expected to be used. Two different material models were considered: an elastic-plastic with strain hardening model[3.4] and a soils or crushable foam model.[3.4,3.5]

A test problem for the material models was used with the two-dimensional large deformation, transient code, HONDO.[3.4] The axisymmetric model is shown in Figure 3.4.1. The balsa is the same size as the end piece of balsa on the lead-steel cask. A plate was attached to simulate the approximate weight of the lead-steel cask, 195 000 pounds. The assembly was impacted at 528 in./s into a rigid foundation.

The "unyielding" foundation was simulated with an elastic foundation, consisting of an elastic spring at each contacting point on the balsa limiter with a spring constant of 10^7 lb/in./radian. By varying the spring constant from 10^6 to 10^8 lb/in./radian and noting that the axial displacement beyond the Z = 0 in. location was very small, the 10^7 lb/in./radian spring constant was deemed adequate to simulate a rigid foundation. The axial displacement at the contact points could have been set equal to zero to provide a rigid foundation, but, if the springs are used, the total force acting upon the limiter by the foundation can be monitored by summing the force in each spring at a specific time.

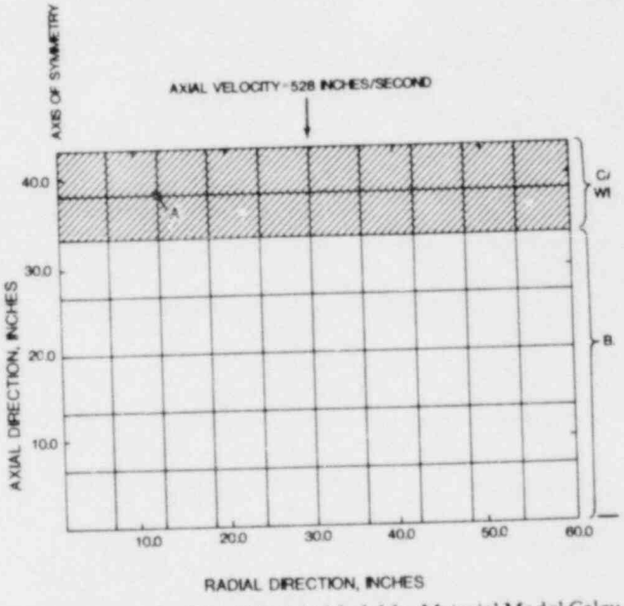

Figure 3.4.1. Balsa-Wood-Weight Model for Material Model Calculations

For the elastic-plastic model the following properties were chosen.

Young's modulus, E = 590 000 psi
Plastic modulus, $E_T = 0.0$
Poisson's ratio, $\nu = 0.0$
Yield stress = 1 700 psi

Isotropic hardening conditions were assumed.

For the crushable foam model, because bulk pressure vs volumetric strain data were not available for balsa wood, the following assumptions were made. Using the data of Reference 3.6, for 9 lb/ft^3 material, the elastic Young's modulus is 590 000 psi. Assuming that Poison's ratio is zero because the material is highly orthotropic E_r = 28 000 psi and E_θ = 8 660 psi, then the elastic shear and elastic bulk moduli would be 295 000 and 197 000 psi, respectively.

It is further assumed that the crush strength under hydrostatic pressure is 1/3 of the uniaxial crush strength of 1 700 psi. Above a pressure of 570 psi the bulk modulus is zero.

A cylindrical yield surface is also defined when an effective stress of 1 700 psi occurs and further loading is perfectly plastic.

The results of the two calculations are shown in Figures 3.4.2 through 3.4.7. Figures 3.4.2, 3.4.3, and 3.4.4 show the acceleration, velocity, and displacement of point A in Figure 3.4.1 when the elastic-plastic model is used. Figures 3.4.5, 3.4.6, and 3.4.7 show the acceleration, velocity, and displacement of the weight at point A when the crushable foam model is used.

A one-dimensional transient analysis can also be performed if the cask is simulated by a rigid mass with an initial velocity of 528-in./s, and the balsa wood is simulated by an elastic-perfectly plastic spring. Newton's second law of motion could be integrated exactly to obtain the response of the cask. A lumped spring-mass computer program called SHOCK[3.6] was used, however, to accomplish the integration numerically. The elastic stiffness of the spring is 2.8 x 10^8 lb/in., which is valid until the crush strength of 1 700 psi of the balsa wood is reached. The elastic stiffness is calculated by

$$k = \frac{AE}{\ell},$$

where E is the Young's modulus, ℓ is the compression height of 33 in., and A is the cross-sectional area of the balsa wood limiter. Using the 1 700 psi crush strength of the balsa wood, the maximum force which can be sustained is 19.0 x 10^6 lb.

A maximum displacement of 3.7 in. at 0.01425 s was calculated. If Newton's second law of motion is integrated using a perfectly plastic spring (no elastic portion), nearly the same results are calculated. If the kinetic energy of the mass is equated to the crushing force times the crush distance, a crush distance of 3.7 in. is calculated. The acceleration, obtained by dividing the crushing force by the mass of the cask, is a constant 37 600 in./(s)^2 (97 g's).

The results for the acceleration and velocity are plotted on Figures 3.4.2, 3.4.3, 3.4.5 and 3.4.6 for comparison purposes. The curves are quite similar. However, the best comparison of the effect on an analysis of an actual cask is shown in Figure 3.4.8, where the force versus time at the interface between the balsa and the rigid target is plotted. Also shown is the force obtained in the one-dimensional solution. Because both the elastic-plastic and foam models predict closely the same response and are both conservative towards a cask safety analysis, the elastic-plastic model will be used in further calculations.

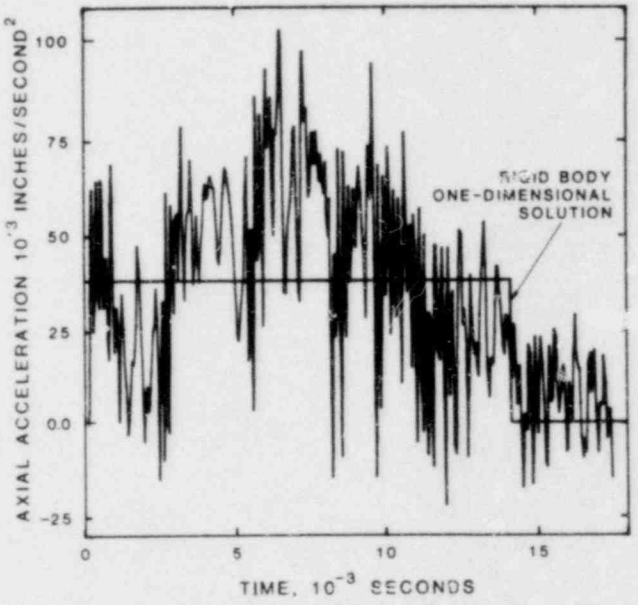

Figure 3.4.2. Axial Acceleration of Plate at Point A When Elastic-Plastic Material Model Is Used

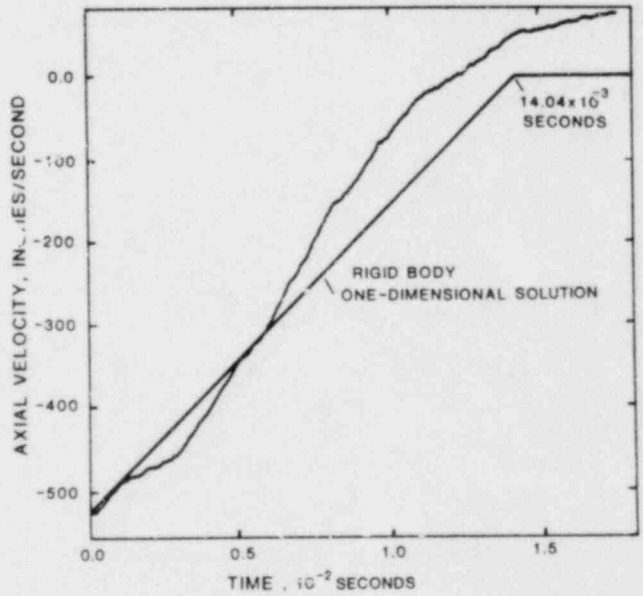

Figure 3.4.3. Axial Velocity of Plate at Point A When Elastic-Plastic Material Model Is Used

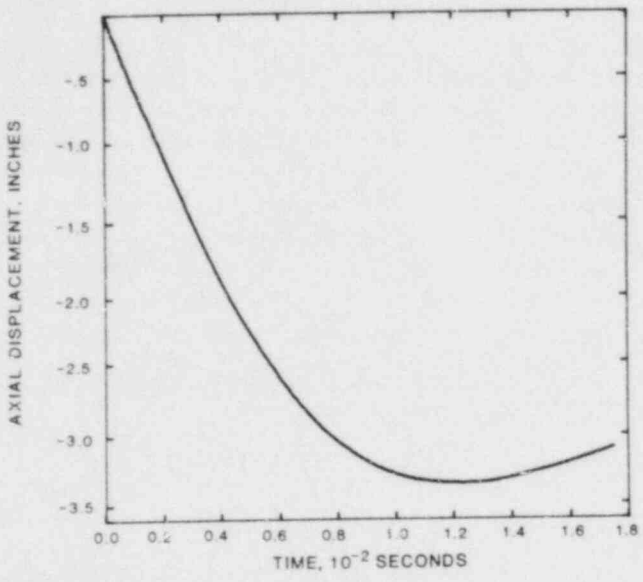

Figure 3.4.4. Axial Displacement of Plate at Point A When Elastic-Plastic Material Model Is Used

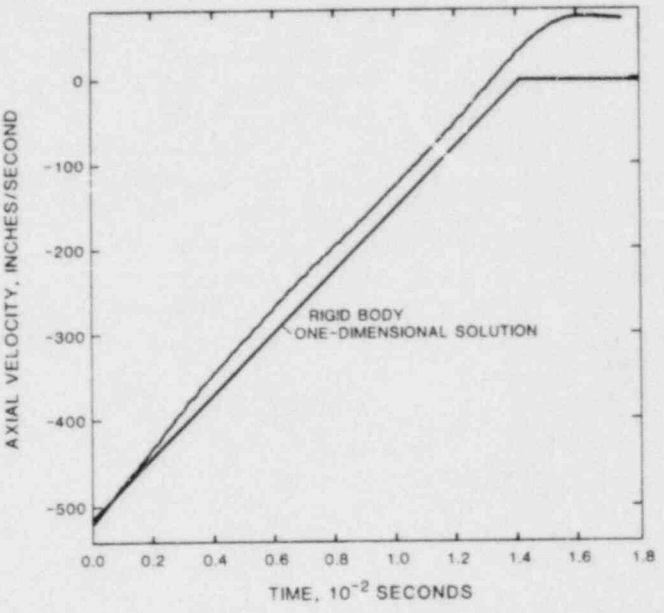

Figure 3.4.6. Axial Velocity of Plate at Point A When Crushable Foam Model Is Used

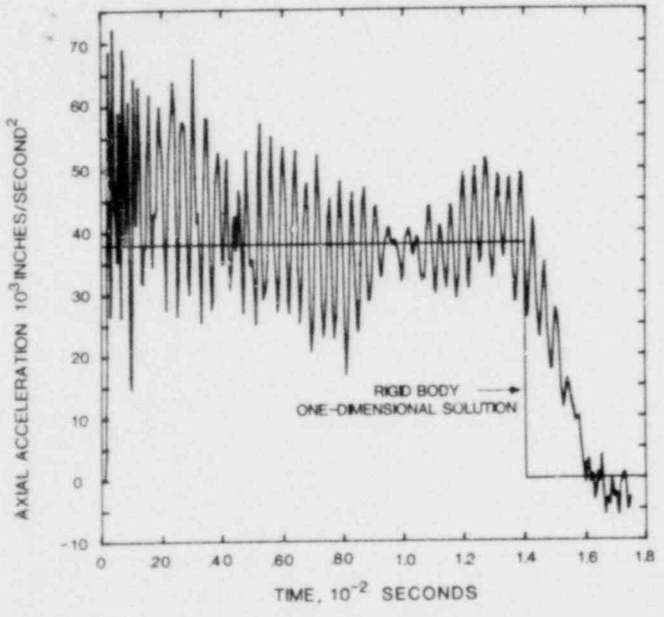

Figure 3.4.5. Axial Acceleration of Plate at Point A When Crushable Foam Model Is Used

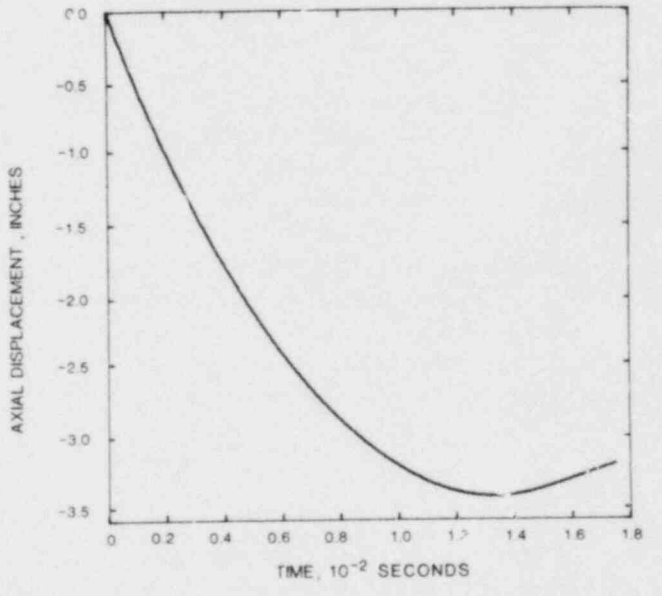

Figure 3.4.7. Axial Displacement of Plate at Point A When Crushable Foam Model Is Used

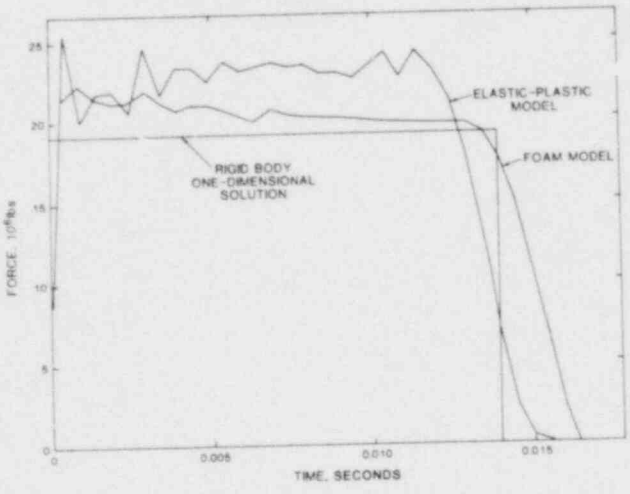

Figure 3.4.8. Total Force vs Time at the Balsa-Wood-Foundation Interface

3.5 Water

Water is used for shielding, and when it is necessary to include it in the calculations, the following properties will be used.[3.2]

Shear modulus, $\mu = 1\,000$ psi
Bulk modulus, $K = 300\,000$ psi
Density, $\rho = 9.34 \times 10^{-5}$ lb-s^2/in.^{4}

For use later with the HONDO[3.4] code for two-dimensional finite element transient analyses, the water will be assumed to be linear in bulk behavior and perfectly plastic with a conical yield surface defined by

$$\phi = \frac{1}{2}\sigma_e^2 - (1.0 + 1\,000\ p) \quad ,$$

where p is the hydrostatic pressure and σ_e is the von Mises effective stress. The result is a material which has a low shear strength that is pressure dependent and will not sustain any hydrostatic tension.

3.6 References

3.1 T. D. Moore, *Structural Alloys Handbook*, Vol. 2 (Traverse City, MI: Mechanical Properties Data Center, Belfour Stulen, Inc., 1977), p 67.

3.2 T. Baumeister and L. S. Marks, *Standard Handbook for Mechanical Engineers* (New York: McGraw Hill Book Co., 1967).

3.3 J. H. Evans, *"Structural Analysis of Shipping Cask*, Vol. 8, Experimental Study of the Stress-Strain Properties of Lead Under Specified Impact Conditions," Report, ORNL-TM-1318, Vol. 8 (Oak Ridge, TN: Oak Ridge National Laboratory, August 1970).

3.4 S. W. Key, "A Finite Element Procedure for the Large Deformation Dynamic Response of Axisymmetric Solids," *Computer Methods in Applied Mechanics and Engineering*, 4, 1974, pp 195-218.

3.5 R. D Krieg, *A Simple Constitutive Description for Soils and Crushable Forms*, Report SC-DR-72-088. Albuquerque, NM: Sandia Laboratories, 1972).

3.6 V. K. Gabrielson and R. T. Reese, *SHOCK Code Users Manual — A Computer Code to Solve the Dynamic Response of Lumped Mass Systems*, Report No. SCL-DR-69-98 (Livermore, CA: Sandia Laboratories, 1969).

3.7 *Design and Analysis Report IF-300 Shipping Cask* (San Jose, CA: General Electric Co., February 1972).

4.0 Analysis of End-On Impact

In this section the analysis of the two spent-fuel shipping casks for an end-on oriented, 30-ft free-fall drop onto an unyielding target is described.

For this drop orientation, the lead-steel-balsa cask is considered to be axisymmetric about the axial direction, and since no distinction has been made regarding the ends of the cask, the response is the same whether the "top" or "bottom" impacts. The symmetry about the axial direction means that only a two-dimensional analysis is required. That is, the displacement in the circumferential direction is zero. As explained previously, one-dimensional analyses, with restrictions, may also be used.

For the analysis of the complete uranium-steel cask for the end-on orientation a three-dimensional analysis would be required because of the fin impact limiters. Plastic buckling of the fins results in deformation out of the plane of the fin upon impact. However, if the fins on the impact end are removed the response of the remaining structure is axisymmetric except for that portion of the cask near the fins. The method of analysis without the actual fin is described in Section 4.2.2.

Finite element techniques can be used to calculate stresses at many locations on the cask, e.g., at the center of each element used in modeling the cask. However, when using a strength-of-materials approach, critical locations are chosen by the analyst where maximum values of stress are expected for different portions or components of the casks. Also, as explained in Section 1.2.1, a strength-of-materials analysis does not capture the actual variation of stress over a complicated cross section. Hence, a few points were selected, mainly on the basis of engineering judgment, to compare the different techniques. The chosen locations do not necessarily include the locations of maximum stress.

Thermal effects are not considered in the analyses in this report. During construction of a spent-fuel shipping cask sizeable residual stresses may be induced because of the difference in the coefficients of thermal expansion between the steel and the shielding materials. When the stresses due to an impact are added to the residual stresses caused by initial temperatures and pressures, some or all of the materials may behave inelastically. When lead shielding is used, the residual stress calculation is a varying-temperature creep analysis with possible complications due to elastic-plastic behavior. This analysis will not be attempted here. If elastic-plastic behavior occurs during the residual and initial stress calculations, the residual and initial stresses and stresses due to impact cannot be added directly. The residual stresses must be used as initial conditions for the transient response calculation.

For the lead-steel-balsa cask the analyses are described in Section 4.1. The analysis of the uranium-steel cask is described in Section 4.2. The analysis of the impact limiters (steel fins) for this cask is discussed in Section 4.2.1, while the analysis of this cask using a model without fins is described in Section 4.2.2. Section 4.3 discusses and compares the results for the end-on impact condition.

4.1 Lead-Steel-Balsa Cask

4.1.1 Cask Analysis

Four analysis techniques were selected to be used for the analysis of the lead-steel-balsa cask. First, a two-dimensional large deformation finite element program is used to obtain a transient dynamic solution of the complete cask with the balsa impact limiter. The second technique is a two-dimensional static simulation of the dynamic problem and is accomplished by using a static finite element calculation and applying a constant axial acceleration to the cask without the impact limiter. This method predicts the average response of the cask.

The third technique predicts a one-dimensional dynamic response of the cask by lumping the cask into a system of springs and masses with which a dynamic transient response is calculated. The results are forces in the springs as functions of time from which stresses are calculated. The fourth technique involves obtaining, by experimental and/or analytical means, a value of constant acceleration and applying a strength-of-materials approach to calculate stresses at selected locations of the cask system. Based on the one-dimensional calculations (Section 3.4) of the balsa wood impact limiter, the analytical results will be compared until 24.0×10^{-3} s after the time of impact.

The locations at which the analytical results are compared are shown in Figure 4.1.1. Stress components and the von Mises effective stress, σ_e, are compared at points A through D. The axial acceleration, velocity, and displacement are compared at points A,

E and F. Locations A and B were chosen to represent the response of the non-impacting end plate of the cask. Locations were not chosen on the impacting end plate because it was desirable to reduce the amount of data to be presented, and because it was thought that the support provided by the limiter would prevent the plate from experiencing significant stress values. Locations A and B should be points of maximum radial stress during flexure of the end plates. Also, for an actual cask, the integrity of a bolted or otherwise connected end plate would have to be assessed. Because the bottom plate will vibrate following the impact, the kinematic quantities of the plate at point A are also compared. At location C the response of the inner steel shell due to the pressure exerted by the lead shielding and the axial loading is compared. It will be assumed for all the finite element analyses that the lead is perfectly bonded to the steel cylinders throughout the 30-ft-drop impact. If this assumption is not valid, it is expected that significantly different stresses would result at points A, B and C. Experimental verification of the assumption should be made for the 30-ft-drop condition. At location D, the response of the lead is compared, although the stress in the lead is not expected to be critical. This point was selected after the two-dimensional transient analysis was completed because it is the point of maximum stress in the side lead shielding. The axial acceleration, velocity and displacement at locations E and F are compared because these points represent the most massive sections of the cask. The best agreement of kinematic quantitites between the different analyses should be at these points.

4.1.1.1 Two-Dimensional Dynamic Analysis

For the two-dimensional transient response using the geometry and materials shown in Figure 4.1.1 the cask was modeled for the analysis as shown in Figure 4.1.2. The balsa wood limiter on the top end was removed because its weight and structural characteristics were not deemed important to the two-dimensional analysis. The finite element mesh was created

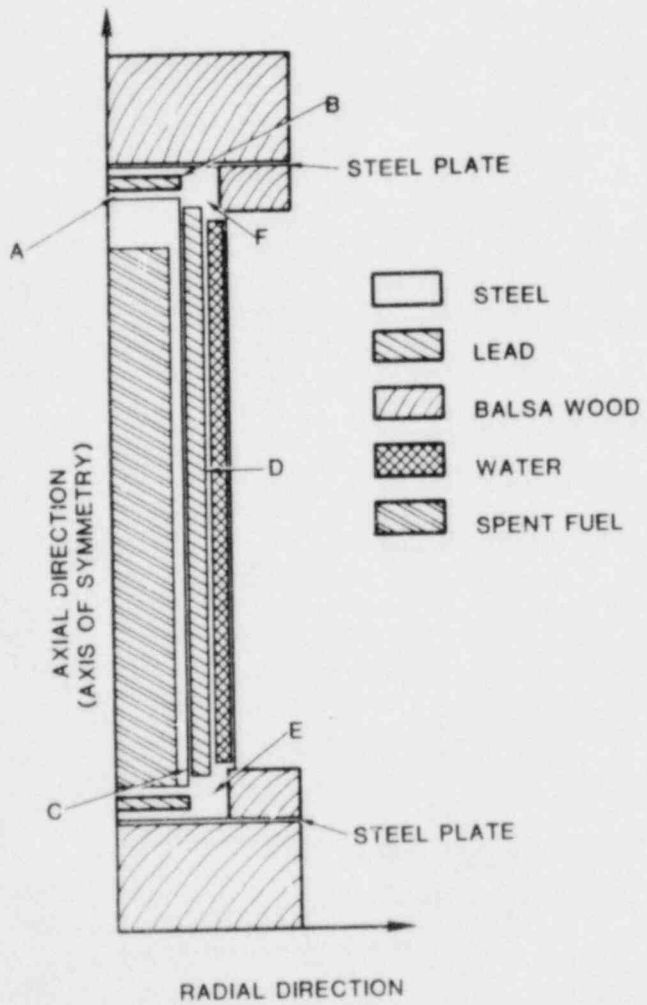

Figure 4.1.1. Axisymmetric Outline Lead-Steel-Balsa Cask

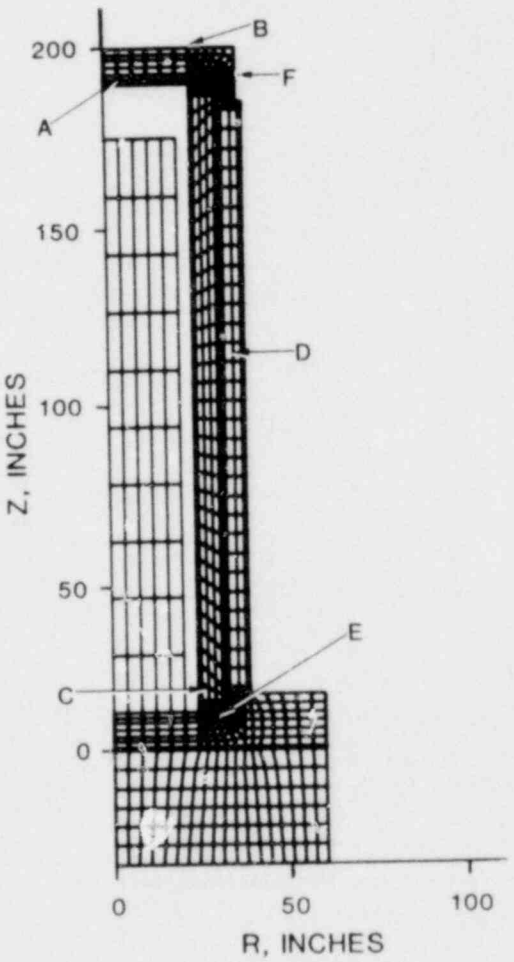

Figure 4.1.2. Finite Element Mesh of Lead-Steel Cask for End-On Impact Analysis

with the two-dimensional mesh generator program, QMESH.[4.1] The number of elements used through the end plates and the cylindrical portion should adequately predict the elastic stress response of the cask. No attempt was made to refine the mesh to substantiate the modeling; only experience was relied upon. A total of 738 elements and 819 nodes are in the model. The computer time required for the HONDO[4.2] computer program to calculate transient response for 24 x 10^{-3} s on a CDC 7600 computer was 2 800 central processor seconds. A total of 18 000 time steps was needed, with the average step size being 1.33 x 10^{-6} s. The computer time required to generate the mesh and plot the results is insignificant when compared to the dynamic analysis solution computer time.

The unyielding target was simulated by an elastic foundation consisting of an elastic spring at each contacting point on the balsa limiter with a spring constant of 10^7 lb/in./radian (see Section 3.4). An initial axial velocity of -528 in./s was given all nodes in the model to simulate the 30-ft-drop conditions.

As stated before, the steel was modeled elastically; the lead and balsa wood, elastic-plastically. The exception is the steel plate directly behind the balsa wood limiter on the end of the cask. Since a preliminary elastic analysis showed that this plate undergoes very large elastic stresses, it was modeled as an elastic-plastic material. The plate is a part of the impact limiter and consequently not a structural component of the cask when the limiter is removed.

The material properties have been described previously (Section 3.0) with the exception of the nonstructural fuel material which was given a Young's modulus of 500 000 psi and a density of 0.3648 x 10^{-3} lb·s^2/in.^{4} The modulus was chosen so the material would have little structural significance and the density was chosen to obtain the correct weight of the fuel.

The results of the computer calculations at the six locations are shown in Figures 4.1.3 through 4.1.13. The quantities are plotted as functions of time, and the plotted points are at every 0.24 x 10^{-3} s or at approximately every 180th calculational time step in the analysis. The quantities plotted at each of the points are representative of other quantities which are not plotted. The maximum values of the quantities are presented in Section 4.3.

The results are typical of output from dynamic finite element codes. Relatively smooth variations are shown for displacement and velocity components at the nodes of the model. The acceleration and stress components have a large amount of high-frequency content. The data plotted have some of the high-frequency variation filtered out because of plotting every 180 calculational steps. Much higher frequencies are also usually obtained if the mesh is refined. However, if the mesh is fine enough and the plot increments are not too large, the accuracy in the plotting of the maximum and minimum of the acceleration and stress component is not lost.

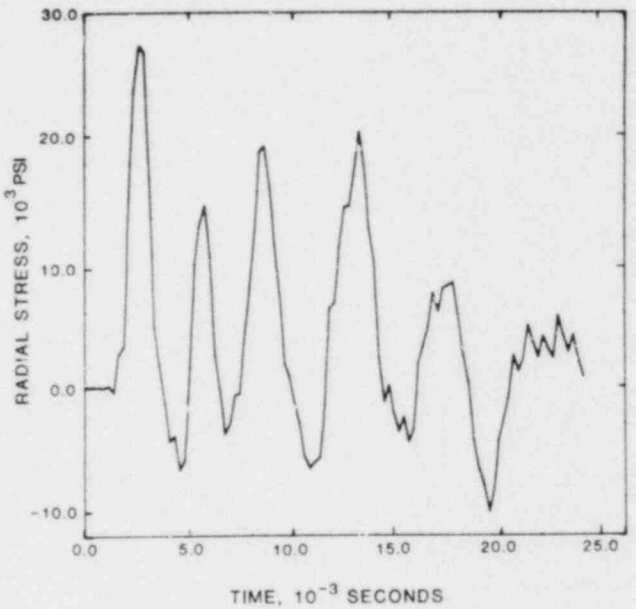

Figure 4.1.3. Radial Stress vs Time at Location A for the Lead-Steel-Balsa Cask End-On Two-Dimensional Dynamic Impact Calculation

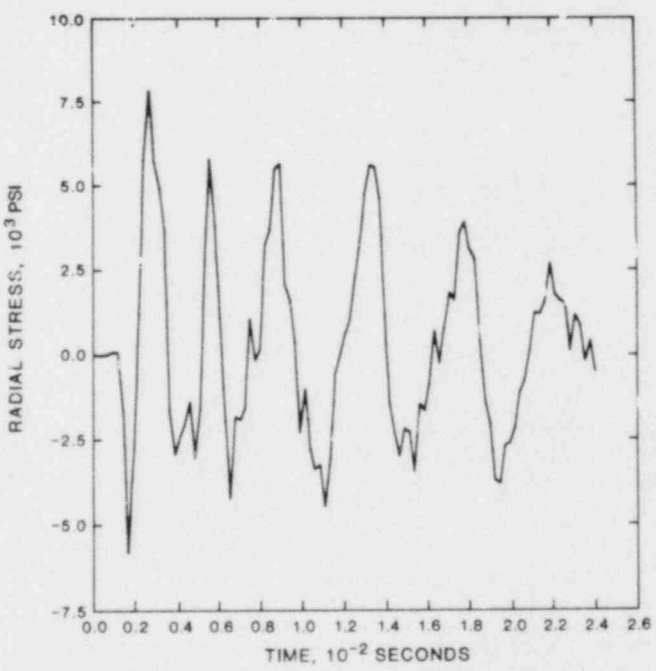

Figure 4.1.4. Radial Stress vs Time at Location B for the Lead-Steel-Balsa Cask End-On Two-Dimensional Dynamic Impact Calculation

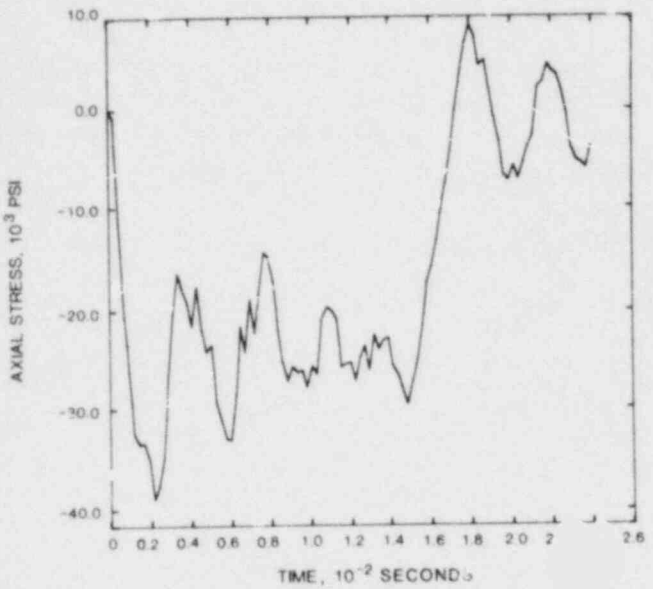

Figure 4.1.5. Axial Stress vs Time at Location C for the Lead-Steel-Balsa Cask End-On Two-Dimensional Dynamic Impact Calculation

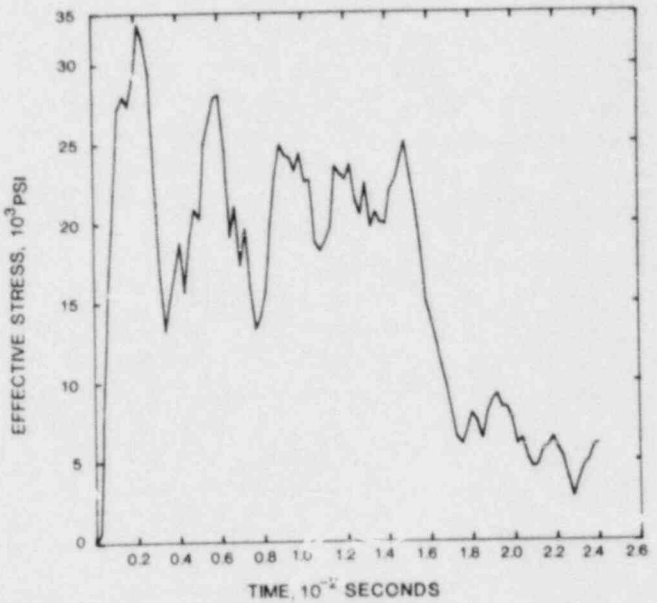

Figure 4.1.7. Effective Stress vs Time at Location C for the Lead-Steel-Balsa Cask End-On Two-Dimensional Dynamic Impact Calculation

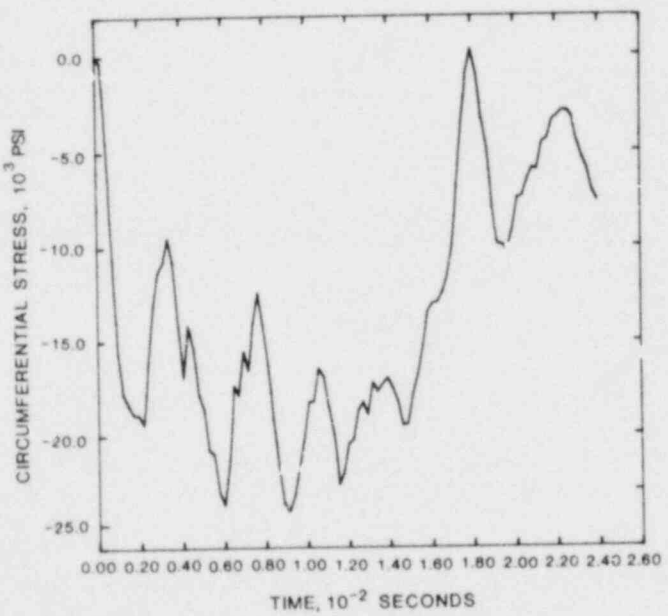

Figure 4.1.6. Circumferential Stress vs Time at Location C for the Lead-Steel-Balsa Cask End-On Two-Dimensional Dynamic Impact Calculation

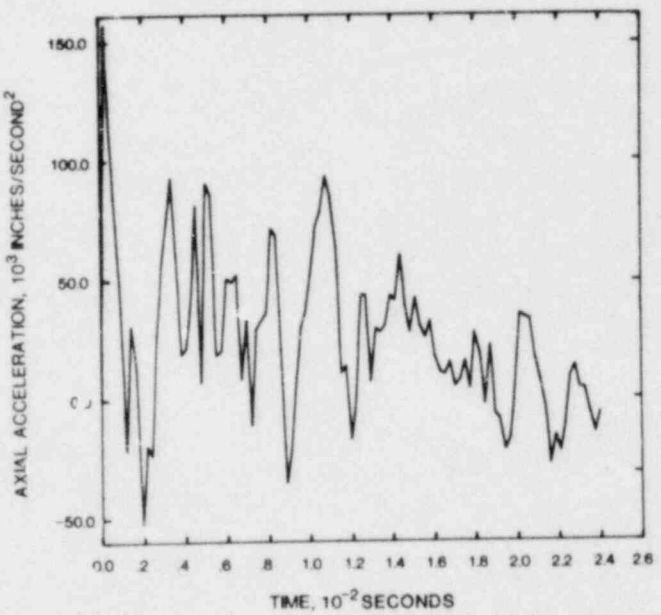

Figure 4.1.8. Axial Acceleration vs Time at Location E for the Lead-Steel-Balsa Cask End-On Two-Dimensional Dynamic Impact Calculation

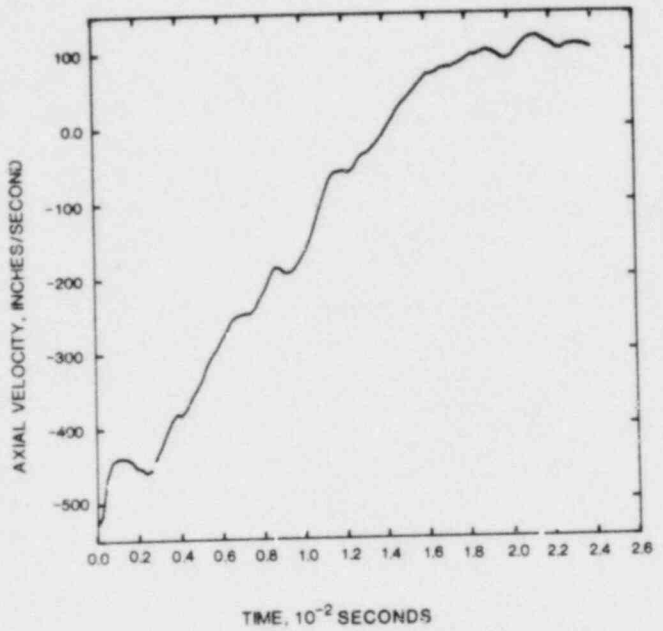

Figure 4.1.9. Axial Velocity vs Time at Location E for the Lead-Steel-Balsa Cask End-On Two-Dimensional Dynamic Impact Calculation

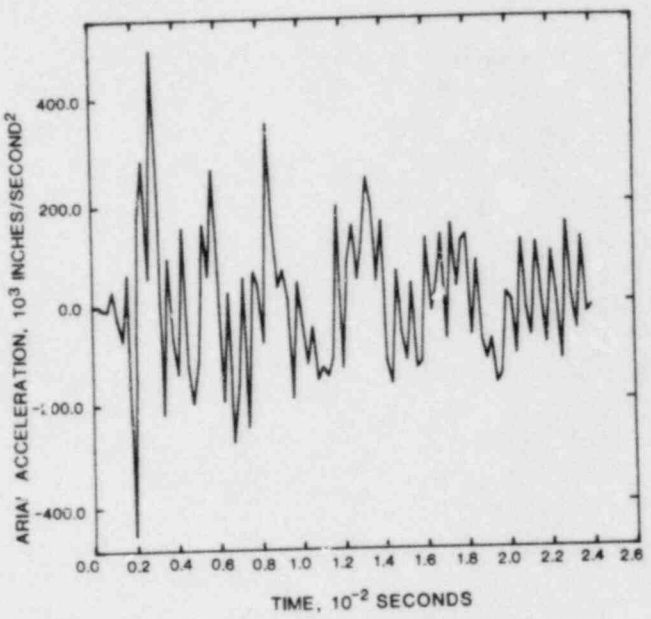

Figure 4.1.11. Axial Acceleration vs Time at Location A for the Lead-Steel-Balsa Cask End-On Two-Dimensional Dynamic Impact Calculation

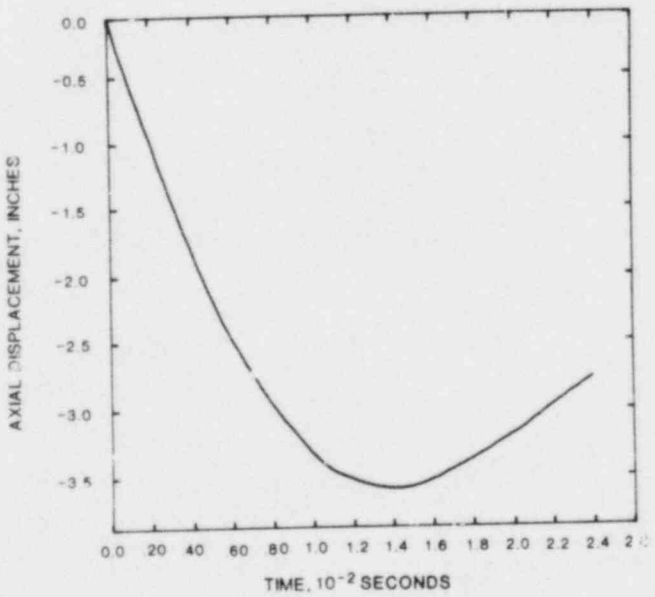

Figure 4.1.10. Axial Displacement vs Time at Location E for the Lead-Steel-Balsa Cask End-On Two-Dimensional Dynamic Impact Calculation

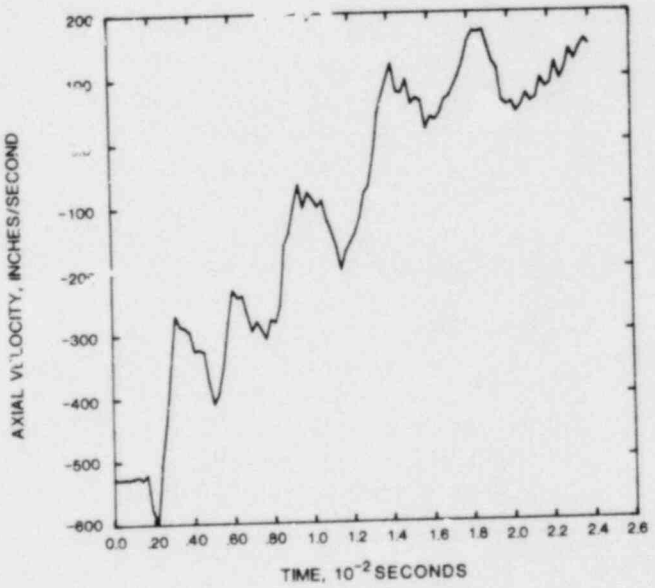

Figure 4.1.12. Axial Velocity vs Time at Location A for the Lead-Steel-Balsa Cask End-On Two-Dimensional Dynamic Impact Calculation

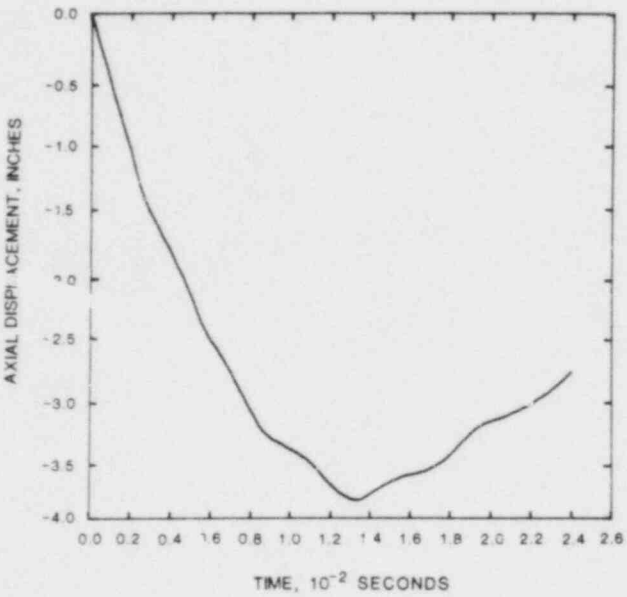

Figure 4.1.13. Axial Displacement vs Time at Location A for the Lead-Steel-Balsa Cask End-On Two-Dimensional Dynamic Impact Calculation

4.1.1.2 Two-Dimensional Static Analysis

The second method of analysis is a two-dimensional static solution of the cask without the balsa wood impact limiters. The same finite element mesh (Figure 4.1.2), without the balsa wood, was used. The nonlinear finite element code ADINA[4.3] was used because it was thought the stresses in the lead might exceed the yield point. However, with the material description used in the analysis, the lead did not yield and a linear code would have sufficed. A constant axial acceleration for every element of -38 000 in./s² (-98 g's) was applied. The end at Z = 0 in. was held fixed in the axial direction, and no radial movement was allowed at the centerline.

The acceleration was calculated using Newton's second law of motion, which is

$$\text{Axial acceleration (in./s}^2) = \frac{\sigma_c A}{W} \quad ,$$

where σ_c is the crush strength of the balsa wood, A is the crush area, and W is the loaded weight of the cask. It is assumed that the complete area of the balsa wood is crushed uniformly by the total weight of 195 000 lb. The method applied an average acceleration to all components of the cask; therefore, for example, there is no amplification of the acceleration at the center of the end plate at point A. The resulting static stresses at the comparison points are shown in Table 4.1 of Section 4.3.

Computer time to accomplish the linear static analysis was 90 central processor seconds for mesh generation and calculation of the stress and displacements. Since only selected point values of stresses are reported, contour plotting of results and post-processing to find maximum and minimum values of stresses was not necessary.

4.1.1.3 One-Dimensional Dynamic Analysis

In this section the one-dimensional dynamic analysis of the lead-steel-balsa cask using the lumped parameter computer program SHOCK[4.4] is discussed. The use of one-dimensional analysis and modeling for the end-on impact orientation is described in Section 1.3.1.

Figure 4.1.14 illustrates a schematic of the model formulated for this analysis. Dynamic stress values at the various cask locations illustrated in Figure 4.1.1 were obtained from the computed loads or elastic deformations in the couplings.

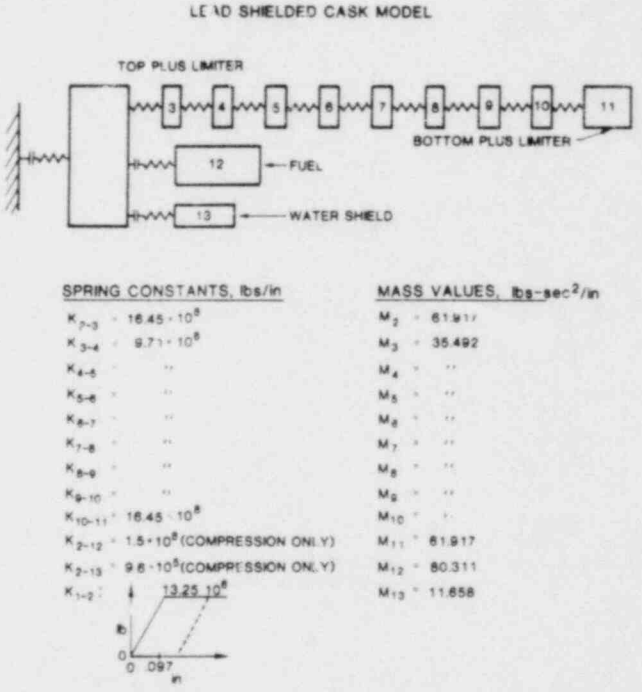

Figure 4.1.14. Schematic of the Lumped Parameter Model

Because the stainless steel plate imbedded in the balsa wood impact limiter was calculated to be insufficiently rigid to allow uniform compaction of the balsa, an effective balsa wood crush area was assumed. This area was computed by taking the average of the cask and impact limiter diameters. A 100-in.-dia value was used to compute the effective crush area of the balsa and define coupling 1-2 in the

model. This force-displacement characteristic could be accurately determined by use of a finite element computer program. However, since the analysis was restricted to a one-dimensional dynamic model, an effective crush area was simply assumed. The calculated deflections were checked to ensure that they were below values which would cause "lockup" of the balsa.

Stresses in the bottom of the cask, at locations A and B (Figure 4.1.1), were calculated by using a plate equation and the computed load in the coupling connecting the last mass element in the model. The bottom of the cask was conservatively modeled as a simply supported circular plate. The following equations were used to compute the radial and tangential stresses.[4,5]

$$S_r = \frac{3W}{8\pi mt^2}\left[(3m + 1)\left(1 - \frac{r^2}{a^2}\right)\right]$$

$$S_t = \frac{3W}{8\pi mt^2}\left[(3m + 1) - (m + 3)\frac{r^2}{a^2}\right] ,$$

where

W = total load
m = reciprocal of Poisson's ratio
a = plate radius
t = plate thickness
r = radial coordinate

The composite plate thickness was used in the computations. Compressive stresses were plotted as negative and tensile stresses as positive.

Figure 4.1.15 illustrates the force pulse input to the end of the cask in the impact and comes from the calculated load in coupling 1-2. As can be seen, the force level remains at the crush strength of the impact limiter for approximately 20 ms.

The motion of the cask body will be examined by looking at the results for the first and last mass elements along the cask structure. Figures 4.1.16, 4.1.17 and 4.1.18 illustrate the displacement, velocity, and acceleration of the front end of the cask, location E, as a function of time. As can be seen, the cask was calculated to displace about 5.3 in. into the balsa wood limiter. The cask decelerates from its impact velocity of 528 in./s to zero in 20 ms (the rebound indicated in Figure 4.1.16 is fictitious and is due to the absence of a gravity field in the model). The acceleration plot exhibits levels as high as 450 g's.

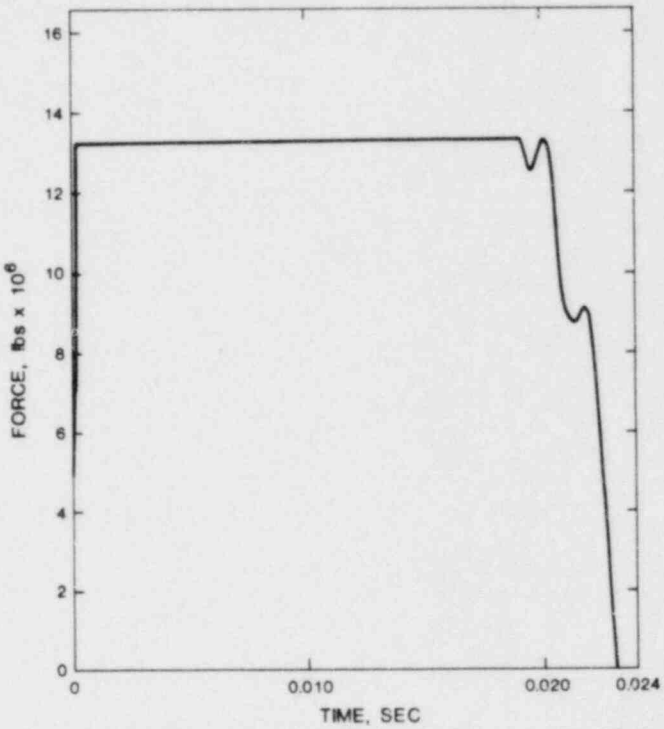

Figure 4.1.15. A Force Input to the Bottom End (Location E) of Cask vs Time for the Lead-Steel-Balsa Cask End-On One-Dimensional Impact Calculation

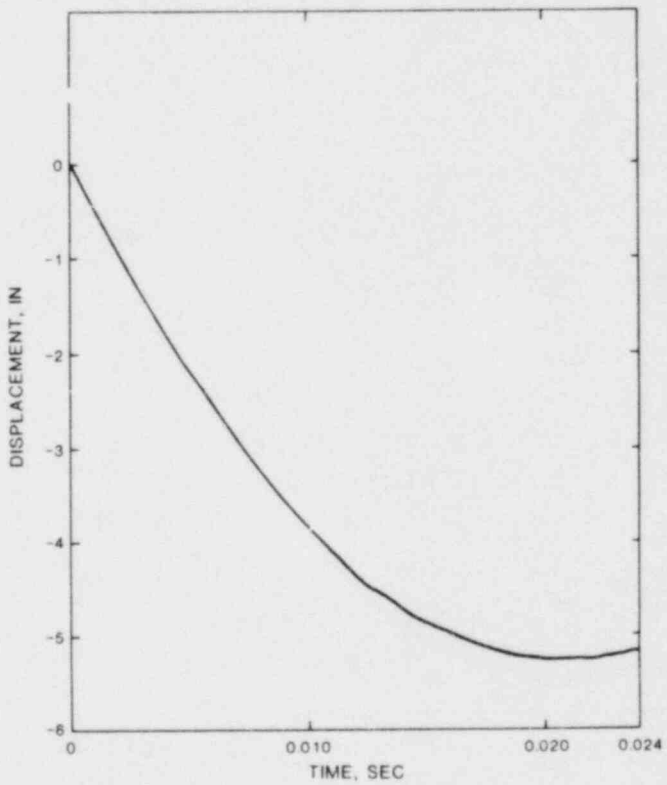

Figure 4.1.16. Displacement of Location E vs Time for the Lead-Steel-Balsa Cask End-On One-Dimensional Impact Calculation

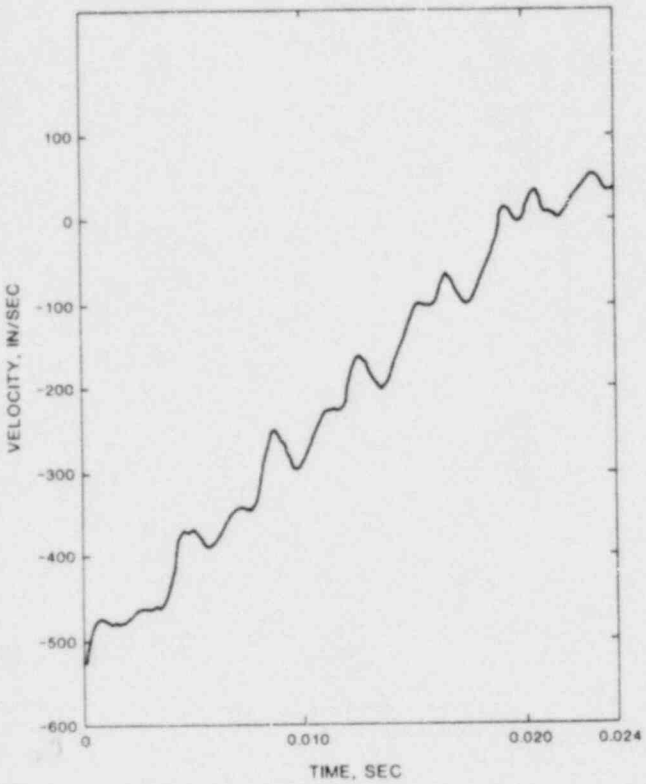

Figure 4.1.17. Velocity of Location E vs Time for the Lead-Steel-Balsa Cask End-On One-Dimensional Impact Calculation

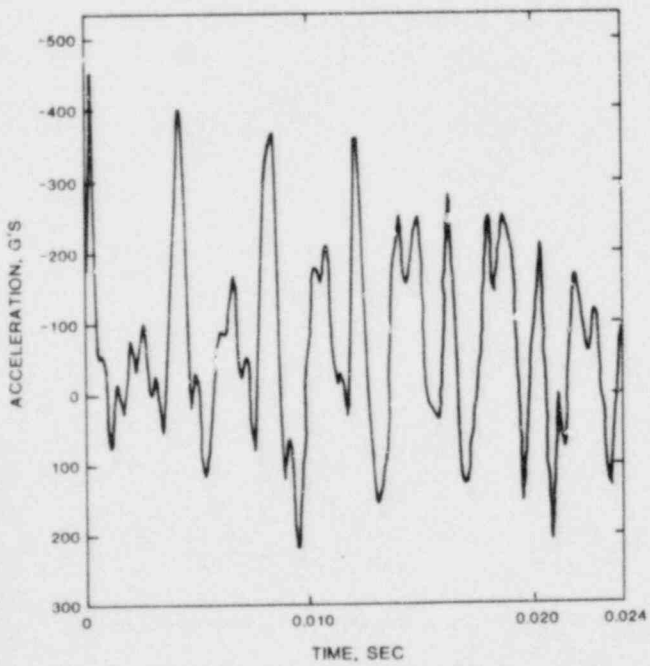

Figure 4.1.18. Acceleration of Location E vs Time for the Lead-Steel-Balsa Cask End-On One-Dimensional Impact Calculation

Results for location F, on the top end of the cask, were very similar, as can be seen by examining Figures 4.1.19, 4.1.20 and 4.1.21. The initial acceleration pulse is delayed about 2 ms and is only slightly attenuated.

The axial stress value at location C was calculated from the calculated load in coupling 2-3. The stress value was obtained by considering the load paths and dividing by the proper cross-sectional area. The stress in the stainless steel was obtained by dividing the load transmitted by the steel by the cross-sectional area of the steel. Figure 4.1.22 illustrates the results for this location. As can be seen, the peak stress was calculated to be about -20 000 psi.

The axial stress in the lead shielding material at location D was calculated from the deformation results for coupling 6-7 by computing a strain for the coupling and multiplying by the elastic modulus for lead. The resulting stress was extremely low, with the peak value being about 15 psi, as indicated in Figure 4.1.23.

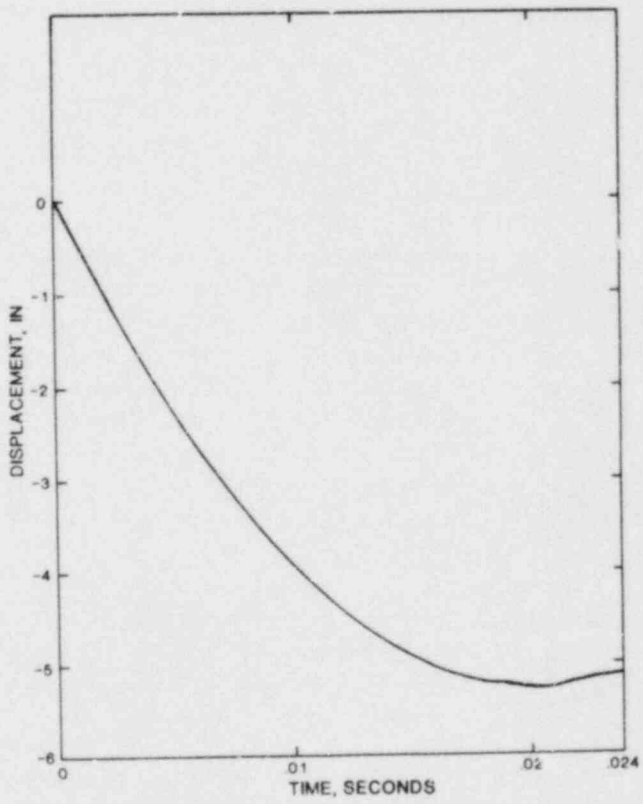

Figure 4.1.19. Displacement of Location F vs Time for the Lead-Steel-Balsa Cask End-On One-Dimensional Impact Calculation

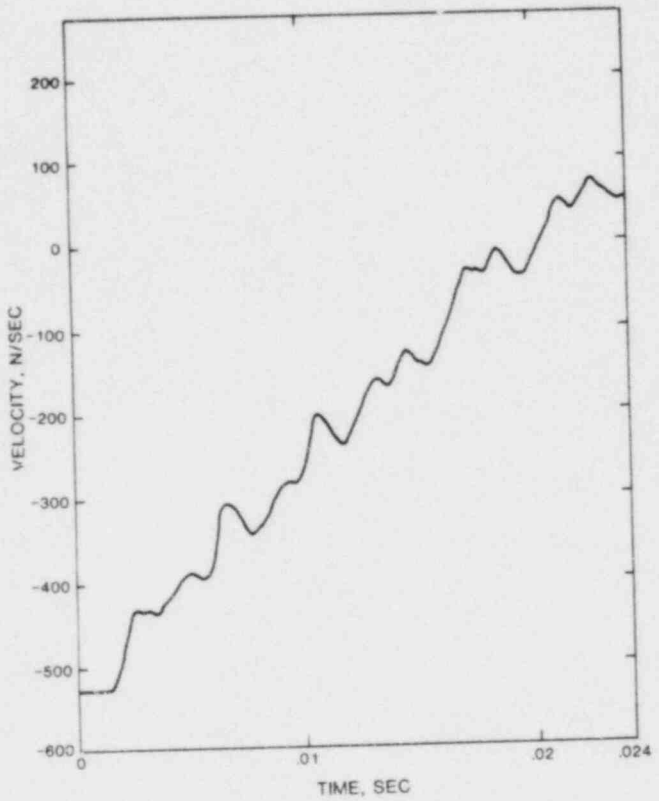

Figure 4.1.20. Velocity of Location F vs Time for the Lead-Steel-Balsa Cask End-On One-Dimensional Impact Calculation

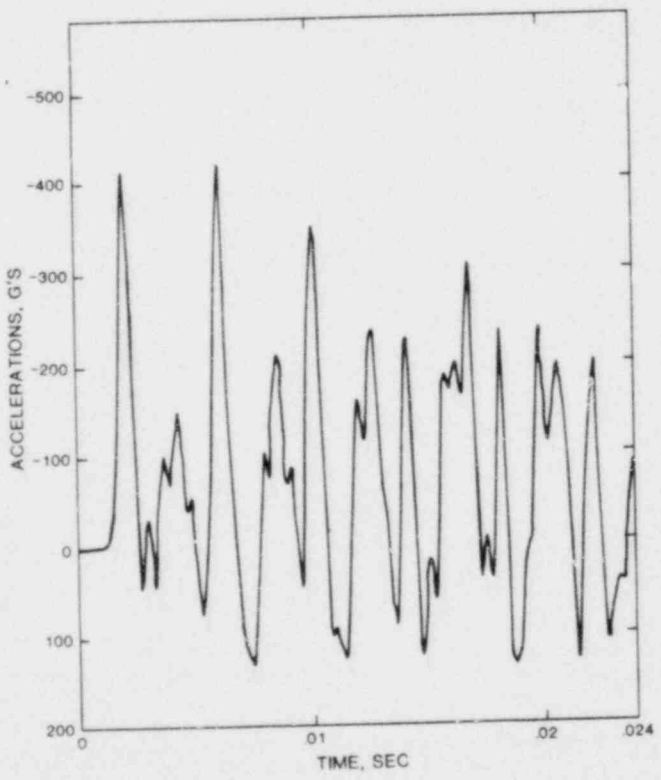

Figure 4.1.21. Acceleration of Location F vs Time for the Lead-Steel-Balsa Cask End-On One-Dimensional Impact Calculation

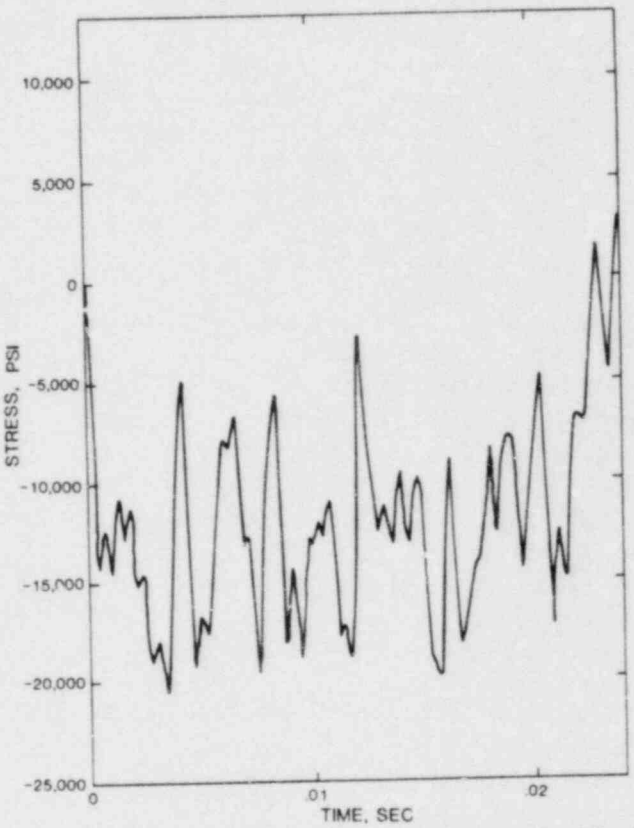

Figure 4.1.22. Axial Stress at Location C vs Time for the Lead-Steel-Balsa Cask End-On One-Dimensional Impact Calculation

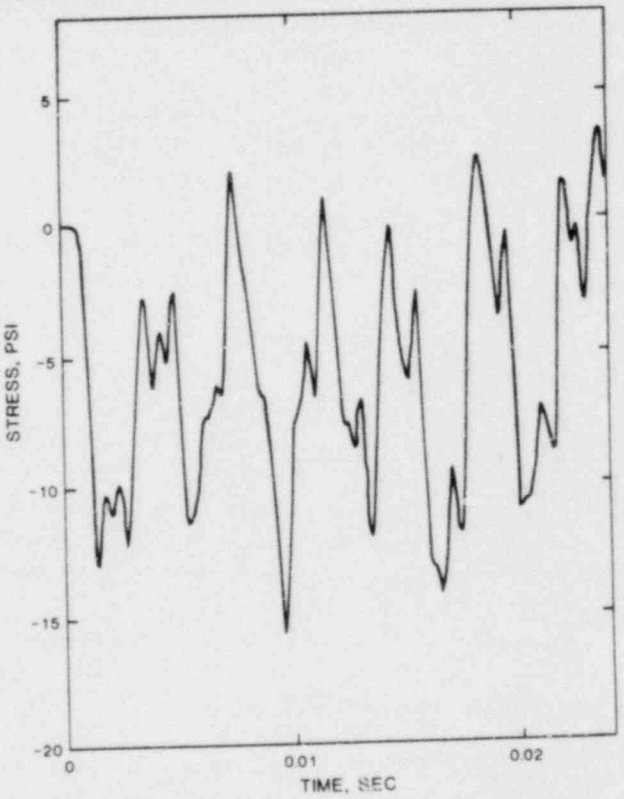

Figure 4.1.23. Axial Stress at Location D (Lead) vs Time for the Lead-Steel-Balsa Cask One-Dimensional End-On Impact Calculation

The stresses at locations A and B on the top end of the cask were computed from the load calculated for coupling 10-11 using the method described in Section 4.1.1.3. Figure 4.1.24 illustrates results for the plate center, location A, where the tangential and radial stresses are the same. The calculated peak value at this location was 40 000 psi. Figures 4.1.25 and 4.1.26 illustrate the radial and hoop stresses at location B (r = 24 in.). The tangential stress is the higher of the two, having a peak value of 30 000 psi. The peak radial stress is approximately 23 000 psi.

4.1.1.4 One-Dimensional Static Analysis

In this section, an elementary engineering stress analysis of the lead-steel-balsa cask for the end-on (vertical) impact is presented. The analysis methods used, and their implications, are discussed in Section 1.2.1.

Briefly, the lead-steel-balsa cask end-on impact dynamic problem is analyzed as an equivalent static problem. The balsa wood impact limiter is assumed to crush uniformly such that a constant deceleration of the cask body is produced. The constant deceleration expressed in g's is used to calculate a static load for use with the strength-of-materials models of the cask components. The ends of the cask are analyzed as linear elastic circular plates. The cask wall stresses are evaluated by assuming that a uniaxial state of stress is present in each wall layer. The remainder of this analysis section is directed toward calculating the stresses at cask locations A through D (Figure 4.1.1).

The first step in the static equivalent analysis of the lead-steel-balsa cask is to determine the cask deceleration. If the balsa wood impact limiter is assumed to crush uniaxially during impact at a constant crush stress, then the cask deceleration may be calculated by applying Newton's second law of motion. Accordingly, by the method of Section 4.1.1.2, the cask deceleration (d) is calculated to be 98 g's.

Each end of the lead-steel-balsa cask is a layered structure having a 4-in.-thick lead layer sandwiched between two 3-in.-thick layers of 304 stainless steel. In the present analysis, the 48-in.-dia cask end structure is modeled as three thin circular plates which function as parallel structures. The parallel function of the three plates is defined by the compatibility condition that the transverse center deflections at the plate interfaces are equal. This method of modeling is chosen because it neglects the composite behavior of the end plate due to a lead-steel bond. Thus, the present modeling of the end plate produces a more flexible structure than would be expected for a composite plate and, as a consequence, should produce conservative stress results.

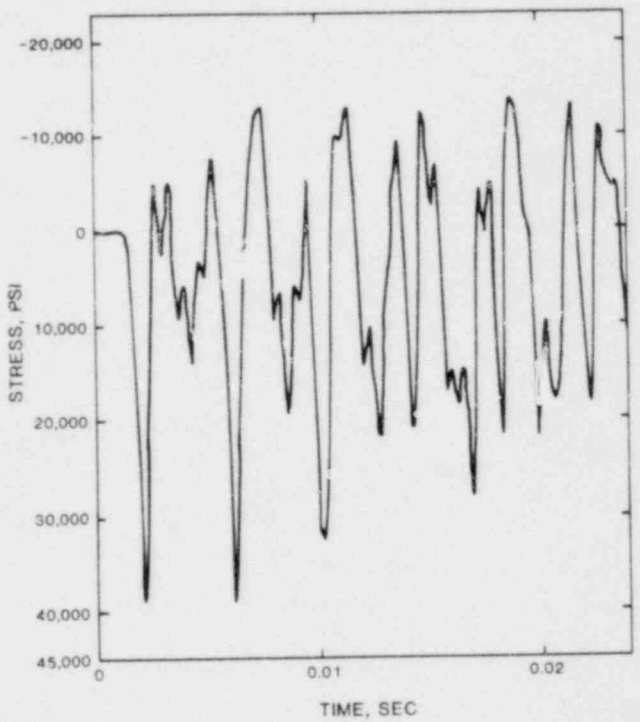

Figure 4.1.24. Tangential Radial Stress at Location A vs Time for the Lead-Steel-Balsa Cask End-On One-Dimensional Impact Calculation

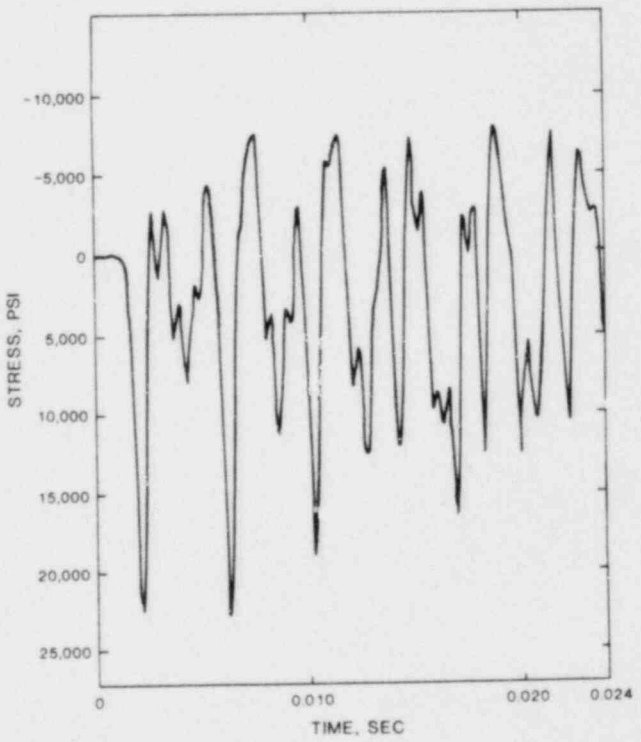

Figure 4.1.25. Radial Stress at Location B vs Time for the Lead-Steel-Balsa Cask One-Dimensional End-On Impact Calculation

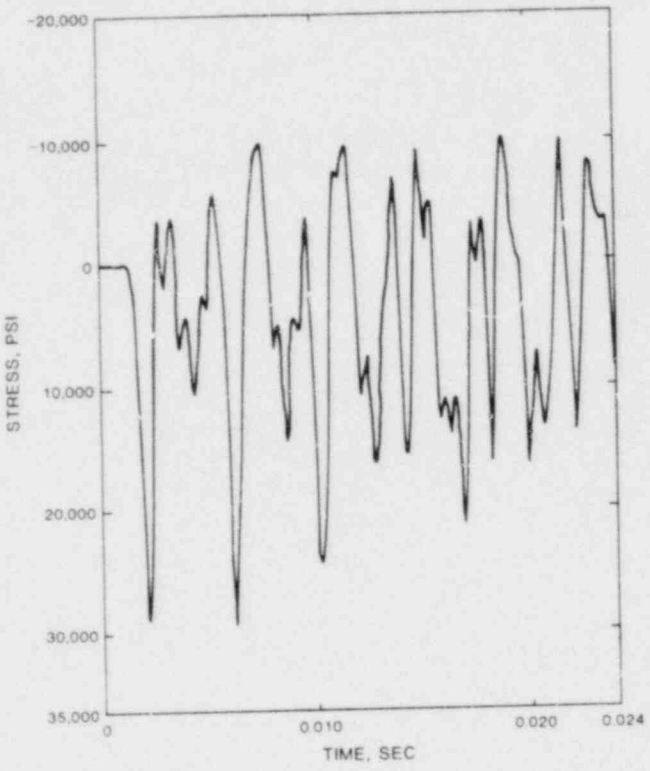

Figure 4.1.26. Tangential Stress at Location B vs Time for the Lead-Steel-Balsa Cask End-On One-Dimensional Impact Calculation

A similar modeling philosophy is used to choose the boundary conditions for the three parallel plates. Since the steel layers of the end plate are integral to the cask walls, the boundaries of the steel plates are assumed to be clamped. The boundaries of the lead plate layer are assumed to be simply supported because there is a lead-steel interface at the edges of the end plate lead layer.

The top end structure on the lead-steel-balsa cask during vertical impact is assumed to support the inertial force due to its own weight and also a bearing pressure due to the impact limiter inertial force. The bearing pressure (P_{IL}) on the end plate resulting from the impact limiter is calculated as

$$P_{IL} = \frac{W_{IL} d}{A_{IL}} = 130.2 \text{ psi} \quad ,$$

where $W_{IL} = 5694$ lbs, $d = 98.4$ g's, and $A_{IL} = 4301$ in^2

in which W_{IL} is the impact limiter weight and A_{IL} is the bearing area between the end of the cask and the impact limiter. The inertial load due to the end plate weight is expressed as a pressure load (P_p) in the following manner:

$$P_p = (2\rho_s t_s + \rho_\ell t_\ell) = 324.9 \text{ psi} \quad ,$$

where ρ_s and t_s are respectively the weight density and thickness of the stainless steel layers, and ρ_ℓ and t_ℓ are similar properties for the lead. The total impact load on the end plate is expressed as a total pressure load (P_T)

$$P_T = P_{IL} + P_p = 455.1 \text{ psi} \quad .$$

For each stainless steel plate layer with clamped edges, the lateral center deflection (y_C^S)[4.5, Table 24-10b] the internal bending moment at the plate center (M_C^S), and the internal bending moment at the plate edges (M_R^S) are given respectively by

$$y_C^S = \frac{q_s R^4}{64 D_s} \quad ,$$

$$M_C^S = \frac{1}{16} q_s R^2 (1 + \upsilon_s) \quad ,$$

and

$$M_R^S = -\frac{1}{8} q_s R^2 \quad ,$$

in which

$$D_s = \frac{E_s t_s^3}{12 (1 - \upsilon_s^2)}$$

where q_s is the plate load per unit area, R is the plate radius, t_s is the plate thickness, E_s is Young's Modulus, and υ_s is Poisson's ratio.

Similarly, for the simply supported lead plate layer[4.5, Table 24-10a] the center deflection (y_C^L) is given by

$$y_C^L = \frac{q_L R^4 (5 + \upsilon_L)}{64 D_L (1 - \upsilon_L)} \quad ,$$

in which

$$D_s = \frac{E_L t_L^3}{12 (1 - \upsilon_L^2)} \quad ,$$

where q_L is the load per unit area, R is the plate radius, t_L is the plate thickness, E_L is Young's modulus, and υ_L is Poisson's ratio.

The calculations which follow apply the assumed deflection compatibility condition, $y_c^s = y_c^L$, in order to determine the loads, q_s and q_L, supported by each plate layer.

$$D_s = \frac{(28 \times 10^6)(3)^3}{12\ [1 - (0.33^2)]} = 7.07 \times 10^7 \text{ (lb in.)} ,$$

$$y_c^s = \frac{-q_s\ (24)^4}{64\ [7.07 \times 10^7]} = -\ (7.336 \times 10^{-5})\ q_s ,$$

$$D_L = \frac{(27750)\ (4)^3}{12\ [1 - (0.42)^2]} = 1.797 \times 10^5 \text{ (lb in.)} ,$$

and

$$y_c^L = \frac{-q_L\ (24)^4\ (5 + 0.42)}{64\ (1.797 \times 10^5)\ (1 + 0.42) = -\ (0.11011) q_L} .$$

Setting the center deflection of the lead equal to the center deflection of a steel layer yields

$$q_L = (6.659 \times 10^{-4}) q_s .$$

Using superposition, the sum of the loads carried by the plate layers is equal to the total end plate load.

$$P = 2q_s + q_L ,$$

$$p = (2 + 6.659 \times 10^{-4})\ q_s = 455.1 \text{ psi} ,$$

or

$$q_s = 221.8 \text{ psi}$$

and

$$q_L = 0.15 \text{ psi} .$$

The radial and hoop stress at the centerline of the steel plate, location A in Figure 4.1.1, is given by the formula

$$\sigma_A = \pm \frac{6M_c^2}{ts^2} = \pm \frac{3q_sR^2(1 + \upsilon_s)}{8ts^2}$$

$$\sigma_A = \pm \frac{3\ (221.8)\ (24)^2(1 + 0.33)}{8\ (3)^2}$$

$$= \pm 7\,080 \text{ psi} .$$

And the radial stress and the hoop stress at the outer edge of the top steel plate layer, location B, is given by

$$\sigma_B^{radial} = \pm \frac{6M_R^s}{ts^2} = \pm \frac{3q_sR^2}{4ts^2}$$

$$= \pm \frac{3(221.8)(24)^2}{4(3)^2} = \pm 10\,646 \text{ psi}$$

and

$$\sigma_B^{hoop} = \upsilon_s\ \sigma_B^{radial} = \pm 3\,193 \text{ psi} .$$

The impact stresses in the cask wall are calculated for location C and D in Figure 4.1.1. The impact force supported by the wall is assumed to produce a compressive uniaxial state of stress as discussed in Section 4.1.1.3.

Location C is in the interior stainless steel layer toward the impact end of the cask body, adjacent to where the radiation shield layers end. The impact force of the wall, the end plate, and the top impact limiter is assumed to produce a compressive uniaxial stress state in the steel layers of the cask walls. The wall weight load is conservatively calculated to be the empty weight of the cask (164 000 lb) less the weight of one impact limiter (5 694 lb) and one end plate (5 975 lb) or a weight load (W^c) of 152 331 lb. Then, the axial stress at location C is

$$\sigma_c = -\frac{W^cd}{A^c} = -20\,341 \text{ psi} ,$$

where d = 98.4 g's and A^c = 736.9 in^2 and where A^c is the cross-sectional area of the steel layers. The lead wall layer is neglected as a load-carrying structure in the above calculation.

At location D in the side wall lead layer, the axial stress is assumed to be due to the weight of the lead in the wall. Consequently, it is assumed that there is no structural bonding between the steel shells and the lead shielding. The weight of the lead, W^D, above location D is

$$W^D = (0.401)\frac{\pi}{4}[(55)^2 - (49)^2]\ (87) = 17\,098 \text{ lb} .$$

Then the axial stress at location D is

$$\sigma_c = -\frac{W^Dd}{A_D}$$

$$= -\frac{(17098)\ (98.4)}{\frac{\pi}{4}\ [(55)^2 - (49)^2]} = -3\,433 \text{ psi} .$$

4.1.2 Comments on Accomplishing Analyses

Several major assumptions have been made which must be verified if the preceding analyses are to be assumed to be correct. The effectiveness of the balsa impact limiter is severely degraded if it is not confined to crushing in a one-dimensional mode along

the longitudinal direction of the wood. The design has no provision to confine the balsa, as would be necessary in an actual cask design. As stated before, the crushable foam model would be a better material model for the two-dimensional transient analysis. After the analyst obtains a value of stress or displacement at critical locations on the cask an assessment as to the safety of the cask must be made, and this study has not attempted to undertake the assessment. Only an elastic analysis of the steel components of the cask was necessary for this comparison of methods, but the situation may be different if residual stresses due to temperature are to be included. It was also assumed that the lead was bonded to the steel in the cask during impact. If this is not the case, the stresses in the steel wall at location C would definitely increase. Again, residual stress may play a role in the results at location C. When the finite element technique is used, the actual values of the stress components will vary slightly with the individual analyst, depending upon how the mesh is defined to describe the object. The main ingredient in obtaining an accurate calculation of the stress components is experience on the part of the analyst.

4.1.3 Comparison of Results for the Lead-Steel Cask

Some results have been tabulated for purposes of making comparisons between the different stress analysis methods. These results are included in Tables 4.1 and 4.2. Table 4.1 also includes results from the analysis included in the materials section (Figure 3.6), where the cask was lumped into a very dense volume behind the balsa wood impact limiter, which was modeled as an elastic-plastic material.

Table 4.1 lists the maximum cask displacement (impact limiter crush), the average deceleration, and the time to reach the maximum displacement. The average acceleration is simply computed by dividing the velocity change (the impact velocity) by the calculated time to reach the maximum displacement. As can be seen by examining Table 4.1 the average deceleration values ranged from 72 to 119 g's. It is apparent here that the one-dimensional dynamic technique indicated a significantly lower value. The reason for this can be traced to the assumption that was made regarding the effective crush area of the balsa wood impact limiter (see Section 4.1.1.3). In retrospect, the crush area which was assumed was probably on the low side.

The deceleration values indicated in Table 4.1 are only average values and are what one might expect if the cask behaved as a perfectly rigid body and the impact limiter provided a smooth deceleration force. In reality, different points on the cask will see different oscillating acceleration traces with high peaks and a broad range. For example, although the calculated average cask acceleration is about -100 g's, both the one- and the two-dimensional dynamic analysis indicated peak g values of about -400 on the solid part of the cask immediately behind the impact limiter. Acceleration levels were amplified even more at a point on the center of the cask's bottom plate (Point A). Here peak acceleration values of -1300 g's were calculated with the two-dimensional dynamic analysis. This, however, represented a fairly high frequency vibration (~1200 Hz).

The dynamic analyses indicate peak stress values that can be considerably higher than those that would be calculated using a static technique. For example, if one considers the locations at the bottom of the cask (Points A and B) the static analyses indicate stress levels that are below 10 000 psi. The dynamic analyses, however, indicate stress excursions to 40 000 psi, but these stress waves are high frequency and of questionable significance. The bottom plate locations (Points A and B) are where the greatest deviations between the dynamic and static analyses occur. Much better agreement was obtained at locations C and D. If one examines the results for the axial stress at point C, which is on the inner stainless steel shell near the impact end, it can be seen that there was less deviation in stress levels among the different techniques than occured at other locations. The static analyses indicated a stress level of

Table 4.1. Kinematic Comparison of Dynamic Analyses, End-On Impact of Lead-Steel-Balsa Cask

Analysis Type	Maximum Displacement (in.)	Average Acceleration (g)	Time to Reach Maximum (s)
2D Dynamic Rigid Case (Figure 3.6)	-3.3	-119.0	0.0115
2D Dynamic Location E (Figure 4.1.5)	-3.6	-98.0	0.014
1D Dynamic Location E (Figure 4.1.25)	-5.3	-72.0	0.019
2D and 1D Static	--	-98.0	--

Table 4.2. Stress Components Comparison, End-On Impact of Lead-Steel-Balsa Cask

Analysis Type		σ_r	σ_z	σ_{rz}	σ_θ	σ_e
LOCATION A						
2D Dynamic	maximum	27 300	630	2 310	27 300	28 400
	minimum	-10 000	-1 100	-1 200	-10 000	--
2D Static		3 967	-20	761	3 967	5 939
1D Dynamic	maximum	40 000	--	--	40 000	40 000
	minimum	-13 000	--	--	-13 000	--
1D Static		7 080	--	--	7 080	7 080
LOCATION B						
2D Dynamic	maximum	8 000	810	1 [illegible]	1 500	11 000
	minimum	-6 100	-1 360	-700	-7 600	--
2D Static		-782	-97	365	2 294	4 056
1D Dynamic	maximum	23 000	--	--	30 000	27 200
	minimum	-7 000	--	--	-10 000	--
1D Static		10 646	--	--	3 194	9 462
LOCATION C						
2D Dynamic	maximum	3 400	8 000	1 690	300	33 300
	minimum	-1 100	-39 000	-300	-24 000	--
2D Static		-935	-22 745	1 126	-5 940	36 473
1D Dynamic	maximum	--	4 000	--	--	21 000
	minimum	--	-21 000	--	--	--
1D Static		--	-20 341	--	--	20 341
LOCATION D						
2D Dynamic	maximum	158	111	216	104	177
	minimum	-112	-106	-141	-92	--
2D Static		-5	-13	89	-5	205
1D Dynamic	maximum	--	3	--	--	3
	minimum	--	-16	--	--	16
1D Static		--	-3 433	--	--	3 433

*σ_e is the effective or von Mises stess.

about -20 000 psi and the two-dimensional dynamic analysis indicated a peak level of -39 000 psi. The one-dimensional dynamic results indicated a peak level of -21 000 psi, which is very much in agreement with the static results. However, it should be remembered that in this analysis the impact limiter was probably modeled on the soft side as it produced a rigid body deceleration that was about 30% lower than the other techniques. Had the impact limiter been modeled stiffer to produce comparable rigid body decelerations, the peak stress values calculated with this technique would have been higher than the levels obtained using the static techniques.

In comparing static results for the bottom plate (Points A and B), the one-dimensional technique produced stress levels that were higher than those obtained with the two-dimensional analysis. At location C the two static techniques produced results that agreed quite well.

All methods except the one-dimensional static gave stress results for the location in the lead shielding material (Point D) which were very comparable and quite low, as can be seen by examining Table 4.2. The one-dimensional static technique produced results which were very significantly higher. The reason for this is that the lead was assumed to be completely unbonded to the steel.

Further discussion of the techniques will be included in the conclusions section (5.0) after the description of the uranium-steel cask analysis.

4.2. Uranium-Steel Cask

The analysis of the uranium-steel cask is more involved than the lead-steel-balsa cask because the impact limiter is a set of metal fins. The analysis method can vary from applying test data to obtain the acceleration loads or forces imposed on the cask during crushing of the fins to a complete three-dimensional finite-element, large deformation, elastic-plastic analysis of a circumferential section including one fin and a section of the cask. The radial-axial symmetry planes between each fin could be used in a three-dimensional analysis. Since it would be very expensive to do the complete three-dimensional analysis and since the fins act on a very stiff location on the cask, the analysis was separated into two parts. First, a fin was modeled both two- and three-dimensionally to obtain loads for the analyses of the cask without the fins. A weight was attached to the fin to simulate the cask portion associated with one fin. (If the fins had been supported by the end plate of the cask, it probably would not have been possible to separate the analysis into two parts.)

The four different methods used to analyze the lead-steel-balsa cask were applied to analyze the uranium-steel cask with the fins removed. The first analysis is an axisymmetric, two-dimensional, transient finite element analysis of the cask. The applied load, a time varying force between the essentially unyielding target and the fin, predicted by the three-dimensional fin analysis was used as a time varying pressure on the end of the cask. The second technique is a two-dimensional static simulation of the dynamic problem and is accomplished by using a static finite element calculation and applying a constant axial acceleration to the cask without the fin impact limiters. The third technique is the lumped-mass one-dimensional transient solution. The fourth technique is the static strength-of-materials approach with a constant value of acceleration as the load.

In choosing the location at which to compare the four different analysis techniques, the same philosophy was used as for the lead-steel-balsa end-on impact calculation. The locations are shown on Figure 4.2.1, an outline of the axisymmetric parts of the cask. At locations A, B, E, and F, the response in terms of the stress components and the effective stress of the end plates was monitored. The kinematic response of the end plates at locations A and F was also chosen. At location C, the stress in the steel shell due to the pressure exerted by the uranium was compared along with the stresses in the uranium at D. The overall kinematic response at locations H and G was also compared. Locations E and F were included for the end plate on the impacting end because, unlike the lead-steel-balsa cask, the end plate is not supported by the impact limiters, and therefore significant stresses are expected at these locations.

4.2.1 Fin Impact Analysis

4.2.1.1 Three-Dimensional Dynamic Analysis

Before the four methods of analyzing the cask are presented, the analysis of a fin will be discussed. The computer code WULFF,[46] which is capable of obtaining the large deformation, elastic-plastic response of the fin, was used for the three-dimensional calculation. Other analyses of impact fins have been conducted using the WULFF program.[47,48] In Reference 4.7, when a mild steel was used, very good agreement between experimental[49] and calculated values of the energy absorption characteristics of the fins was obtained. For the geometries considered, strain rate effects are apparently not important; however, force versus time (e.g., acceleration versus time using experimental results and theoretical calculations) were

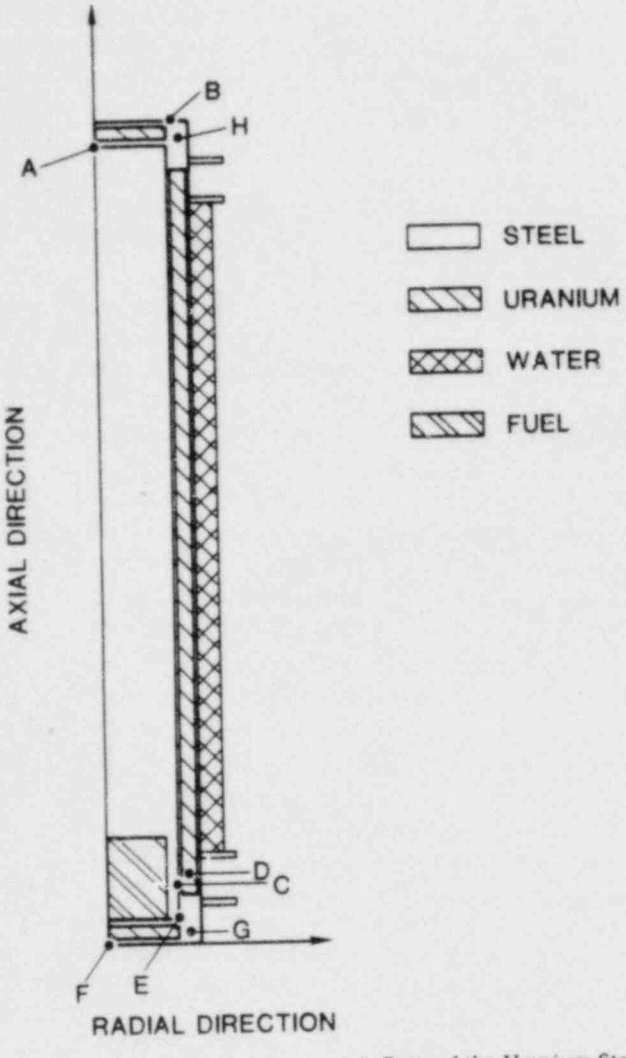

Figure 4.2.1. Outline of Axisymmetric Parts of the Uranium-Steel Cask.

not compared in Reference 4.7. In Reference 4.8 the experimental data showed significant strain rate sensitivity for 304 stainless steel, which is the material considered here. This effect was so important that correlation between dynamic analysis and dynamic experimental results for this report was not possible because a strain-rate-sensitive material model was not available in WULFF. However, when static test results were compared with a velocity-controlled dynamic calculation, the correlation was good. The velocity-controlled dynamic calculation is achieved by holding one end of a fin fixed and moving the other end at a constant velocity while a transient dynamic calculation is performed. Such factors as height-to-width ratio and the amount of lateral imperfection may play major roles when the material used is strain rate sensitive. The three-dimensional analysis is included here as an example of how it is accomplished, but will only be valid when a good strain rate material model is used or the material is strain rate insensitive.

From previous analyses[4.8] it was determined that 14 elements in the impact direction and 2 elements through the thickness were adequate for modeling the fin.

Since the fins are equally spaced circumferentially around the cask, a plane of symmetry exists between every pair of fins. A plane of symmetry exists on either side of the fin (Figure 4.2.2), and only one fin need be modeled. The 10 elements at the bottom of the model represent the weight of a section of the remainder of the cask.

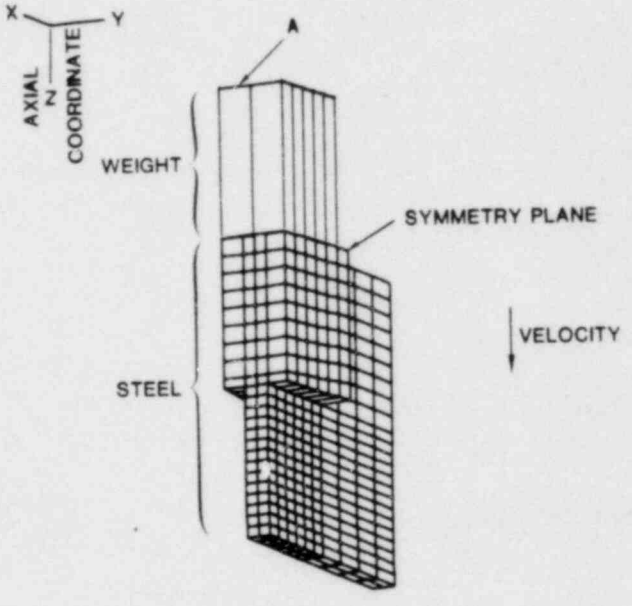

Figure 4.2.2. Finite Element Mesh for Three-Dimensional Fin Impact Analysis.

The model was given a velocity of 528 in./s (30-ft-drop condition) and the downward motion was resisted by the Winkler spring foundation on the end of the fin. Each node on the end of the fin was resisted by a spring with a stiffness of 10^7 lb/in. when its end plane moved past its original position. The springs were necessary because the number of nodes in contact with the plane varies in time. In similar fin studies,[4.8] the value of the stiffness was varied and 10^7 lb/in. was found to give a stiffness low enough so that instabilities did not develop, only a small amount of rebound occurred at early times, and only a small penetration of the foundation was calculated. The total force in all the resisting springs at each time step was summed and the results are shown in Figure 4.2.3. The acceleration, velocity, and displacement, as a function of time in the z direction at node A on the

weight, are shown in Figures 4.2.4, 4.2.5, 4.2.6. The deformed shape of the fin at 7.00 and 7.75 x 10^{-3} s after impact, which is close to the time when the velocity of the weight is zero, is shown in Figures 4.2.7 and 4.2.8.

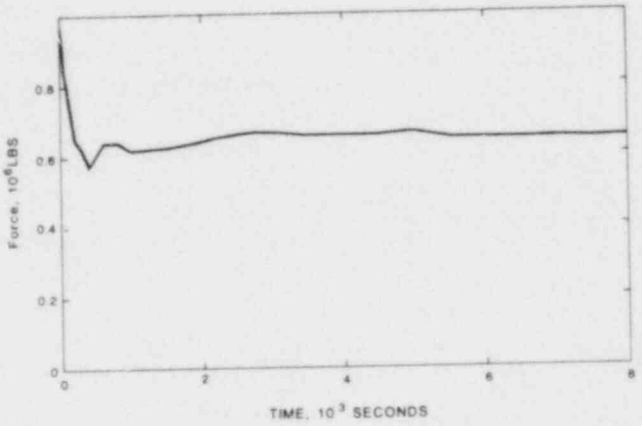

Figure 4.2.3. Total Force vs Time on End of Fin From Three-Dimensional Transient Analysis.

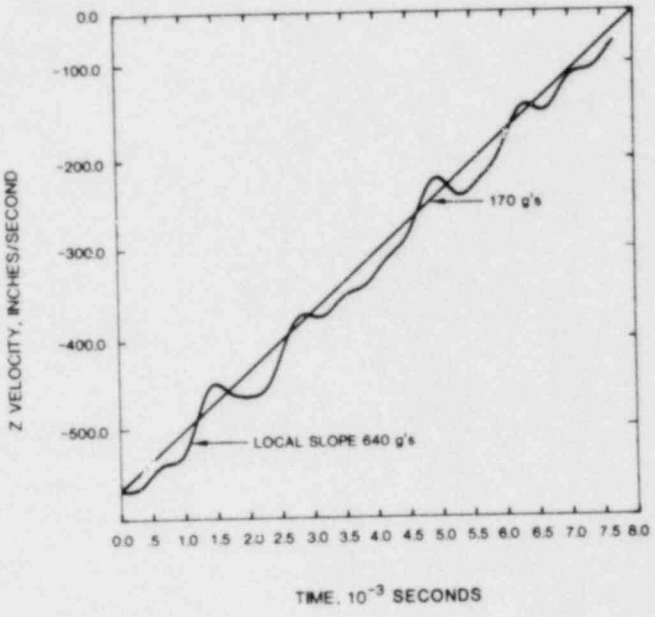

Figure 4.2.5. Z Veloicity vs Time for Simulated Cask.

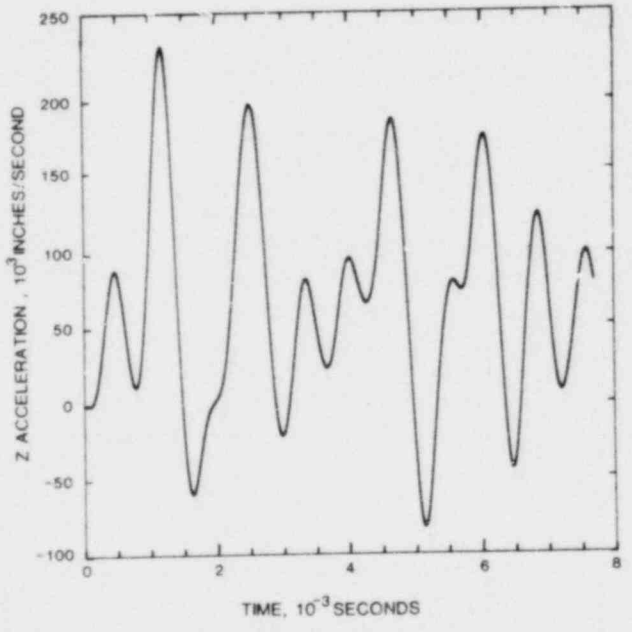

Figure 4.2.4. Z Acceleration vs Time for Simulated Cask.

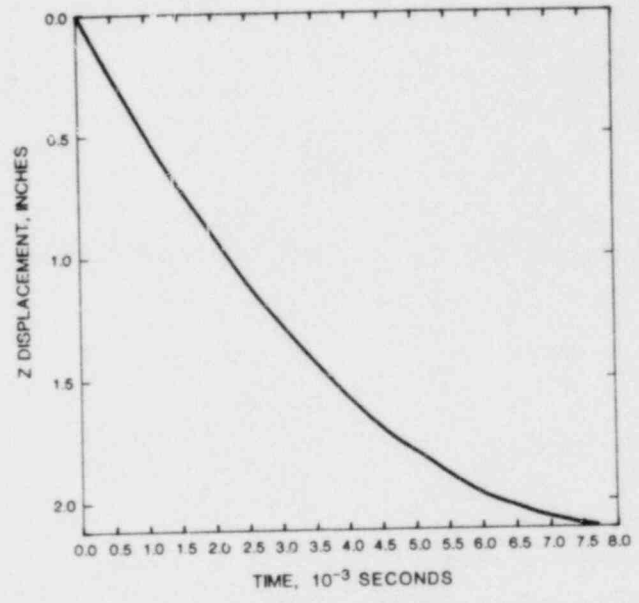

Figure 4.2.6. Z Displacement vs Time for Simulated Cask.

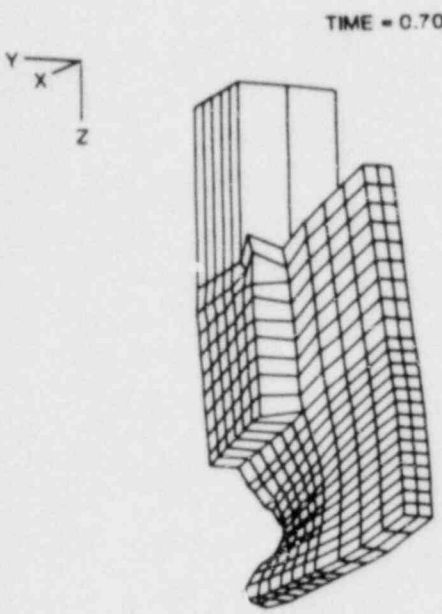

Figure 4.2.7. Deformed Mesh of Fin at 7.00×10^{-3} s After Impact.

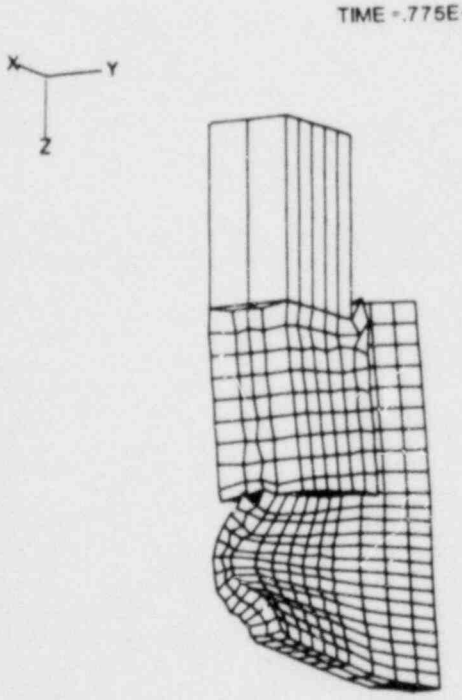

Figure 4.2.8. Deformed Mesh of Fin at 7.75×10^{-3} s After Impact.

An average acceleration of approximately 170 g's was calculated from Figure 4.2.5, and a maximum displacement of the weight of 2.2 in. in 8.00×10^{-3} s was obtained. A maximum acceleration of approximately 640 g's was also obtained from Figure 4.2.4. After the initial spike each fin presents an essentially constant 650 000-lb force to the body of the cask. The assumption most important to the analysis is the pinning of the top of the fin to prevent its movement in the y (lateral) direction. This assumption is substantiated by tests.[4.8] If, however, the fin does not hit vertically and slides laterally, its energy absorption capability will be less.

Much difficulty was encountered in performing the analysis when the steel material directly above the fin was considered to be elastic. Severe distortions of the bottom of the fin occurred. When elastic-plastic properties were used, part of the section deformed plastically, absorbing some of the impact, and therefore keeping extremely high strains from occurring at the base of the fin. It should be noted that if a sealing ring were located in the section of cask directly above the fin, then the severe rotations about the circumferential directions could jeopardize the integrity of the seal. The computer time to calculate the response for an analysis of the fin was approximately 3.0 h of CDC 7600 central processor time.

4.2.1.2 Two-Dimensional Dynamic Analysis

The purpose of the two-dimensional analysis of the fin impact limiter is to calculate a characteristic average deceleration of the uranium-steel cask for use in the elementary stress analysis presented in Section 4.2.2.4. A plane strain finite element analysis of the large-displacement, elastic-plastic, time-dependent fin impact problem is obtained by using the HONDO computer code.[4.2] The plane strain theory allows displacements in the two-dimensional plane of the model but lateral strain is set to zero.

The finite element model of the 304 stainless steel fin is shown in Figure 4.2.9. The model represents a unit slice of the 1.25-in.-thick x 8.0-in.-high fin. The finite element model has 6 elements through the thickness and 38 elements along the height. In order to initiate buckling, the fin is given an initial curvature such that the maximum deviation from a straight fin is 10% of the fin thickness.

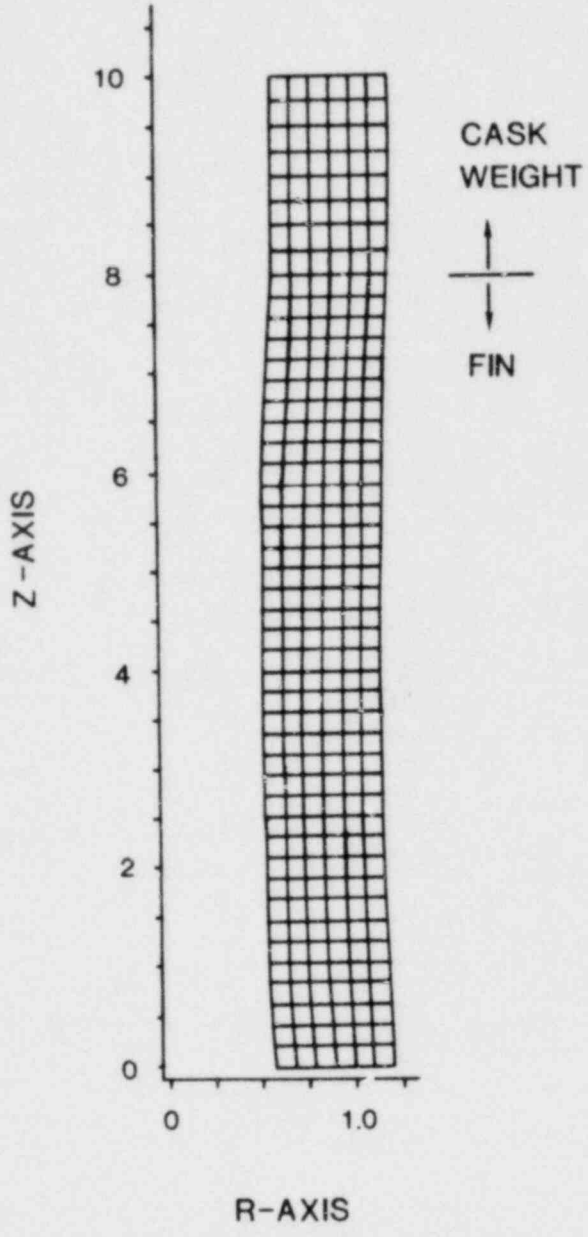

Figure 4.2.9. Cask Fin Finite Element Model

The cask weight is modeled with the 1.25 x 2.0 in. area at the top of the fin model (Figure 4.2.9). The weight density of this area is adjusted to a value such that the weight simulates the portion of the cask stopped by a unit slice of the fin. The total radial length of each fin is assumed to be effective in dissipating the impact energy.

The initial impact conditions are set by giving the finite element model a 528 in./s velocity in the z direction. As in Section 4.2.1.1, the rigid target is modeled with a Winkler spring foundation attached to the impact end of the fin model. The radial displacements of the cask portion of the fin model are fixed to simulate no rotation of the cask about its longitudinal axis. Also, the radial displacements of the impact end of the fin are fixed so that no sliding occurs between the fin and the rigid target.

According to the analysis results, the fin impact limiter deforms 1.18 in. in absorbing the cask impact energy in 4.25 ms. The deformed shape of the fin model is shown in Figure 4.2.10. The acceleration and

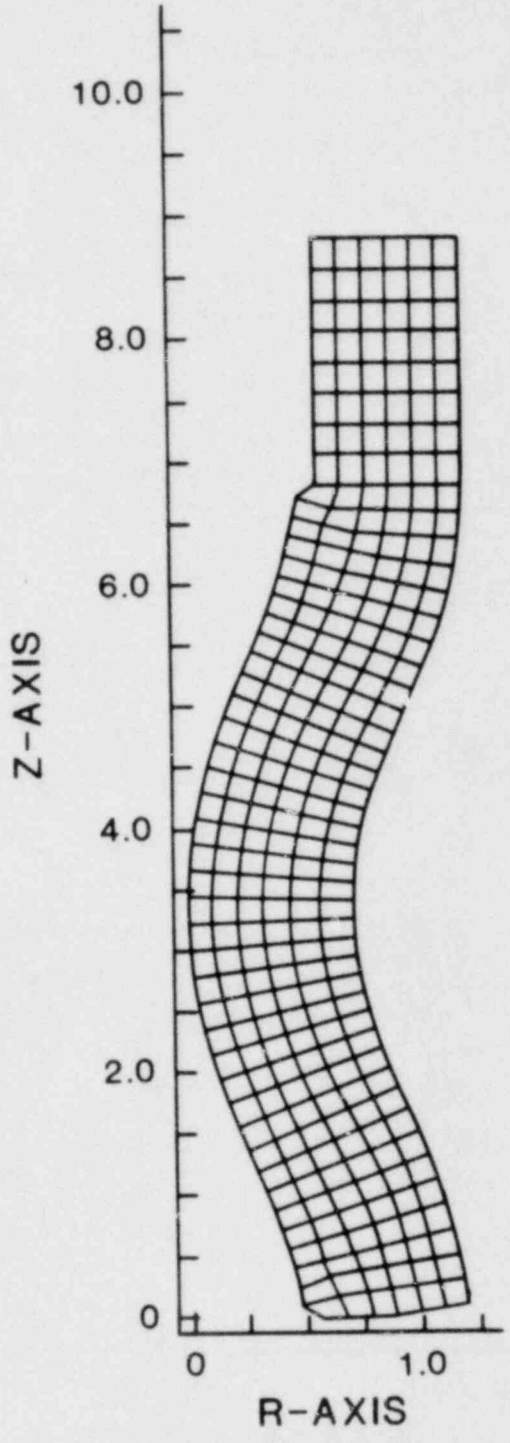

Figure 4.2.10. Deformed Fin Model at 4.25 ms

velocity for a representative cask model point are presented in Figures 4.2.11 and 4.2.12, respectively. The nodal point is chosen on the line separating the fin portion of the model from the cask portion and at the center of the fin thickness. An average cask deceleration of 345 g's is obtained from the velocity change of the cask over the 2.0- to 2.25-ms time period. The finite element analysis with HONDO took about 1420 s of CDC 7600 central processor time for one computer run.

The present two-dimensional analysis predicts a cask deceleration load twice as large as the three-dimensional analysis of Section 4.2.1.1. The reason the present analysis produces a larger deceleration is the assumption that the entire radial length of each fin is fully effective in dissipating the impact energy (Figure 4.2.13). However, apparently only the portion of each fin directly under the cask body is fully effective in absorbing impact energy. As seen in Figure 4.2.13, the length of the fin directly under the cask body is approximately one-half the total radial length of the fin. Since the deceleration force is directly proportional to the fin length assumed, a fin length that is too large would produce a high deceleration.

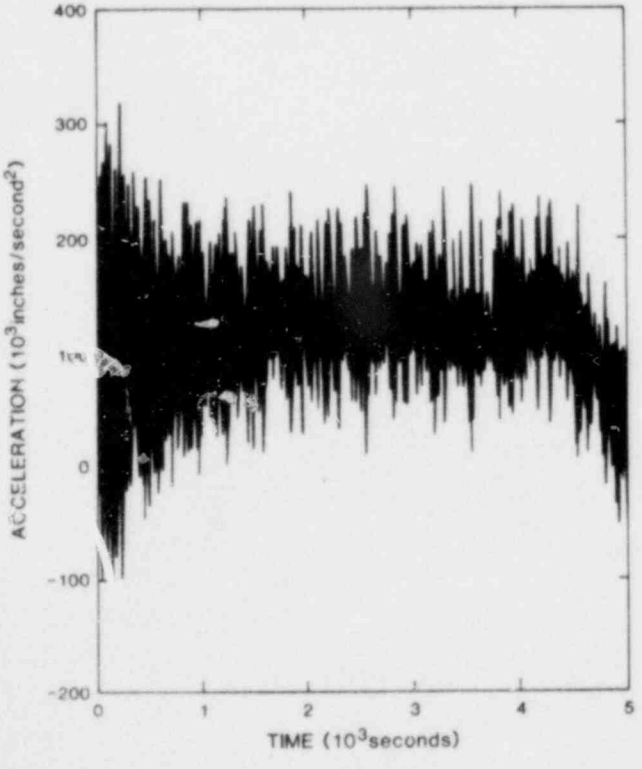

Figure 4.2.11. Cask Acceleration During Impact

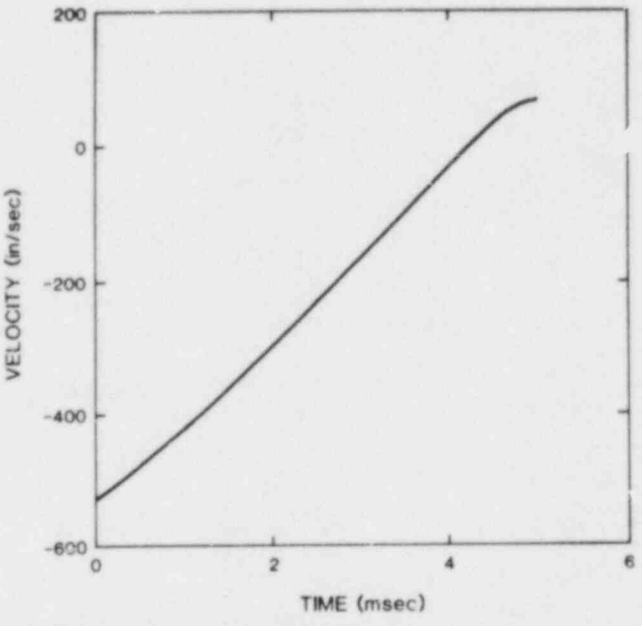

Figure 4.2.12. Cask Velocity During Impact

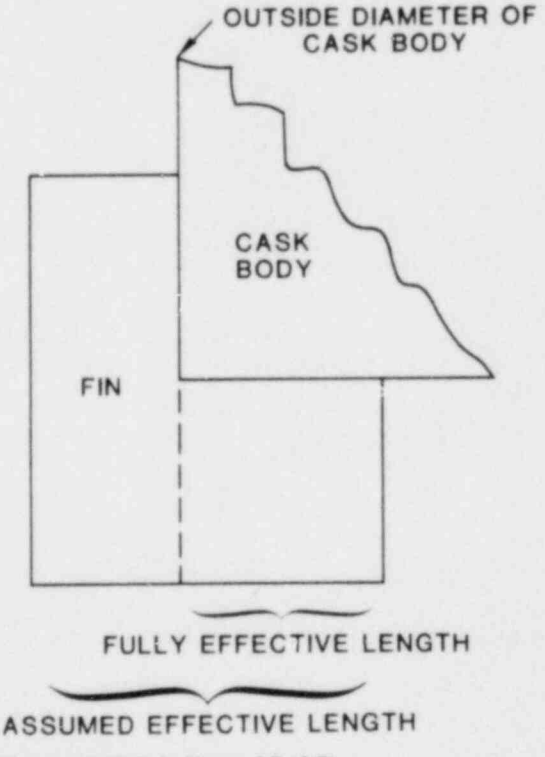

Figure 4.2.13. Side View of End Fin

4.2.2 Cask Analysis

4.2.2.1 Two-Dimensional Dynamic Analysis

The two-dimensional transient analysis of the uranium-steel cask proceeds as with the lead-steel-balsa cask. The outline of the axisymmetric finite element model showing material interfaces is shown

in Figure 4.2.1. The finite element model is shown in Figure 4.2.14, which was obtained with the QMESH[41] program. The cask was modeled with two elements through each steel section and three elements through each uranium section. As with the lead-steel-balsa cask, several locations were chosen at which to compare the results of the various analyses. The model contains 384 elements and 448 nodes. The boundary conditions consist of an initial axial velocity of -528 in./s with an applied pressure-versus-time force applied to the surface at which the end fins are attached. The pressure-versus-time input is obtained by mutiplying the force in Figure 4.2.3 (three-dimensional fin analysis) by 32, the number of fins, and dividing by the circumferential area of the surface where the fins are attached.

The water, water jacket and the four circumferential fins were not modeled because it was not felt that the structural response of these components was important in the end-on impact. The material properties for the weight simulating the fuel were Young's modulus = 500 000 psi, Poisson's ratio = 0.3 and a density of 0.0026697 lb/s²/in.⁴ No structural capability was expected of the fuel. A computer time of 500 s was needed for the calculations. The results of the dynamic two-dimensional calculations for locations A through H are shown in Figures 4.2.14 through 4.2.28.

The responses at points A and B are greatly influenced by the vibration of the end plate on the rear of the cask. The response at C is due to the weight of the cask above this point and the pressure exerted on the steel shell by the uranium. The response of the bottom end plate is forced by its own weight plus the entire weight of the fuel. It should be noted that the finite element model is underweight by 5 800 lb, or 4.8%, because the outside water jacket and the fins were not included. When comparing this analysis to the other analyses, the 4.8% less weight is unimportant.

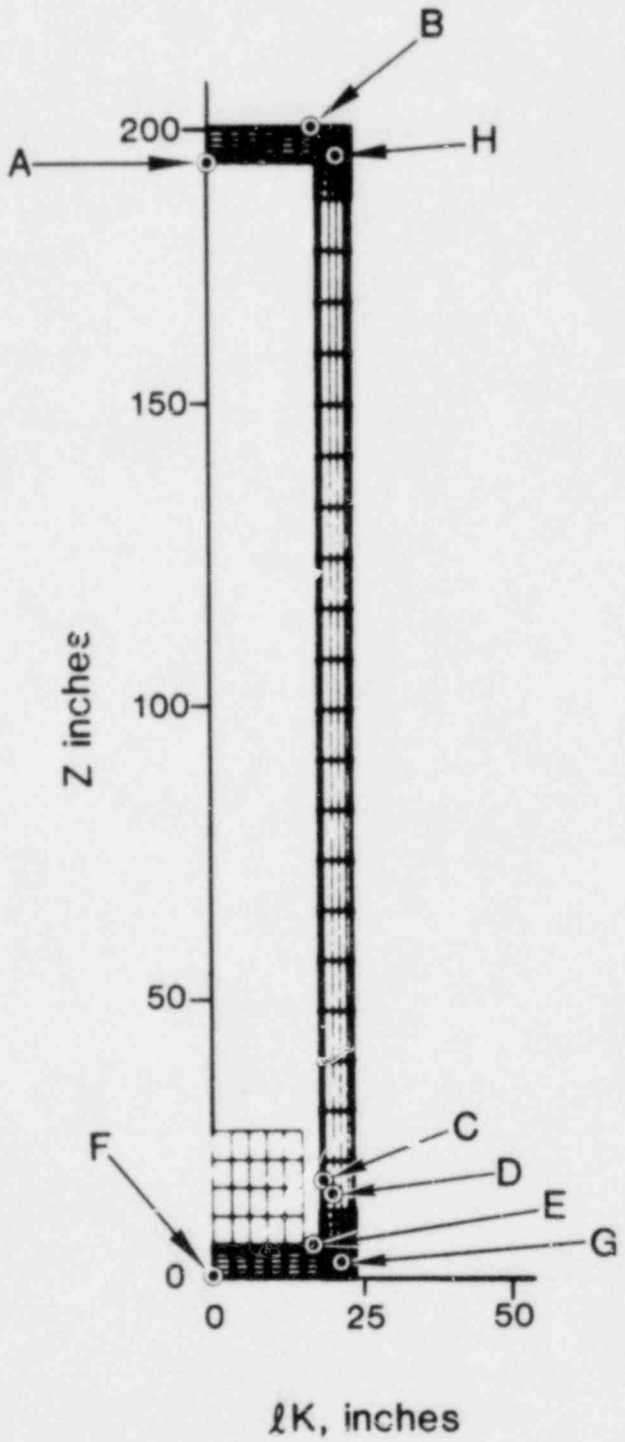

Figure 4.2.14. Axisymmetric Finite Element Model of Uranium-Steel Cask Without Fins

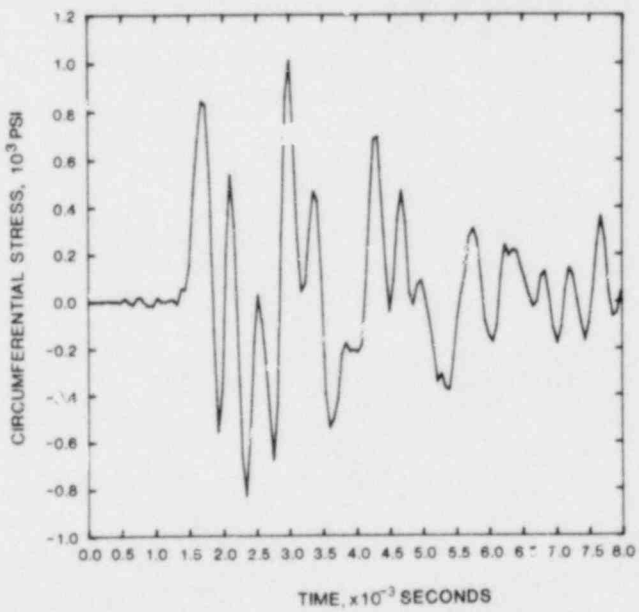

Figure 4.2.15. Circumferential Stress vs Time at Location A for the Uranium-Steel Cask End-On Two-Dimensional Impact Calculation

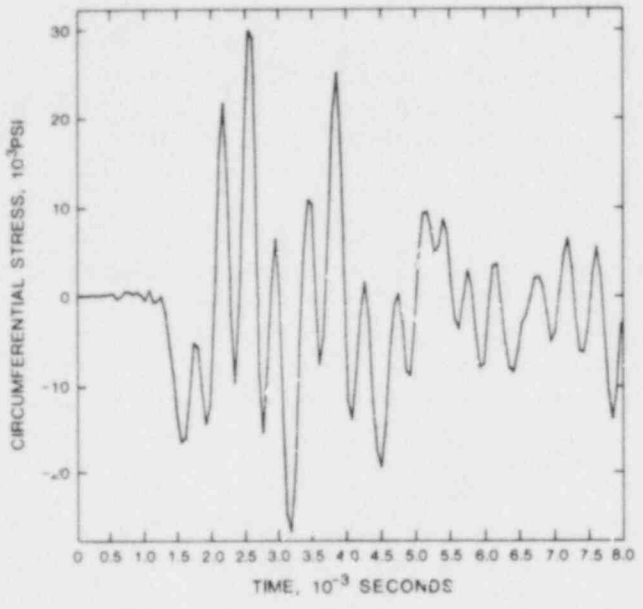

Figure 4.2.16. Circumferential Stress vs Time at Location B for the Uranium-Steel Cask End-On Two-Dimensional Impact Calculation

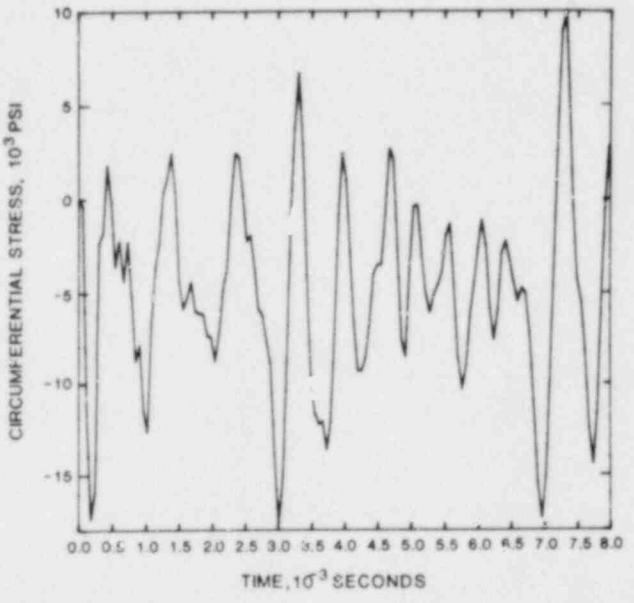

Figure 4.2.18. Circumferential Stress vs Time at Location C for the Uranium-Steel Cask End-On Two-Dimensional Impact Calculation

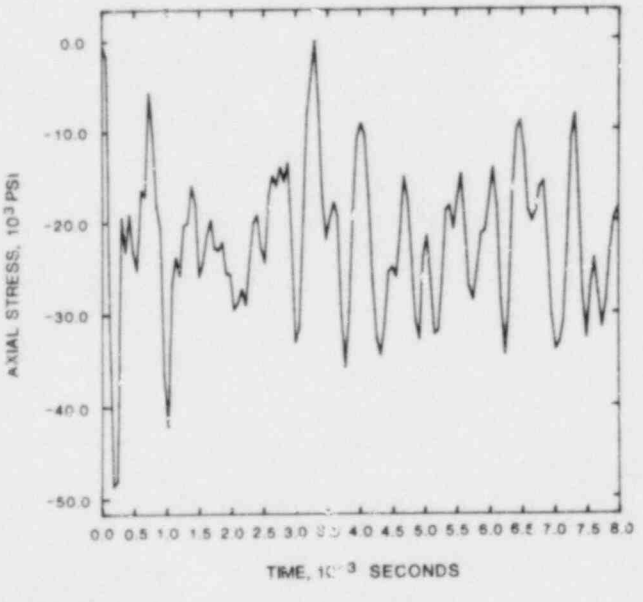

Figure 4.2.17. Axial Stress vs Time at Location C for the Uranium-Steel Cask End-On Two-Dimensional Impact Calculation

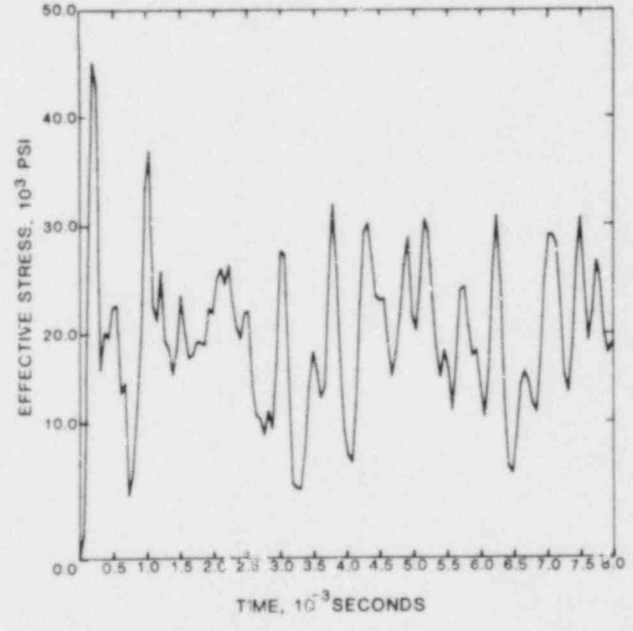

Figure 4.2.19. Effective Stress vs Time at Location C for the Uranium-Steel Cask End-On Two-Dimensional Impact Calculation

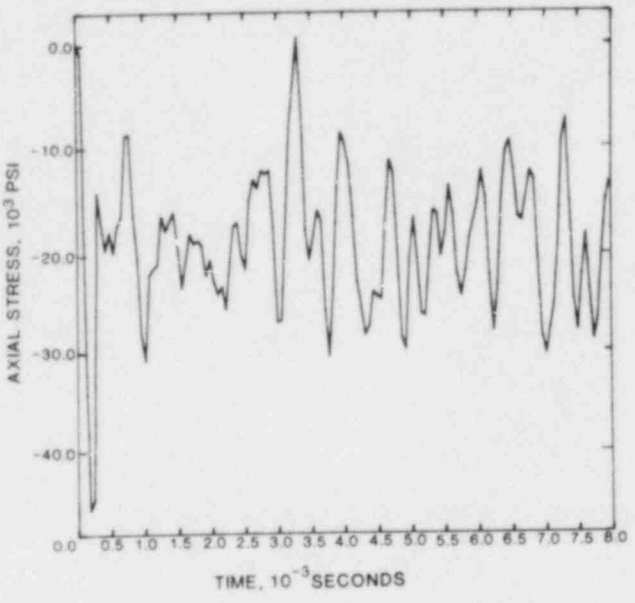

Figure 4.2.20. Axial Stress vs Time at Location D for the Uranium-Steel End-On Two-Dimensional Impact Calculation

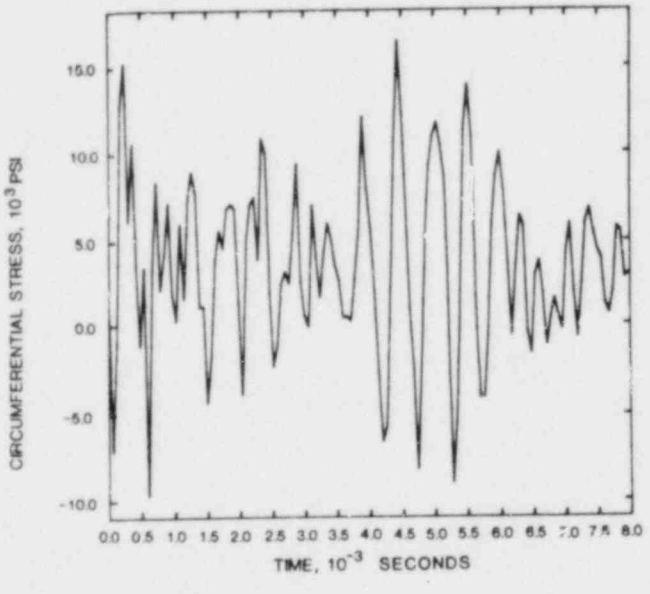

Figure 4.2.21. Circumferential Stress vs Time at Location E for the Uranium-Steel Cask End-On Two-Dimensional Impact Calculation

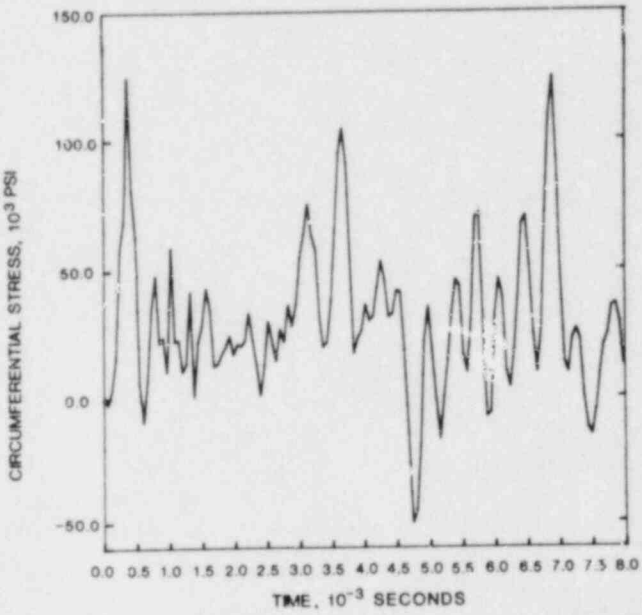

Figure 4.2.22. Circumferential Stress vs Time at Location F for the Uranium-Steel Cask End-On Two-Dimensional Impact Calculation

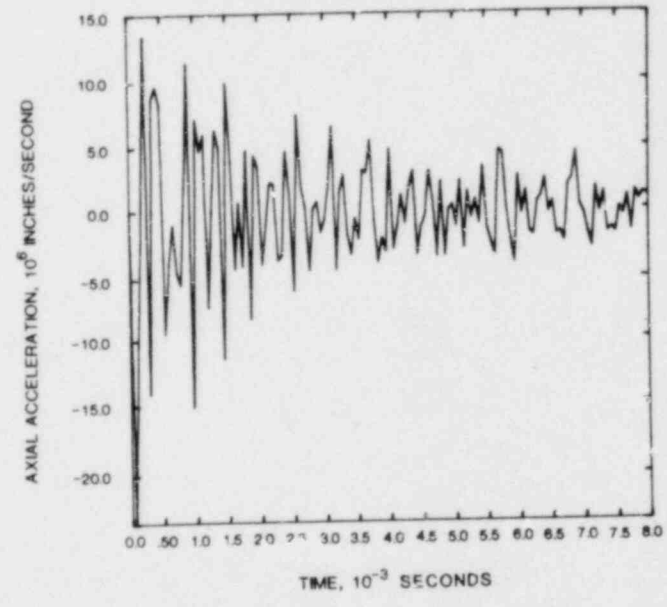

Figure 4.2.23. Axial Acceleration vs Time at Location F for the Uranium-Steel Cask End-On Impact Calculation

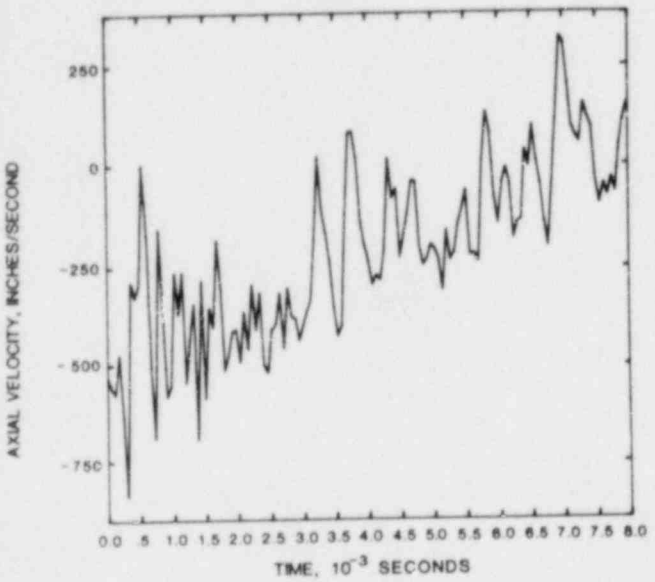

Figure 4.2.24. Axial Velocity vs Time at Location F for the Uranium-Steel Cask End-On Two-Dimensional Impact Calculation

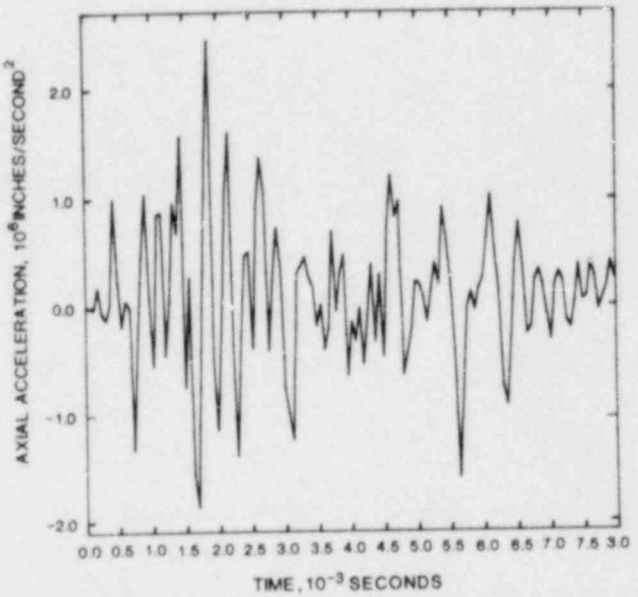

Figure 4.2.26. Axial Acceleration vs Time at Location H for the Uranium-Steel Cask End-On Two-Dimensional Impact Calculation

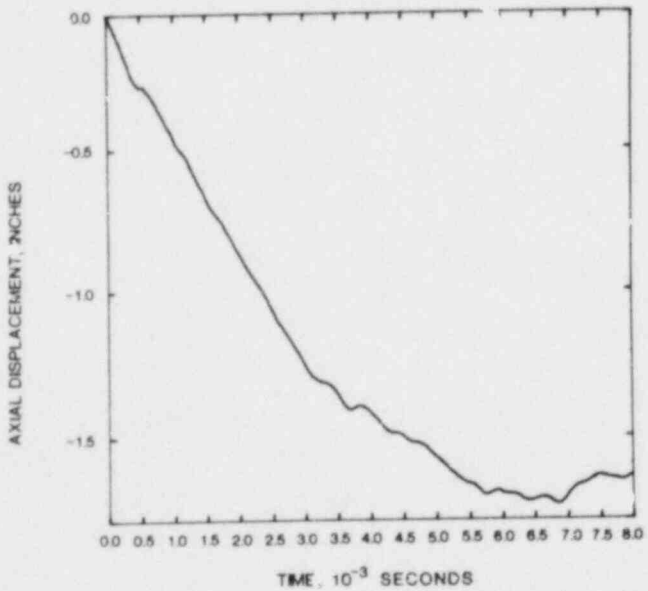

Figure 4.2.25. Axial Displacement vs Time at Location F for the Uranium-Steel Cask End-On Two-Dimensional Impact Calculation

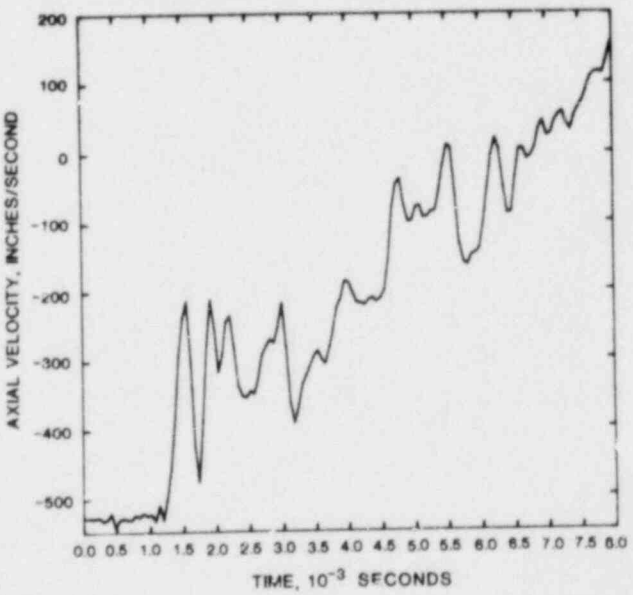

Figure 4.2.27. Axial Velocity vs Time at Location H for the Uranium-Steel Cask End-On Two-Dimensional Impact Calculation

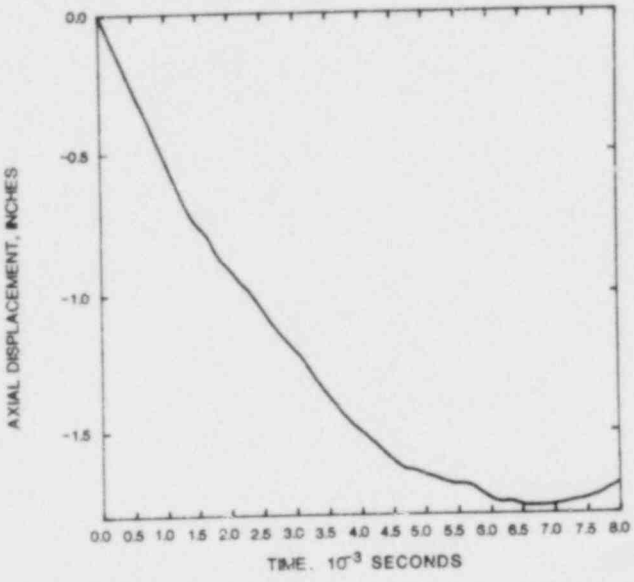

Figure 4.2.28. Axial Displacement vs Time at Location H for the Uranium-Steel Cask End-On Two-Dimensional Impact Calculation

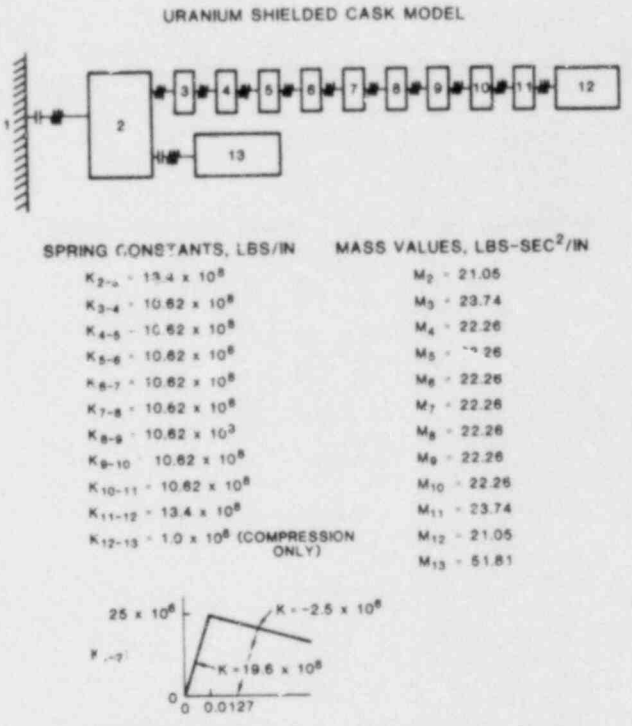

Figure 4.2.29. Schematic of the Lumped Parameter Model

4.2.2.2 Two-Dimensional Static Analysis

With the second technique, which is the two-dimensional static solution, the same finite element mesh without the fins was used (Figure 4.2.13).

To simulate the dynamic loads, a constant axial acceleration of 345 g's was applied. The details of calculating the g level from a two-dimensional transient analysis are explained in the fin analysis section, 4.2.1.2. The resulting stresses at the designated locations are shown in Table 4.4, Section 4.2.4, where a comparison of results is made. The stresses reported are at the center of the element nearest the point in question.

4.2.2.3 One-Dimensional Dynamic Analysis

The uranium shielded cask of this study was modeled employing the same technique used with the lead shielded cask. Figure 4.2.29 schematically illustrates the lumped parameter mode. Mass elements 2-12 represent the cask and impact limiter structures. The impact limiter mass was apportioned between the two mass elements on each end. Mass element 13 represents the fuel assembly. The force-deflection characteristic of the impact limiter, coupling 1-2, was obtained by using data from Reference 4.7 as a guidline.

As with the lead shielded cask, the mass elements of the model were given an initial velocity of 528 in./s against a fixed target mass. The computational results, including displacements, loads in couplings, and accelerations, were used to calculate stresses at the various cask locations (Figure 4.2.1).

Figure 4.2.30 illustrates the computed force in coupling 1-2, the impact limiter. This coupling transmits force directly into the cask body. As can be seen, the dynamic loading of the cask is calculated to last approximately 9 ms and decline rapidly after 8 ms. (The dip in the force level seen in these figures is a dynamic effect which results from a hammer and rebound effect of the fuel inside the cask.)

Figure 4.2.31 illustrates the calculated displacement of the front end (location G) of the cask. This indicates that the fin impact limiter crushes about 1.8 in. The front part of the cask body travels the distance in approximately 7 ms. Figure 4.2.32 illustrates the velocity-time behavior for the same location. Figure 4.2.33 is the corresponding acceleration-time plot. A peak g value of 3 000 is calculated to occur at impact.

Figure 4.2.34 illustrates the displacement of Location H on the top end of the cask. It appears very similar to the displacement curve for the front location, indicating that the cask goes through the impact very much like a rigid body. The top location does displace slightly more, indicating some compression of the cask. Figures 4.2.35 and 4.2.36 illustrate the velocity-time and acceleration-time plots for the top end of the cask. The peak acceleration value (2 000 g's) is approximately 30% lower than for the bottom end.

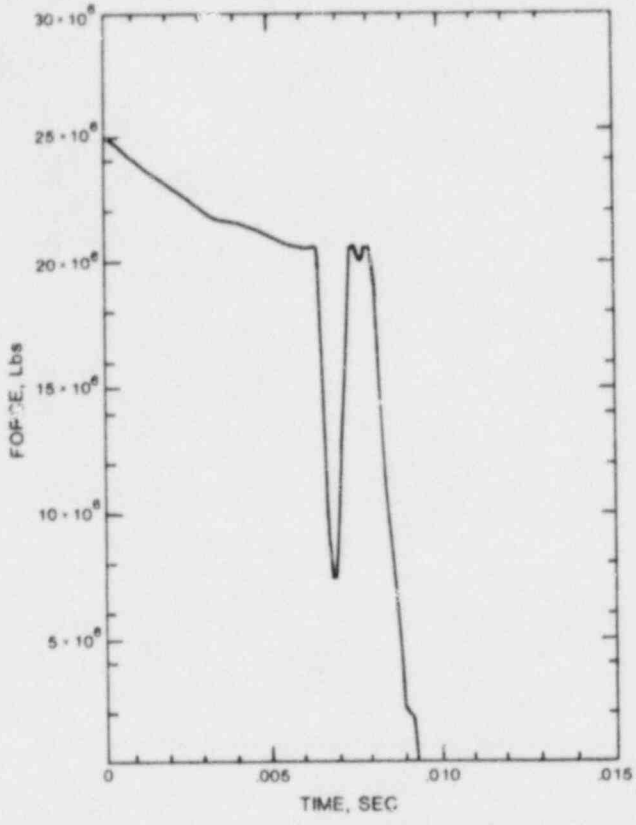

Figure 4.2.30. Force Input to the Front End of the Cask vs Time for the Uranium-Steel Cask End-On One-Dimensional Impact Calculation

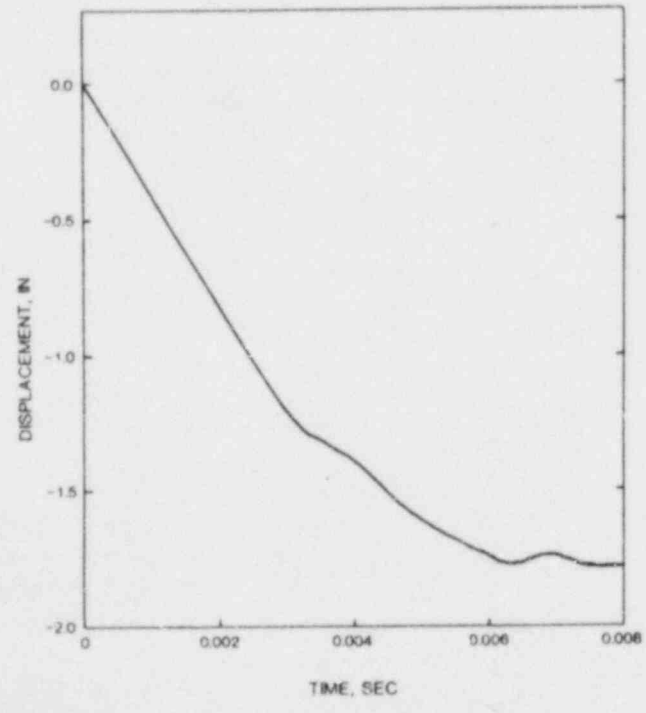

Figure 4.2.31. Displacement of the Bottom End of the Cask (Location G) vs Time for the Uranium-Steel Cask End-On One-Dimensional Impact Calculation

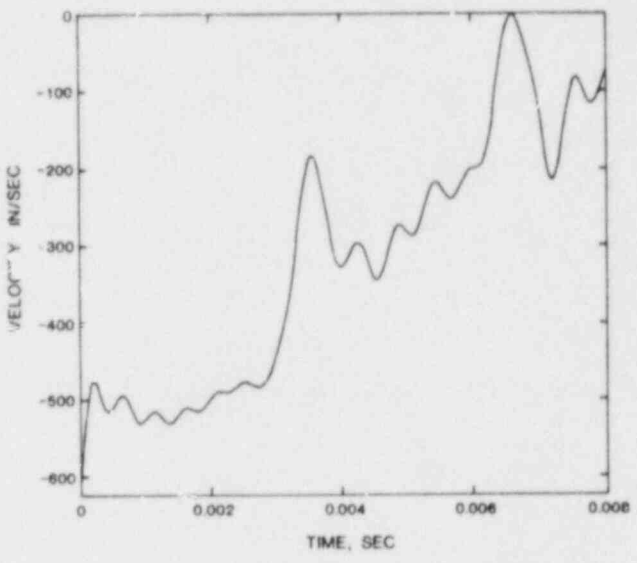

Figure 4.2.32. Velocity of the Bottom End of the Cask (Location G) vs Time for the Uranium-Steel Cask End-On One-Dimensional Impact Calculation

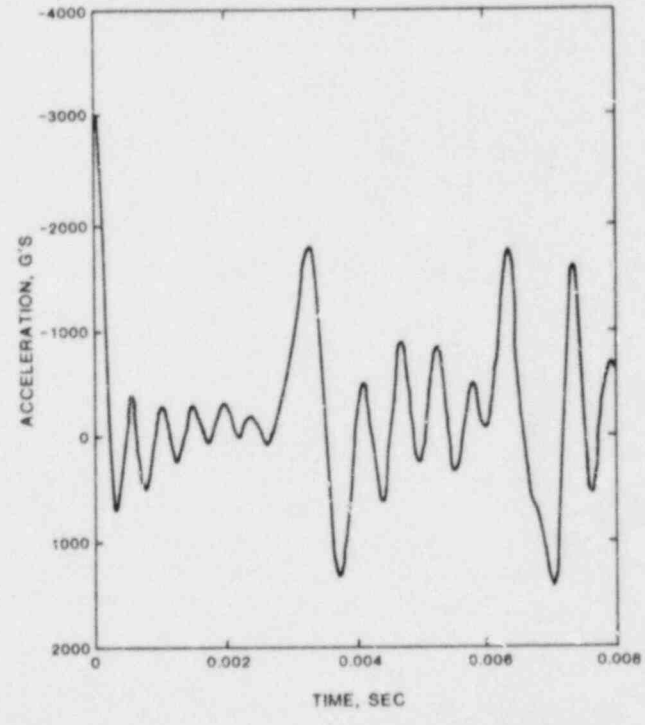

Figure 4.2.33. Acceleration of the Bottom End of the Cask (Location G) vs Time for the Uranium-Steel Cask End-On One-Dimensional Impact Calculation

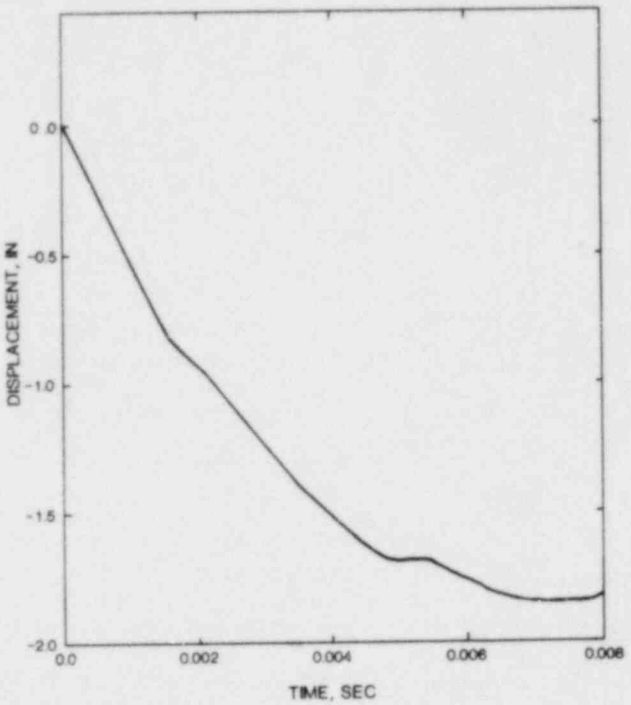

Figure 4.2.34. Displacement of the Top End of the Cask (Location H) vs Time for the Uranium-Steel Cask End-On One-Dimensional Impact Calculation

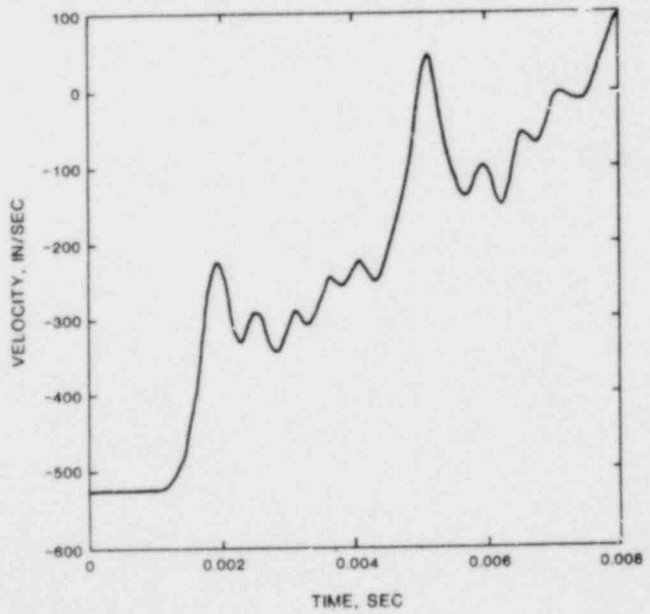

Figure 4.2.35. Velocity of the Top End of the Cask (Location H) vs Time for the Uranium-Steel Cask End-On One-Dimensional Impact Calculation

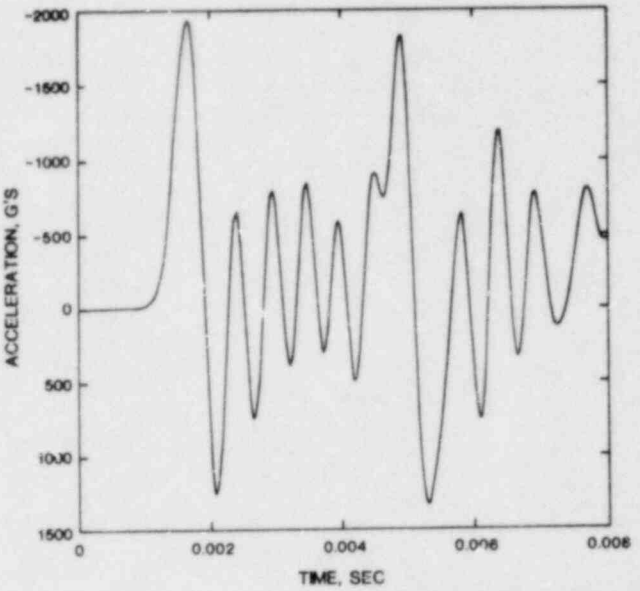

Figure 4.2.36. Acceleration of the Top End of the Cask (Location H) vs Time for the Uranium-Steel Cask End-On One-Dimensional Impact Calculation

Figure 4.2.37 is a plot of the axial stress in the stainless steel shell at location C near the bottom of the cask. The peak compressive stress level for this point was calculated to be 39 000 psi. Figure 4.2.38 illustrates stresses calculated for location D in the uranium shielding material. The peak compressive stress calculated at this point was 34 000 psi. The stress levels at these locations, C and D, were obtained from the calculated load for coupling 2-3 of the model.

Stress levels in the cask ends were calculated by treating the ends as simply supported plates, as described in Section 1.2.1.2. The loading used for calculating the stresses was obtained by taking the calculated acceleration for the corresponding mass element and multiplying it by the weight of the plate. This method was used for calculating stresses at locations A, B, E, and F.

Figure 4.2.39 illustrates the radial stress at point E on the bottom of the cask. The peak radial stress was calculated to be 29 000 psi. Figure 4.2.40 illustrates the hoop stress at this same point. It was calculated to be higher than the radial stress, with a peak value of 44 000 psi. Figure 4.2.41 illustrates the stress at the center of the front end plate, location F. This was calculated to be the highest stressed point in the cask,

with a peak value of about 67 000 psi. Figure 4.2.42 illustrates the stress at the corresponding point at location A at the top end of the cask. Stress levels here are considerably lower, with a peak value of about 44 000 psi.

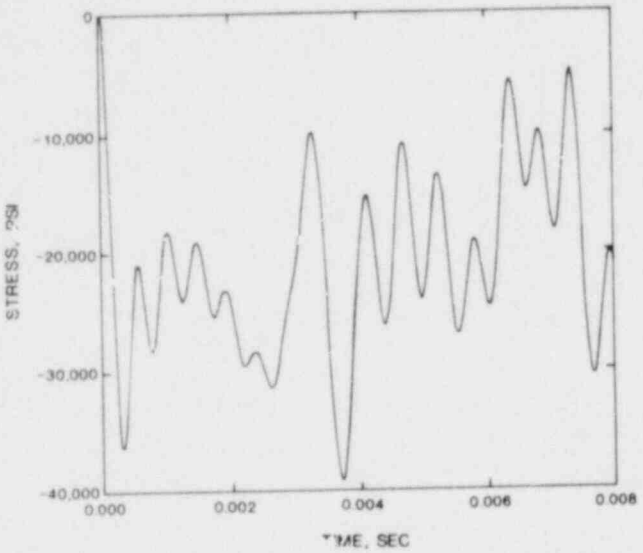

Figure 4.2.37. Axial Stress at Location C vs Time for the Uranium-Steel Cask End-On One-Dimensional Impact Calculation

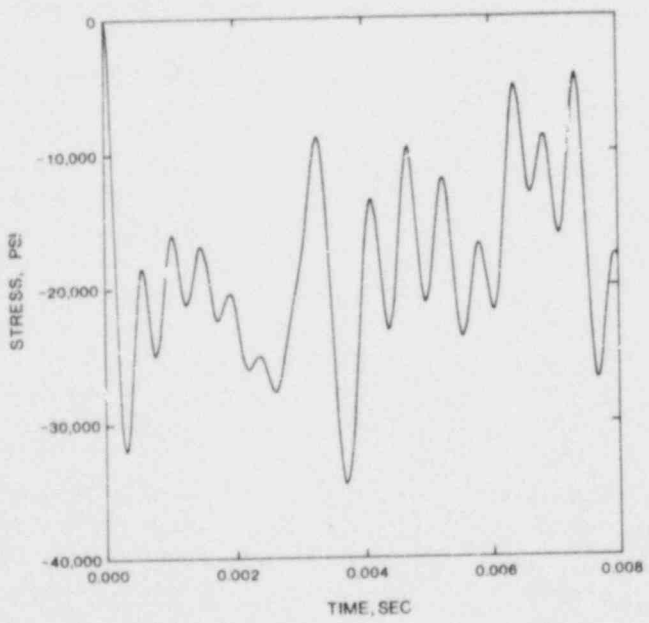

Figure 4.2.38. Axial Stress at Location D vs Time for the Uranium-Steel Cask End-On One-Dimensional Impact Calculation

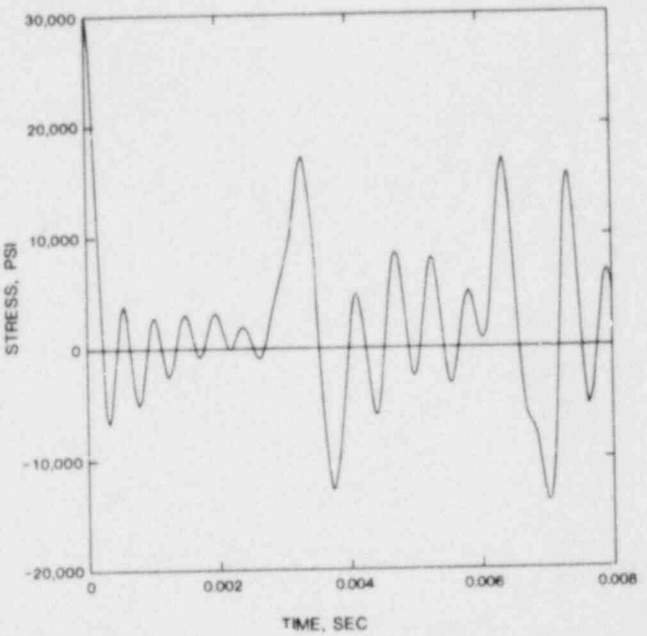

Figure 4.2.39. Radial Stress at Location E vs Time for the Uranium-Steel Cask End-On One-Dimensional Impact Calculation

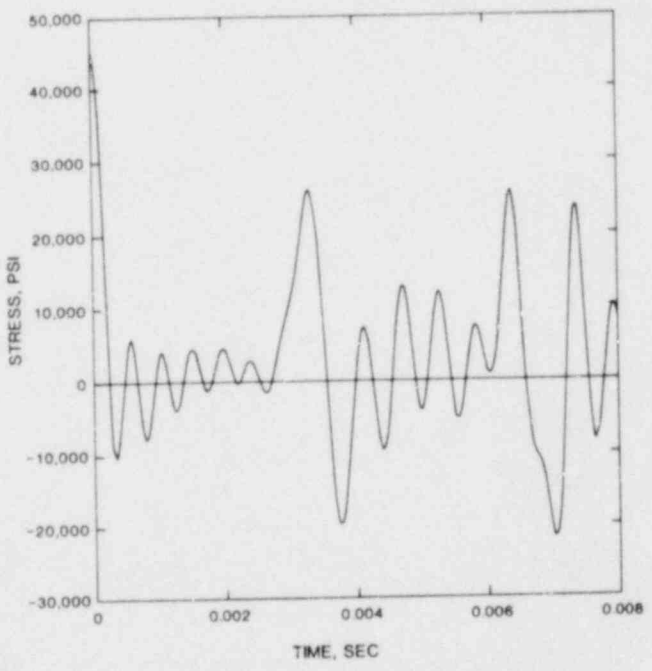

Figure 4.2.40. Tangential Stress at Location E vs Time for the Uranium-Steel Cask End-On One-Dimensional Impact Calculation

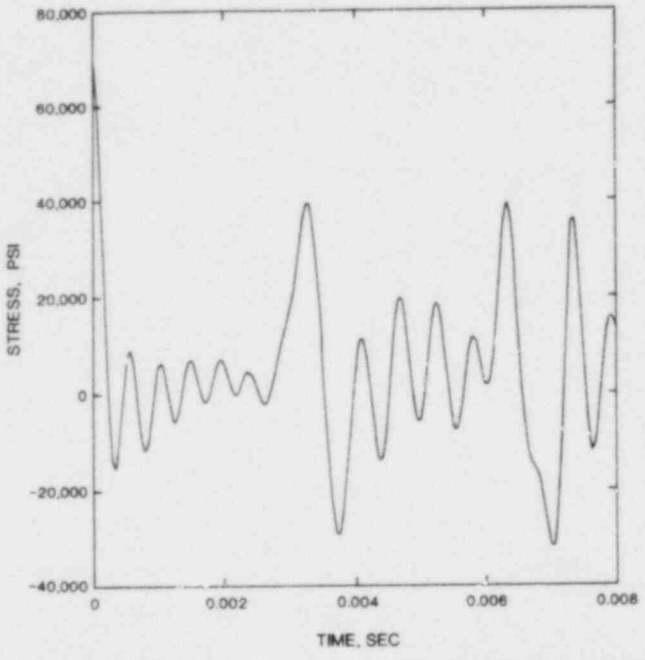

Figure 4.2.41. Tangential and Radial Stress at Location F vs Time for the Uranium-Steel Cask End-On One-Dimensional Impact Calculation

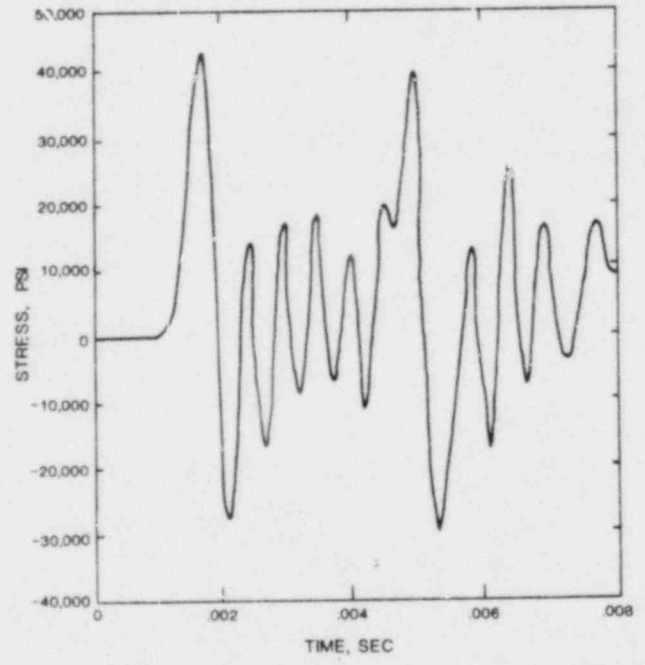

Figure 4.2.42. Tangential and Radial Stress at Location A vs Time for the Uranium-Steel Cask End-On One-Dimensional Impact Calculation

The results for the outer point, B, on the back plate are illustrated in Figures 4.2.43 and 4.2.44. The radial stress had a peak value of 18 500 psi; the maximum hoop stress was 28 500 psi.

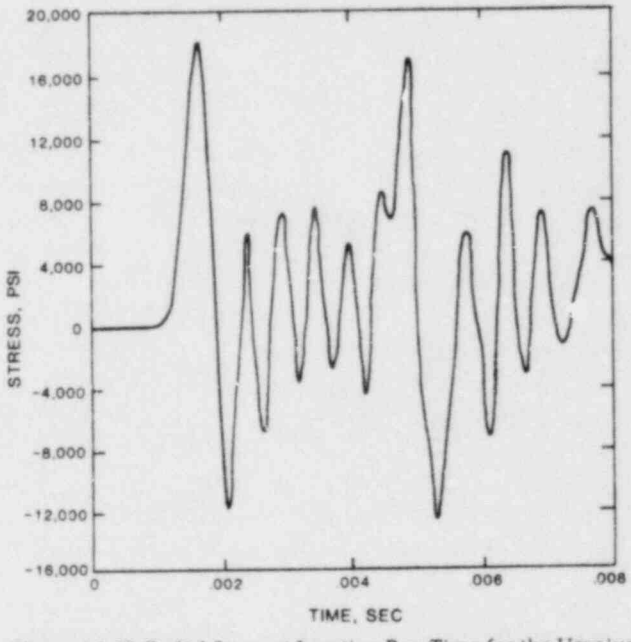

Figure 4.2.43. Radial Stress at Location B vs Time for the Uranium-Steel Cask End-On One-Dimensional Impact Calculation

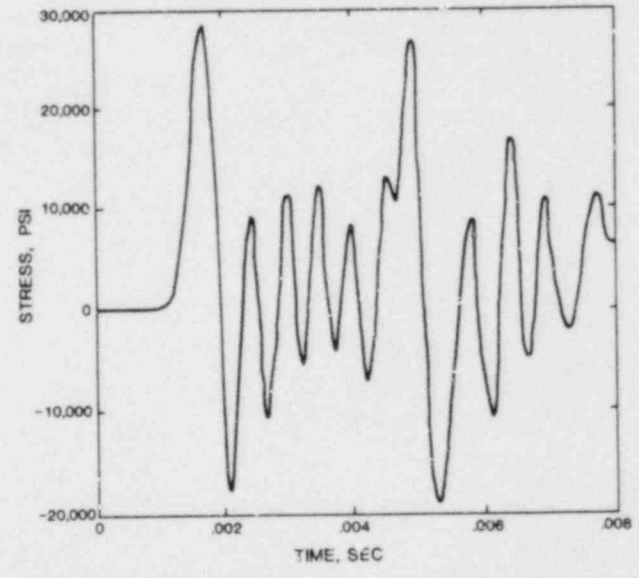

Figure 4.2.44. Tangential Stress at Location B vs Time for the Uranium-Steel Cask End-On One-Dimensional Impact Calculation

4.2.2.4 One-Dimensional Static Analysis

In this section, the stresses in the uranium-steel cask which occur as a result of the vertical impact are calculated by applying basic stress analysis methods. The analysis methods and the implications of these methods have been discussed in Section 1.2.1.

The stress analysis presented in this section is essentially identical to the analysis presented in Section 4.1.1.4 for the lead-steel-balsa cask. The cask impact is treated as an equivalent static problem, with the impact inertial force calculation being based upon the deceleration (d) of 345 g's determined in Section 4.2.1.2. The stresses in the ends of the cask are calculated with thin plate theory. The cask wall stresses are calculated by assuming a uniaxial stress state in the wall layers. The remainder of the section is directed toward the determination of stress values for locations A through F, Figure 4.2.13.

The 36-in.-dia end plate on the uranium-steel cask consists of a 3-in. depleted uranium layer sandwiched between two 1.5-in. layers of 304 stainless steel. In this analysis, the end plate is modeled as three thin plate structures which act as parallel structures having the same center deflection at their interfaces. The two steel layers are modeled as circular plates with clamped edges, because of the integral attachment to the cask wall. The uranium layer is modeled as a simply supported circular plate in order to neglect bonding of the uranium layer to the cask walls. This latter assumption produces conservative stress results in the steel layers by causing the end plate model to be more flexible and by requiring the steel layers to support a larger portion of the impact load.

The center deflection, y_c^s, for one of the steel end plate layers is described by the formula[4.5, Table 24-10b]

$$y_c^s = \frac{-q_s' R^4}{64 D_s} ,$$

where

$$D_s = \frac{E_s t_s^3}{12 (1-\upsilon_s^2)} ,$$

in which q_s' is the load per unit area, R is the plate radius, t_s is the plate thickness, E_s is Young's modulus, and υ_s is Poisson's ratio. Substituting the end plate variables into the above equations yields

$$D_s = \frac{(28 \times 10^6)(1.5)^3}{12 [1.0 - (0.33)^2]} = 8.837 \times 10^6 \text{ lb in.}$$

and

$$y_c^s = \frac{-q_s' (18)^4}{64 (8.837 \times 10^6)} = -(1.856 \times 10^{-4}) q_s' .$$

The center deflection, y_c^u, for the uranium end plate layer is given by[4.5, Table 24-10a]

$$y_c^u = \frac{q_u' R^4 (5 + \upsilon_u)}{64 D_u (1 + \upsilon_u)} ,$$

in which

$$D_u = \frac{E_u t_u^3}{12 (1 - \upsilon_u^2)} ,$$

and where the physical constants have the same meaning as for the steel layer plate equations. Evaluating the above equations yields

$$D_u = \frac{(25.8 \times 10^6)(3)^3}{12 [1 - (0.21)^2]} = 6.073 \times 10^7 \text{ lb in.}$$

and

$$y_c^u = \frac{-q_u' (18)^4 (5 + 0.21)}{64 (6.073 \times 10^7) (1 + 0.21)}$$

$$= -(1.353 \times 10^{-4}) q_u' .$$

Setting the steel plate deflection equal to the uranium plate deflection yields the relationship that

$$q_u' = 1.596 q_s' .$$

The inertial impact load on the top plate is assumed to be due to the plate weight only. Expressed in terms of load per unit plate area, the impact load on the plate is given by

$$Q' = (2t_s\rho_s + \rho_u t_u)d ,$$

in which ρ is the weight density. Evaluating the above expression yields

$$Q' = [2(0.283)(1.5) + (.682)(3)](345) = 998.8 \text{ psi} .$$

By superposition, the total load is equal to the sum of the loads on the individual plate layers; that is,

$$Q' = 2q_s' + q_u' = (2 + 1.596) q_s' ,$$

which yields

$$q_s' = 277.7 \text{ psi} .$$

The radial stress and the hoop stress at the center of the steel plate, location A, are given by

$$\sigma_A^{radial} = \sigma_A^{hoop} = \pm \frac{6M_c^s}{t^2 s} = \pm \frac{3q_s'' R^2 (1 + \upsilon_s)}{8t_s^2}$$

and

$$\sigma_A = \pm \frac{3(277.7)(18)^2(1 + 0.33)}{8(1.5)^2} = \pm 19\,944 \text{ psi}$$

The radial stress and the hoop stress at the edge of the steel plate, location B, are calculated as

$$\sigma_B^{radial} = \pm \frac{6M_R^s}{t_s^2} = \pm \frac{3q_s'' R^2}{4t_s^2} = \pm \frac{3(277.7)(18)^2}{4(1.5)^2}$$

$$= \pm 29\,922 \text{ psi}$$

and

$$\sigma_B^{hoop} = \upsilon_s \sigma_A^{radial} = 8\,998 \text{ psi} \quad ,$$

Since the bottom end plate is structurally the same as the top plate, the analysis method applies to both. However, the bottom plate not only carries the impact load due to its own weight, but also carries the inertial load due to the cask payload, which is 21 000 lb.

Thus, the total inertial load on the bottom end plate is calculated as

$$Q'' = Q' + \frac{W_{PL} d}{A_p}$$

$$Q'' = 998.8 + \frac{(21\,000)(345)}{\frac{\pi}{4}(36)^2} = 8\,117 \text{ psi} \quad .$$

Q' is the load per unit area for the plate as calculated in the previous section, W_{PL} is the cask payload, and A_p is the plate area. Again using superposition, the impact load carried by the stainless steel layer is calculated as

$$Q'' = 2q_s'' + q_u'' = (2 + 1.596)\, q_s''$$

or

$$q_s'' = 2\,257 \text{ psi} \quad .$$

Since linear theory is used on the plate calculations, the stresses at locations F and E are proportional to those at locations A and B, respectively. Thus,

$$\sigma_F^{hoop} = \sigma_F^{radial} = \sigma_A^{radial} \frac{q_s''}{q_s'} = \pm 19\,444 \left(\frac{2257}{227.7}\right)$$

$$= \pm 162\,100 \text{ psi} \quad ,$$

$$\sigma_E^{radial} = \sigma_B^{radial} \frac{q_s''}{q_s'} = \pm 29\,992 \left(\frac{2257}{227.7}\right)$$

$$= \pm 243\,800 \text{ psi} \quad ,$$

and

$$\sigma_C^{hoop} = \upsilon_s \sigma_E^{radial} = \pm 73\,140 \text{ psi} \quad .$$

all of which for exceed the yield strength of the material.

The cask wall stresses at locations C and D, Figure 4.2.1, are calculated by assuming that a state of uniaxial stress exists in each layer of the cask wall. The weight supported by the cask wall is taken to be the empty cask weight less the weights of the bottom end plate, the lower impact limiters, and one circumferential impact limiter or a weight (W^{CD}) of 90 281 lb.

The depleted uranium wall layer and the stainless steel wall layers are assumed to act as parallel uniaxial structures. Axial displacement compatibility between the parallel systems is assumed to calculate the proportion of the total inertial load carried by the uranium wall layer and the steel wall layers, respectively. The longitudinal deflection of the uranium layer is given by the expression

$$\delta_u = \frac{F_u L_u}{A_u E_u} \quad ,$$

where δ_u is the deflection, F_u is the layer force, L_u is the length, A_u is the cross-sectional area, and E_u is Young's modulus. Similarly, the longitudinal displacement of the steel layers is expressed as

$$\delta_s = \frac{F_s L_s}{A_s E_s} \quad .$$

Setting, the layer displacements equal to each other yields

$$F_u = \frac{A_u E_u}{A_s E_s} F_s$$

since the lengths of the layers are equal.

$$A_u = \frac{\pi}{4}[(46)^2 - (38)^2] = 527.8 \text{ in.}^2$$

and

$$A_s = \frac{\pi}{4}[(48)^2 - (46)^2 + (38)^2 - (36)^2] = 263.9 \text{ in.}^2$$

Then,

$$F_u = \frac{(527.8)(25.8 \times 10^6)}{(263.9)(28 \times 10^6)} F_s = 1.843 F_s$$

By the principle of superposition, the sum of the layer forces is equal to the total inertial wall force; thus,

$$F_s + F_u = -W^{CD}d = (-90\,281)(345)$$
$$= -3.115 \times 10^7 \text{ lbs}$$

Solving the latter two expressions for F_u and F_s produces

$$F_s = -1.102 \times 10^7 \text{ lbs}$$

and

$$F_u = -2.013 \times 10^7 \text{ lbs}$$

The axial stresses at locations C and D are calculated as

$$\sigma_C = \frac{F_s}{A_s} = -41\,760 \text{ psi}$$

and

$$\sigma_D = \frac{F_u}{A_u} = -38\,480 \text{ psi}$$

4.2.3 Comparison of Results for the Uranium-Steel Cask

As with the lead-steel-balsa cask, the results for the uranium-steel cask will be compared at the discrete points on the cask indicated in Figure 4.2.14. First, some kinematic quantities will be compared. The kinematic data for the four calculations are tabulated in Table 4.3. The average acceleration is again calculated by dividing the velocity change by the time to reach maximum displacement. It should be pointed out that the average acceleration calculated is highly dependent on the method by which the fin impact limiter was modeled. The two-dimensional dynamic calculation utilized the results of the three-dimensional finite element model of the limiter. This calculation produced an average acceleration of -170 g's. The one-dimensional dynamic calculation, which used experimental results for fin crushing from Reference 4.7, produced an average acceleration of -182 g's. The one- and two-dimensional static calculations produced identical kinematic quantities as they both used the same assumptions for the impact limiter crush (the two-dimensional fin calculation). The average acceleration for this calculation was significantly higher at -345 g's, for reasons explained in Section 4.2.1.2. The maximum cask displacement (impact limiter crush) varied from 1.18 in. to 2.2 in., with the dynamic calculations being fairly close and indicating less crush.

Table 4.3. Kinematic Comparison of Dynamic Analyses, End-On Impact of Uranium-Steel Cask

Analysis Type	Maximum Displacement (in.)	Average Acceleration (g)	Time to Reach Maximum (s)
2D Dynamic*	-2.2	170	8.0×10^{-3}
1D Dynamic	-1.8	182	7.5×10^{-3}
2D and 1D** Static	-1.18	345	4.3×10^{-3}

*From 3D dynamic fin calculation
**From 2D dynamic fin calculation

The results for use in the comparison of the stress components predicted by each analysis technique are summarized in Table 4.4. For Point A, at the center of the top end plate, the two-dimensional dynamic solution is considered the most accurate solution based on the assumption that the uranium is bonded to the steel and plates. All the other analysis techniques under-predicted the stresses in the end plates because the dynamic characteristics of the plate were neglected. The static solutions greatly underestimated the stress at this top plate location. The results for the static analyses would have been even lower if 170 g's were input as a load instead of the 345 g's, predicted by the two-dimensional dynamic fin analysis.

Table 4.4. Stress Component Comparison, End-On Impact of Uranium-Steel Cask

Analysis Type		σ_r	σ_z	σ_{rz}	σ_θ	σ_e
LOCATION A						
2D Dynamic	maximum	102 000	2 700	4 800	102 000	102 000
	minimum	-82 000	-1 950	-6 700	-82 000	--
2D Static		6 116	45	0	6 142	6 084
1D Dynamic	maximum	44 000	--	--	44 000	44 000
	minimum	-30 000	--	--	-30 000	--
1D Static		-19 944	--	--	-19 944	19 944
LOCATION B						
2D Dynamic	maximum	28 000	1 530	3 350	30 000	30 000
	minimum	-28 000	-1 800	-3 400	-27 000	--
2D Static		1 082	72	367	-2 127	2 914
1D Dynamic	maximum	18 500	--	--	28 500	25 000
	minimum	-13 000	--	--	-19 000	--
1D Static		-29 992	--	--	8 998	26 657
LOCATION C						
2D Dynamic	maximum	2 650	1 000	6 250	10 000	45 000
	minimum	-2 700	-49 000	-4 200	-18 000	--
2D Static		-197	-38 752	213	-5 092	+36 358
1D Dynamic	maxinum	--	-5 000	--	--	39 000
	minimum	--	-39 000	--	--	--
1D Static		--	-41 760	--	--	41 760
LOCATION D						
2D Dynamic	maximum	2 470	1 000	7 800	9 200	42 600
	minimum	-1 420	-46 000	-5 200	-12 000	--
2D Static		-421	-33 710	271	194	34 022
1D Dynamic	maximum	--	-4 000	--	--	34 000
	minimum	--	-34 000	--	--	--
1D Static		--	-38 480	--	--	38 480

Table 4.4. (Continued)

Analysis Type		σ_r	σ_z	σ_{rz}	σ_θ	σ_e
LOCATION E						
2D Dynamic	maximum	49 000	17 000	16 800	16 300	49 000
	minimum	-16 000	-10 000	-3 400	-11 500	--
2D Static		30 503	-3 026	5 974	8 611	31 250
1D Dynamic	maximum	--	29 000	--	44 000	38 700
	minimum	--	-14 500	--	-22 000	--
1D Static		243 800	--	--	73 140	216 694
LOCATION F						
2D Dynamic	maximum	137 000	5 000	122 000	127 000	127 000
	minimum	-51 000	-5 800	-17 300	-50 000	--
2D Static		41 530		-112	41 717	41 485
1D Dynamic	maximum	67 000	--	--	67 000	67 000
	minimum	-34 000	--	--	-34 000	--
1D Static		162 100	--	--	162 100	162 100

At location B, the outer edge of the top plate, the two- and one-dimensional dynamic analyses are in agreement. A comparison with the static results indicates some differences with the dynamic results and even between the two static solutions. These differences are caused mainly by the assumption that the uranium is bonded to the steel for the two-dimensional static analysis and unbonded for the one-dimensional static or strength-of-materials analysis. In order to compare the static results to the dynamic results, the load for the static analysis should be changed to -170 g's, which means a reduction of the predicted stress values by 50%. When the load is changed, the static analyses significantly under-predict the stresses at Point B.

The stresses at Points C and D, in the wall of the cask, are in good agreement if the load is not adjusted. If the 50% reduction in load is applied to the two static solutions, the stresses are under-predicted by about 50%.

The results at Points E and F on the lower end plate for the dynamic calculations are similar to the results for Points B and A, respectively. Again the two-dimensional dynamic results are considered the most accurate. The one-dimensional dynamic calculations capture the dynamic response of the point at which the ends of the plate are attached, but do not model the dynamic response of the plate itself. Hence, this method tends to underestimate the magnitude of the stresses at end plate locations.

The static results at the plate locations E and F again differed from the dynamic calculations. The two-dimensional static calculation, which assumes perfect bonding between the uranium and the steel, under-predicted the stresses at these plate locations. The one-dimensional static calculation, which assumes no bonding between the uranium and the steel, proved to be very conservative by greatly overestimating the stress at both points.

4.3 References

4.1 R. E. Jones, *Users Manual for QMESH, A Self-Organizing MESH Generation Program*, Report No. SLA-74-0239 (Albuquerque, NM: Sandia Laboratories, July 1974).

4.2 S. W. Key, "A Finite Element Procedure for the Large Deformation Dynamic Response of Axisymmetric Solids," *Computer Methods in Applied Mechanics and Engineering*, 4, 1974, pp 195-218.

4.3 K. J. Bathe, *ADINA, A Finite Element Program for Automatic Dynamic Incremental Nonlinear Analysis*, Report 82448-1 (Cambridge, MA: Massachusetts Institute of Technology, 1976).

4.4 V. K. Gabrielson and R. T. Reese, *SHOCK Code Users Manual — A Computer Code to Solve the Dynamic Response of Lumped Mass Systems*, Report No. SCL-DR-69-98 (Livermore, CA: Sandia Laboratories, 1969).

4.5 R. J. Roark and W. C. Young, *Formulas for Stress and Strain*, 5th ed (New York: McGraw-Hill Book Company, 1975).

4.6 J. H. Biffle and M. H. Gubbels, *WULFF — A Set of Computer Programs for the Large Displacement Dynamic Response of Three-Dimensional Solids*, Report SAND76-0096 (Albuquerque, NM: Sandia Laboratories, 1976).

4.7 L. I. Weingarten, *Impact Energy Mitigation in LMFBR Spent Fuel Shipping Casks*, Report SAND76-0601 (Albuquerque, NM: Sandia Laboratories).

4.8 J. H. Biffle, M. J. Sagartz, L. I. Weingarten, *Inelastic Response of Metallic Impact Limiters*, 4th International Conference on: Structural Mechanics in Reactor Technology, San Francisco, CA, August 15-19, 1977.

4.9 F. C. Davis, *Structural Analysis of Shipping Casks, Volume 9 — Energy Absorption Capabilities of Plastically Deformed Streets Under Specified Impact Loading Conditions*, ORNL-TM-1312 (Vol. 9) (Oak Ridge National Laboratory, TN, February 1971).

5.0 Summary and Conclusions

This report has described a number of analytical techniques which can be used to analyze the response of a spent-nuclear-fuel shipping cask subjected to an end-on impact. These same techniques can be used to analyze a side impact and possibly a corner impact; however, these cases fall beyond the scope of the present study.

Two basic types of casks have been analyzed: one has a "soft" balsa wood impact limiter and the other has a more rigid stainless steel fin impact limiter. These hypothetical casks were designed to be representative of commercial casks as determined by a cask survey described in this report. A number of materials commonly used in cask construction were examined, and common material properties were used in the different analyses. The analysis techniques ranged from a simple strength-of-materials method to a dynamic two-dimensional finite element technique.

A comparison of kinematic quantities calculated for the cask motion by the different techniques was made. These results indicated good agreement between the various methods for the quantities of total crush of the impact limiter and the average deceleration of the cask during the impact. The largest discrepancy occurred between the two- and three-dimensional finite element analyses of the fin impact limiter. The two-dimensional results produced an artifically high value for the stiffness of the limiter, which affected the cask body stress calculations based on this analysis.

From the results of the study it can be concluded that if the impact limiter characteristics are well known, all of the techniques yield good results for stresses in the cylindrical part of the cask body (location C, for instance). The results of this study also indicate that an end impact situation can cause high-frequency vibration in the ends of the cask and very high (but of very short time duration) stress peaks. A two-dimensional dynamic analysis is necessary in order to accurately model this behavior. The one-dimensional dynamic analysis, as configured in this report, does not capture the plate dynamics well. This type of one-dimensional dynamic model could possibly be modified to include the mass and stiffness of the end plates. A model modified in this manner would probably model end plate stresses much more accurately using basically the same techniques. The static methods can greatly underestimate stresses at points on flexible parts of the cask, such as end plates, as was clearly shown in this study.

One finding of this study, a result of the dynamic analyses, was a confirmation of the fact that acceleration levels at different points on a cask can vary greatly. The acceleration can also include a very high frequency component, a fact that the experimenter who desires to measure cask deceleration levels in a drop test should keep in mind.

The question of whether the shielding material is well bonded or not bonded to the main structural material is quite important in the stress analyses. All of the techniques used in this study, except the strength-of-materials method, have assumed perfect bonding between these two materials. An unbonded condition could severely alter the results and is certainly something which the analyst should consider. When using a finite element technique, one method of treating an unbonded condition (which will be conservative if bonding exists) is to use sliding interfaces between the two materials.

This work has demonstrated that there are a number of analytical techniques which may be used to analyze a shipping cask. In some instances the results can differ significantly when considering the dynamic response at a given point on the cask. It should be kept in mind that these calculations represent a very detailed analysis of a case where the stress levels were, for the most part, in the linear elastic range. Analyses for a much more severe impact than that investigated here, and which would result in large plastic deformations of the cask, fall into a separate category. For such cases it is probably more practical to construct and test small-scale physical models of the casks.

DISTRIBUTION:

US Nuclear Regulatory Commission (290)
(290 copies for RT)
Division of Document Control
Distribution Services Branch
7920 Norfolk Avenue
Bethesda, MD 20014

US Nuclear Regulatory Commission
SAFER
M.S. 1130 SS
Washington, DC 20555
Attn: W. R. Lahs

US Nuclear Regulatory Commission (2)
FCTC
M.S. 396-SS
Washington, DC 20555
Attn: C. E. MacDonald
C. Ross Chappel

4400 A. W. Snyder
4440 G. R. Otey
4442 W. A. Von Riesemann (5)
4550 R. M. Jefferson (7)
5500 O. E. Jones
5520 T. B. Lane
5521 L. W. Davison
5521 J. H. Biffle
5524 C. R. Adams
8214 M. A. Pound
3141 L. J. Erickson (5)
3151 W. L. Garner (3)
For: DOE/TIC (Unlimited Release)
3154-3 C. H. Dalin (25)
For: NRC Distribution to NTIS

NRC FORM 335 (7 77) U.S. NUCLEAR REGULATORY COMMISSION

BIBLIOGRAPHIC DATA SHEET

1. REPORT NUMBER (Assigned by DDC)
NUREG/CR-2018
SAND80-1870

4. TITLE AND SUBTITLE (Add Volume No., if appropriate)
A Comparison of Analytical Techniques for Analyzing a Nuclear-Spent-Fuel Shipping Cask Subjected to an End-on Impact

2. (Leave blank)

3. RECIPIENT'S ACCESSION NO.

7. AUTHOR(S)
C.R. Adams
M.H. Gubbels
John H. Biffle
M. Huerta

5. DATE REPORT COMPLETED
MONTH June YEAR 1981

9. PERFORMING ORGANIZATION NAME AND MAILING ADDRESS (Include Zip Code)
Sandia National Laboratories
Albuquerque, NM 87185

DATE REPORT ISSUED
MONTH August YEAR 1981

6. (Leave blank)

8. (Leave blank)

12. SPONSORING ORGANIZATION NAME AND MAILING ADDRESS (Include Zip Code)
Office of Nuclear Regulatory Research
U.S. Nuclear Regulatory Commission
Washington, DC 20555

10. PROJECT/TASK/WORK UNIT NO.

11. CONTRACT NO.
FIN No. A1045

13. TYPE OF REPORT

PERIOD COVERED (Inclusive dates)

15. SUPPLEMENTARY NOTES

14. (Leave blank)

16. ABSTRACT (200 words or less)

A requirement of the design of a nuclear shipping cask (10 CFR 71 Appendix B) is that it survive a free drop of 30 feet onto a flat, essentially unyielding target. This report compares various analytical techniques which can be used to determine the dynamic response of a cask. These techniques are compared by defining two hypothetical cask designs, one lead-steel-balsa and the other uranium-steel. The end-on axial impact orientation condition was selected and one-, two-, and three-dimensional analyses were performed. The analysis techniques include strength-of-materials methods, lumped-parameter dynamic modeling, and both static and dynamic two- and three-dimensional finite element techniques. The results are compared in terms of kinematic and stress levels at different points on the casks. The study will be valuable as a guide in selecting analysis techniques for evaluating the dynamic response of shipping casks.

17. KEY WORDS AND DOCUMENT ANALYSIS

17a. DESCRIPTORS

17b. IDENTIFIERS/OPEN-ENDED TERMS

18. AVAILABILITY STATEMENT
Unlimited

19. SECURITY CLASS (This report)
Unclassified

21. NO. OF PAGES

20. SECURITY CLASS (This page)
Unclassified

22. PRICE
$

NRC FORM 335 (7 77)

Org.	Bldg.	Name	Rec'd by *	Org.	Bldg.	Name	Rec'd by *

120555064215 2 ANRT
US NRC
ADM DOCUMENT CONTROL DESK
PDR
016
WASHINGTON DC 20555